Lawrence Berkeley Laboratory
UNIVERSITY OF CALIFORNIA

Materials & Molecular
Research Division

# THE CRYSTALLIZATION OF GLASSES IN THE Mg-Si-O-N SYSTEM

Thomas Carroll Shaw
(Ph.D. thesis)

October 1980



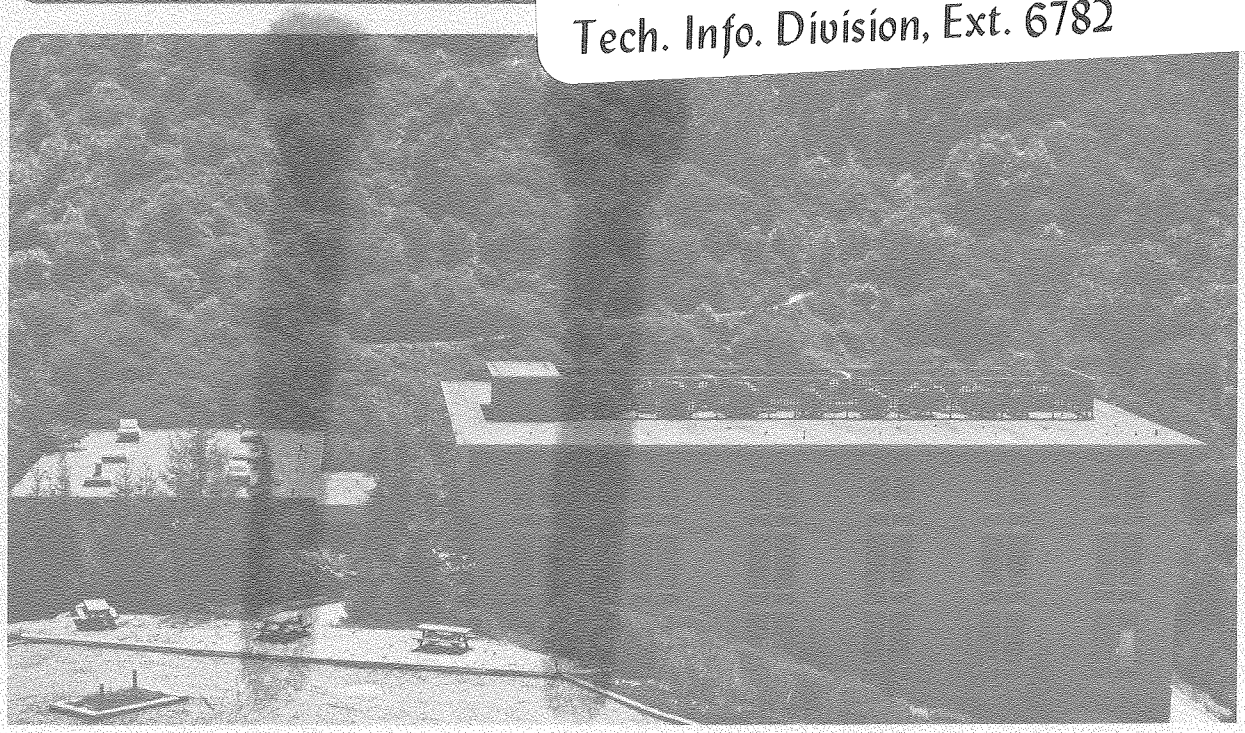

Prepared for the U.S. Department of Energy under Contract W-7405-ENG-48

## DISCLAIMER

LBL-11759

# THE CRYSTALLIZATION OF GLASSES IN THE Mg-Si-O-N SYSTEM

by

Thomas Carroll Shaw
(Ph.D. Thesis)

Materials Science and Mineral Engineering Department
Materials and Molecular Research Division
Lawrence Berkeley Laboratory
University of California
Berkeley, California 94720

October 80

This research was supported by the National Science Foundation grant #DMR-77-24022. Technical staff and facilities were provided by the Director, Office of Energy Research, Office of Basic Energy Sciences, Division of Materials Sciences of the U. S. Department of Energy under Contract No. W-7405-ENG-48.

# THE CRYSTALLIZATION OF GLASSES IN THE Mg-Si-O-N SYSTEM

by

Thomas McCarroll Shaw

## ABSTRACT

The general crystallization behavior of glasses in the Mg-Si-O-N system has been investigated.

In preparation of the glasses, it was found that $Si_3N_4$ was a necessary constitutent of melts for glass formation, but that decomposition reactions limited the range of compositions which produced useful glasses. Melts of $SiO_2$ rich compositions separated into $SiO_2$ rich and MgO rich glassy phases on cooling. Compositional analysis of the phases established that phase separation results from extension of the miscibility gap in the MgO-$SiO_2$ system into the Mg-Si-O-N system.

Crystallization in a glass of composition 59 wt% $SiO_2$, 32 wt% MgO and 9 wt% $Si_3N_4$ was investigated in detail using the techniques of differential thermal analysis, x-ray diffraction, optical microscopy and transmission electron microscopy. Crystallization occurred mainly by internal nucleation of crystals, although some surface crystallization was also observed. Intermediate temperature heat treatments in the temperature range 1000°C-1300°C crystallized the MgO rich phase of the glass to spherulites of enstatite, but had no effect on the $SiO_2$ rich phase. The spherulites developed at intermediate temperatures

consisted of fan like arrangements of plate shaped enstatite grains separated by thin films of uncrystallized glass. After heating to temperatures above 1300°C, faceted grains of enstatite were formed adjacent to the $SiO_2$ rich pockets by recrystallization of the spherulites. Heating to above 1300°C also precipitated crystals of $Si_2N_2O$ from residual glass between enstatite grains in the spherulites. Volume changes on crystallization of the glass caused porosity to form throughout the microstructure.

The effect of two stage nucleation and growth heat treatments on microstructure were investigated. Nucleation treatments at temperatures of 800°C-1000°C brought about a considerable refinement of the microstructure and optimum nucleation occurred at about 850°C. The effect of nucleation treatments were limited, treatments longer than 2 hours producing no further refinement of the microstructure. A brief study of crystallization in glasses of other compositions showed that nucleation was also highly sensitive to the composition of the glass. Circumstantial evidence suggests that nucleation was caused by silicon impurity particles precipitated from the glasses on cooling from the melt.

The results indicate that Mg-Si-O-N glasses may be useful as starting materials for the production of glass ceramics of new compositions. Additional experiments for exploration of this possibility are suggested.

Gareth Thomas

Gareth Thomas
Professor of Materials Science

TABLE OF CONTENTS

Page

# I. INTRODUCTION

Oxynitride glasses represent a new class of glasses in which both oxygen and nitrogen contribute to glass formation. They were originally discovered when it was found that oxide glasses after nitriding contained small amounts of nitrogen.[1-3] More recently interest in oxynitride glasses has been stimulated by the suggestion that they form the bonding layer between $Si_3N_4$ grains in $Si_3N_4$ ceramics hot pressed and sintered with additives.[4,5] This has prompted attempts to prepare oxynitride glasses by melting mixtures of oxides and nitrides in a nitrogen atmosphere. By this method both samples of oxynitride glasses containing up to 10 at% nitrogen have been produced in a variety of systems.[6,7]

Technologically oxynitride glasses are of interest from two points of view. Firstly as thin intergranular films in $Si_3N_4$ based ceramics, oxynitride glasses control properties such as strength,[8,9] creep resistance[10,11] and oxidation resistance[12] in these materials. Secondly, in bulk form, oxynitride glasses are potentially of interest as new materials because of their high refractive index and the possibility of preparing glass ceramics[13] from them. Important to both these aspects of oxynitride glasses is an understanding of their crystallization behavior.

Crystallization of the glassy grain boundary phase in $Si_3N_4$ based ceramics offers a potential method of overcoming the deleterious effects of such a phase on the high temperature properties of $Si_3N_4$. The controlled crystallization of bulk oxynitride glasses is also of interest because of the possibility of producing glass

ceramics of new compositions. In particular the prospect of producing glass ceramics that contain refractory nitride on oxynitride phases is an attractive one. So far however there have been no detailed investigations of the crystallization behavior of oxynitride glasses.

In view of this deficiency, the present investigation was undertaken to characterize crystallization behavior in glasses formed in the Mg-Si-O-N system. This system was chosen because it was already known that glasses formed in the system and important aspects of phase equilibria in the system had previously been established.[14,15] In addition, it was felt that the relative simplicity of the Mg-Si-O-N system would facilitate interpretation of the results. The glasses were prepared by melting mixtures of $SiO_2$, MgO and $Si_3N_4$. The microstructures of as-cooled glass melts were characterized in detail. Differential thermal analysis was used to determine temperature ranges in which crystallization reactions occurred and the crystalline products of reactions were identified by x-ray diffraction. The microstructures of glasses after simple heat treatments were examined using optical and transmission electron microscopy. The effect of two stage nucleation and growth heat treatments on crystallization was also examined to explore the possibility of glass ceramic formation in this system.

Observations made during glass forming experiments are described in Section III, along with a detailed characterization of the composition and microstructures of successful glasses. In Section IV, crystallization reactions observed in the most successful glass are described. Temperature ranges for each reaction and the microstructural

changes that result from the reactions are reported. The results of additional experiments to examine ways in which crystallized microstructures can be controlled are given in Section V. In the discussion section (Section VI), factors affecting glass formation in oxynitride glasses are examined and the crystallization phenomena observed in Mg-Si-O-N glasses are related to crystallization behavior in other systems. Also discussed in Section VI, is the potential for glass ceramic formation in the Mg-Si-O-N system. Additional experiments to examine the possibility of glass ceramic formation from oxynitride glasses are suggested.

# II. EXPERIMENTAL PROCEDURES

## II.1. Glass Preparation

Initial experiments to survey the glass forming region found at $SiO_2$ rich compositions in the Mg-Si-O-N system were carried out by Dr. R. Loehman at Stanford Research Institute, Starting compositions were made up by mixing weighed amounts of Baker reagent grade $SiO_2$ and MgO powders and GTE amorphous SN402 $Si_3N_4$ powder. Ten gram batches of each composition were melted in shallow molybdenum dishes at various temperatures using a graphite element furnace.* Melting was carried out in nitrogen at one atmosphere pressure. Typical melting times were one hour and cooling was effected by turning off the furnace. Exact cooling rates were not determined, but generally melts were cooled to below 1000°C in less than ten minutes. To supplement these experiments some additional compositions were melted using a tungsten element furnace.+ The appearance of quenched melts were noted and inhomogeneous melts were crushed and remelted to improve mixing. Each melt was checked for crystallinity by x-ray diffraction. For a detailed investigation of crystallization behavior a larger sample of the most successful glass was prepared by melting a hundred gram batch of powder for four and a half hours using the graphite element furnace. Compositions of the melts prepared are given in Table I.

---

*Custom built

+Centor New Hampshire

## II.2. Differential Thermal Analysis (DTA)

Reactions occurring on heating glass A were detected by differential thermal analysis. One gram crushed samples of the glass were heated in a platinum crucible to 1400°C at a rate of 10°C per minute. Heating was carried out in air, using a platinum wound tube furnace. The temperature difference between the sample and an equivalent weight of high purity $Al_2O_3$ powder, in good thermal contact with the sample, was continuously monitored using thermocouples. The temperature was recorded from a thermocouple situated midway between the sample and the standard. Temperature ranges in which reactions occurred were identified from exothermic and endothermic peaks in the DTA traces.

In preliminary heat treatments of glasses carried out in air, it was found that crystallization behavior at the surface of samples differed from that in the bulk of the glass. To differentiate peaks in the DTA traces arising from surface reactions from those caused by reactions in the bulk of the glass, samples of two different particle sizes were used for DTA runs. A sample crushed to give coarse particles ($\approx$ 500 μm in diameter) was used to detect reactions in the bulk of the glass. In a second run a finely ground sample was used. As the fine powder had a larger surface area than the coarsely ground sample, peaks corresponding to surface reactions in this DTA trace were larger than in the DTA trace from the coarse powder. Thus temperatures at which surface reactions occurred could be identified by comparison of DTA traces from finely and coarsely ground samples.

## II.3. Heat Treatments

Samples of glass A for microstructural characterization were crystallized in air using isothermal heat treatments. Additional samples were given two stage heat treatments to investigate the possibility of refining the microstructure by controlled nucleation and growth of crystals. Other glass compositions were also crystallized by isothermal heat treatments for examination of microstructure-composition relationships.

## II.4. X-Ray Diffraction

Crystalline phases formed after heat treatment of the glasses were identified using an x-ray diffractometer and monochromatic Cu $K_\alpha$ radiation. Qualitatively the amount of each phase was estimated from relative peak heights in the diffractometer traces.

## II.5. Microstructural Characterization

The microstructures of the as cooled and crystallized glasses were examined using transmitted polarized light microscopy and transmission electron microscopy. Thin sections were cut from samples using a diamond saw and mounted on glass slides with wax. Sections were then ground to a thickness of about 50 μm on silicon carbide papers and polished on both sides with 6 μm diamond paste. Thinned sections were used for both optical microscopy and to prepare specimens for transmission electron microscopy. The final thinning of TEM specimens was carried out by ion milling with 5 KV argon ion beams after sections had been mounted on copper grids.

Thinned foils were examined in a Philips 301 transmission electron microscopy operating at 100 KV. Compositional data from the microstructures was obtained using energy dispersive x-ray (EDSX) and electron energy loss (ELS) spectrometer attachments to a Philips 400 transmission electron microscope.

# RESULTS

## III. GLASS FORMATION IN THE Mg-Si-O-N SYSTEM

### III.1. Melting Experiments

Figure 1 shows the extent of the glass forming region found in the Mg-Si-O-N system for the furnace conditions and cooling rates used in the survey melting experiments. The starting compositions melting temperatures and time at temperature for each melt are tabulated in Table I along with a description of each melt on cooling. The region of glass formation lies predominantly in the $SiO_2$-$Si_2N_2O$-$MgSiO_3$ compatibility triangle of the $SiO_2$-MgO-$Si_3N_4$ phase diagram and is centered around composition A (59 wt% $SiO_2$, 32 wt% MgO, 9 wt% $Si_3N_4$).

The extent of the glass forming region was found to be limited by two factors, crystallization of the melt on cooling and frothing of the melt during melting. Partly crystalline melts resulted from compositions containing less $Si_3N_4$ (melts I and J) or more MgO (melts K and L) than composition A. Estimation of liquidus temperatures from the binary $SiO_2$-MgO phase diagram[16] indicated that compositions I and J were completely molten at the melting temperatures used and therefore crystallized on cooling. The rapid increase in liquidus temperature with increasing MgO content in the MgO-$SiO_2$ phase diagram suggests that the crystallinity in compositions K and L, is in part, due to incomplete melting.

For compositions richer than A in $SiO_2$ or $Si_3N_4$ (melts G and H) copious frothing occurred on melting. This resulted in glassy

materials which contained a large number of bubbles on cooling. Melts A-F all produced glassy materials which were largely bubble free. However, some bubbling was initially observed in all these compositions, particularly in the more $SiO_2$ rich compositions (C and D). In this respect the glass forming region indicated by the dotted line in Fig. 1 is somewhat arbitrary. The most successful glass forming composition A produced a completely bubble free glass after melting for one hour.

Measurement of the nitrogen contents of the glasses, by a fusion technique*, indicated that about 30% of the nitrogen initially added (as $Si_3N_4$) was lost on melting. The exact composition of the glasses could not be determined due to the large uncertainties involved in such measurements. The loss of nitrogen, though, indicates that the compositions were shifted towards the $MgO$-$SiO_2$ binary tie line in the $SiO_2$-$MgO$-$Si_3N_4$ phase diagram during melting.

## III.2. Characterization of the Glasses

On cooling melts A, B, C and D produced opaque glasses. Microstructural examination showed that the opaqueness was caused by phase separation in the glasses. Phase separation in glass A produced a microstructure consisting of groups of droplets of one phase, about 3 μm across dispersed in a continuous matrix of a second glassy phase. A low magnification view of this microstructure is shown in Fig. 2(a). EDS spectra from the two phases in glass A indicated that the minor phase contained mainly silicon and virtually no magnesium (Fig. 2(b)),

*Oregon Metallurgy Laboratories

whereas the matrix phase contained significant amounts of both magnesium and silicon. Similar spectra obtained from the matrix and minor phases in glasses B, C, and D indicated that in each glass the minor phase consisted mainly of $SiO_2$ while the matrix phase contained both $SiO_2$ and MgO. The only other element detected in the glasses was chlorine (nitrogen and oxygen being undetectable by EDSX due to x-ray absoprtion by the beryllium detector window). Chlorine was present in small concentrations in the MgO rich phase, but not in the $SiO_2$ rich droplets. The chlorine was thought to come from the amorphous $Si_3N_4$ powders used to prepare the glasses.[17]

In preparing thin foils of the glasses A - D for TEM it was found that preferential etching of the $SiO_2$ rich phase occurred during ion beam milling. This made preparation of uniformly thinned specimens difficult and in most cases the $SiO_2$ rich phase was almost completely etched from the microstructure leaving holes in the foils. From the size of these holes, however, an idea of the amount of and morphology of the $SiO_2$ rich phase in the glasses could be obtained.

Low magnification views of the microstructures in glasses A, B and C are shown in Figs. 3(a),(b),(c), respectively, for comparison. From the size of the holes in the foils it can be seen that glasses B and C contain considerably more $SiO_2$ rich phase than glass A. From this it is apparent that the amount of $SiO_2$ rich phase increases with the $SiO_2$ content of the glasses. The morphology of the phase separation in glasses A, B and C is unusually coarse but is quite distinct from the macroscopic liquid unmixing observed at melting temperatures in immiscible silicate liquids.[18,19] This

suggests that at the melting temperatures used in the present experiments, glasses A, B and C are homogeneous liquids and that the coarse microstructures result from phase separation occurring as the melts are cooled.

In order to determine the extent of the miscibility gap in the present system, quantitative microanalysis was used to examine the compositions of the $SiO_2$ rich (droplets) and MgO rich (matrix) phases in glasses A - D. Each glass was annealed at a temperature of 850°C for two hours to equilibrate the glasses at the same temperature. The ratio of magnesium to silicon in matrix and minor phases was determined in the TEM using x-ray analysis.

A problem encountered in this analysis was the sensitivity of the MgO rich phase to radiation damage. When a high intensity electron probe was focused on areas of the matrix phase, extensive bubble formation occurred in the exposed region after only short times (see for example Figs. 4(a)-(d)). Similar behavior has been observed in glassy pockets in $Si_3N_4$ ceramics[20,21], and it has been suggested that damage is caused by ionization of atoms in the glass under the influence of the electron beam[21]. EDS analysis showed that accompanying the damage in the MgO rich phase there was a loss in magnesium from the exposed region. This resulted in considerable errors in the analysis of Mg/Si ratios in the glasses when long counting times were used.

To avoid this problem a low intensity beam was used to record all spectra and for each phase spectra were first recorded at 60 second intervals to check for changes in composition with exposure. Counting times were selected for which no change in composition could be detected and were then used to record subsequent spectra.

An example of this analysis is shown in Fig. 5. Using a high intensity electron beam the Mg/Si count ratio changes from 0.44 to 0.31 after an exposure of 500 seconds. Using a lower intensity beam the Mg/Si count ratio remains essentially constant. A further check of the analysis is obtained from extrapolation of the plots of Mg/Si count ratio against time to zero time. The extrapolated value of Mg/Si count ratio for the high intensity beam (0.442) agrees well with the averaged value of Mg/Si count ratio obtained using a low intensity beam (0.437).

To further improve the analysis, spectra were recorded from 10 different regions of phases in each glass using typically 250 sec. counting times and a low intensity beam. Using this technique values of Mg/Si count ratio, for each phase, which were reproducible to within ±2% could be obtained. The count ratios were converted to atomic ratios of the elements using the relation[22]

$$\frac{I_A}{I_B} K_{AB} = \frac{C_A}{C_B}$$

where $I_A$ and $I_B$ are integrated peak intensities and $C_A$ and $C_B$ are atomic fractions of the elements A and B respectively. The constant $K_{AB}$ was found experimentally using two independent standards of known Mg/Si ratio i.e. powdered samples of pure $MgSiO_3$ and $Mg_2SiO_4$. The quantified Mg/Si atomic ratios for MgO and $SiO_2$ rich phases in glasses A - D are given in Table II.

Knowing the Mg/Si ratios of phases in each glass is insufficient to fix their compositions, but indicates lines of constant Mg/Si

ratio in the phase diagram along which each phase must lie. Tie lines then pass through the point representing the average composition of the glass on the phase diagram.[23] The tie line for each composition intersects the lines of constant Mg/Si ratio for phases in the glass at points corresponding to their compositions. The problem of finding the composition of phases in the glasses then becomes one of finding the tie line connecting them.

In order to establish the approximate position of the tie line for glass A energy loss spectra were recorded from both MgO and $SiO_2$ rich phases in this glass. Typical spectra are shown in Fig. 6(a),(b). Spectra from both phases contained prominent oxygen K edges, the nitrogen edges, however, were only clearly seen after background stripping and magnification of spectra. The relative areas of the nitrogen edges after stripping indicated that there was approximately twice as much nitrogen in the matrix glass as in the $SiO_2$ rich minor phase.

If it assumed that the composition of the glasses were unchanged on melting a tie line for glass A can be drawn on the phase diagram through the starting composition for glass A. The tie line intersects the lines of constant. Mg/Si ratio for each phase such that the composition of MgO rich phase fixed the tie line contains twice as much nitrogen as the composition fixed for the $SiO_2$ rich pahse (see Fig. 7). If it is further assumed that the tie lines for other glasses lie parallel to that for glass A the compositions of phases in glasses B - D can similarly be fixed. The compositions determined in this way for $SiO_2$ rich and MgO rich phases in glasses A - D are plotted on the phase diagram in Fig. 7. The

lines plotted then represent a partial plot of the extent of the miscibility gap in the $SiO_2$-MgO-$Si_3N_4$ system at 850°C. Although the position of the miscibility gap in Fig. 7 is only approximate the results show that at 850°C glasses A - D separate into a minor phase with a composition close to the $SiO_2$-$Si_2N_2O$ tie line and a matrix phase whose composition lies close to the $MgSiO_3$-$Si_2N_2O$ tie line. Both phases contain nitrogen but more is segregated to the MgO rich phase.

As a further test for the position of the miscibility gap compositions E and F were prepared and examined for phase separation (see Fig. 7 for the compositions of glasses E and F). Electron microscopy showed that glass E whose composition lies within the experimentally determined miscibility gap phase separated on a fine scale during cooling (see Fig. 8(a)). Glass F, with a composition outside the miscibility gap, was completely clear and showed no evidence of phase separation, even after annealing for two hours at 850°C (see Fig. 8(b)). The consistency of these results with the experimentally determined miscibility gap suggests that Fig. 7 may be used with some confidence to predict immiscibility in glasses in the $SiO_2$-MgO-$Si_3N_4$ system.

As well as phase separation a few crystalline particles were found in some of the glasses. The particles were most common in glasses B and C and a typical example from glass B is shown in Fig. 9(a). The corresponding electron diffraction patterns indicated that the particles were twinned crystals of elemental silicon. This was further confirmed by the finding that EDS spectra from the particles contained only a peak corresponding to silicon Fig. 9(b).

Frequently associated with the silicon crystals were small dark particles (arrowed in Fig. 9(a)). EDS spectra from these regions showed that they contained Si, Ti, Cr and Fe (Fig. 9(c)). These were thought to come from impurities in the starting powders used to prepare the glasses. Similar but smaller particles of silicon were found in glass A, see for example Fig. 10(a), (b). Even after close examination no silicon particles were observed in glass E.

# IV. CRYSTALLIZATION REACTIONS IN GLASS A

## IV.1 Differential Thermal Analysis and X-ray Diffraction Studies

DTA traces from coarse and fine powders of glass A are shown in Figs. 11(a),(b) respectively. Both traces have a small endothermic dip at about 800°C corresponding to the glass transition and strong exothermic peaks centered at 1070°C and 1350°C which arise from reactions in the bulk of the glass. The DTA trace from the finer powder has an additional peak centered at 1020°C and a somewhat larger peak at 1350°C indicating the occurrence of surface reactions at these temperatures.

X-ray diffraction from the bulk of heat treated samples of glass A indicated that below 1000°C little or no crystallization occurred. In the temperature range 1000°C - 1300°C enstatite ($MgSiO_3$) crystallized from the interior of samples. The relative intensities of reflections in the x-ray diffraction patterns indicated that at room temperature the samples consisted largely of the monoclinic polymorph of enstatite clinoenstatite.[24] After heat treatments above 1300°C both clinoenstatite and protoenstatite were found in the interior of samples. From these results it was concluded that the exothermic peak at 1070°C in the DTA traces arose from internal crystallization of the glass to enstatite. The second exothermic peak at 1350°C was attributed to the formation of protoenstatite in the bulk of the glass.

Markedly different behavior was observed on the surface of heat treated samples of glass A. At temperatures just above the glass transition temperature and up to 1300°C, forsterite ($Mg_2SiO_4$)

crystallized from the surface of the glass, more forsterite tending to form at higher temperatures. Above 1300°C protoenstatite and crystobalite ($SiO_2$) formed on the samples surfaces. The exothermic peak at 1020°C in the DTA trace from the finer powder was attributed to the crystallization of the surface of samples to forsterite. The increased size of the exothermic peak at 1350°C in the DTA trade from the fine powder was thought to be caused by reactions forming crystobalite and protoenstatite on the surface of the glass.

IV.2. Surface Crystallization

For microstructural characterization samples of glass A were heated in air to different temperatures, held at temperature for two hours and then cooled. Thinned sections were taken perpendicular to the surface of heat treated samples. Examination of the sections using transmitted polarized light revealed microstructural differences between the surface and interior of the samples. Three types of microstructure were observed at the surface.

(a) After heat treatments at temperatures below 1000°C a thin layer of forsterite crystals formed on the surface of the glass as shown in Fig. 12(a).

(b) After intermediate temperature heat treatments (1000°C to 1300°C) the crystals had grown from the surface to a depth of about 20 μm, Fig. 12(b). The extinction behavior of the crystals in polarized light indicated that they had a high degree of preferred orientation.[25] Beneath the surface layer of crystals a crystalline microstructure developed

which was similar to the bulk microstructure of the sample only finer in scale. Examination of sections cut parallel to the surface of heat treated samples in the TEM showed that the layer of orientated crystals was made up of forsterite dendrites growing with their [001] direction perpendicular to the surface of the sample. An example of the dendrites is shown in Fig. 13. Electron diffraction indicated that each dendrite was a single crystal of forsterite. Dark field imaging using diffuse scattering from residual glass in the microstructure (see Appendix II) showed that each crystal was finely branched and that the branches were separated by considerable amounts of glass (see Fig. 13).

(c) Heat treatments at temperatures above 1300°C resulted in the formation of a fine grained friable layer of crystals on the surface of the sample. This is seen as a uniform gray band about 60 μm thick in the optical micrograph in Fig. 12(c). In agreement with the x-ray diffraction results described in the previous section, the surface layer was found by TEM to consist of crystals of enstatite and crystobalite.

The results suggested that surface crystallization was influenced by the oxidizing atmosphere used in heat treatments. The depth to which the microstructure was affected varied with heat treatment time and temperature, but even after high temperature heat treatments was not greater than 200 μm. The microstructures observed beneath the surface affected layer were uniform throughout the samples indicating that they were unaffected by the furnace atmosphere. For this reason

the remainder of the investigation concentrated on characterization of crystallization in the interiors of samples, as this was thought to be representative of the intrinsic behavior of the glasses.

## IV.3. Bulk Microstructural Development

The effect of heat treatments on the microstructure of glass A could be divided roughly into three temperature ranges, the temperature ranges corresponding to those identified by DTA and x-ray diffraction studies. Each temperature range of behavior is treated separately below.

### IV.3.a. Low temperatures (below 1000°C)

After heating at temperatures below 1000°C little or no crystallization was detected in the interior of samples of glass A even after 4 hour heat treatments. Optical and TEM examination of samples failed to reveal any perceptible changes in the bulk microstructure of the glass, except after heating at temperatures close to 1000°C. Heat treatments in this temperature range produced a dispersion of small internally nucleated crystals in the glass, see for example Fig. 14. Growth of the crystals was very slow at these temperatures preventing extensive crystallization of the glass from occurring. Heat treatments at temperatures well below 1000°C, however, have an appreciable effect on nucleation of crystals in the glass as will be shown in section V(1).

### IV.3.b. Intermediate temperatures (1000°C-1300°C)

In this temperature range crystal growth was sufficiently rapid for extensive crystallization to occur in less than 2 hours.

The microstructures of samples of glass A after heating at 1020°C for 0, 10, 20, 50 and 120 minutes are shown in Figs. 15(a)-(c). No crystallization was evident in the optical microscope when glass A was simply heated to 1020°C and cooled, Fig. 15(a). After 10 minutes at 1020°C internally nucleated crystals formed in the glass, Fig. 15(b). (Later results show these are in fact groups of crystals.) Longer heat treatments produced further growth of the groups of crystals as seen in Fig. 15(c) and (d). By counting the number of groups per unit area in several optical micrographs from sections of the same thickness it was found that the number of groups of crystals remained approximately constant throughout heat treatments ($\approx 1 \times 10^7/cm^3$). This suggests that crystal nucleation was not occurring at the heat treatment temperatures and that the groups of crystals had grown from nuclei established in the glass prior to reaching 1020°C. After 50 minutes the groups of crystals had started to impinge on each other. At this stage porosity started to form throughout the sample. After two hours x-ray diffraction indicated that the crystallization reaction was complete and the groups of crystals had extended throughout the microstructure, Fig. 15(e). Coarse porosity was found to be formed uniformly in the interior of the sample after this heat treatment.

A reflected light micrograph of the porosity in the sample heated for two hours at 1020°C is shown in Fig. 16. The pores are irregular in shape and up to 50 μm across. The sample was found, by a point counting method, to contain about 10% porosity on completion of crystallization. Bulk densities of a sample of glass A before and after crystallization were accurately measured using a sink float

technique (see appendix I) to determine the volume change occurring in the glass on crystallization. In the as quenched condition glass A had a density of 2.663 grams/cc. After completion of crystallization at 1020°C the bulk density of the sample was measured as 2.809 grams/cc indicating that on the order of 5% shrinkage of the sample occurred on crystallization.

A more detailed view of the crystal morphology developed in glass A on crystallization at 1020°C is shown in the polarized light micrograph in Fig. 17. The cross like contrast evident in several regions of the micrograph is characteristic of a so called spherulitic crystal morphology in which fibrous crystals grow radially from a central nucleation site.[26] The x-ray diffraction results of section IV.1 show that the spherulites are made up of clinoenstatite crystals. The effect of varying the crystallization temperature from 1000°C to 1100°C on the spherulites is shown in Fig. 18. The contrast seen in each micrograph is similar but the cross like spherulite contract is less apparent in the micrographs from the samples crystallized at higher temperatures. It is difficult to measure the size of the growth units developed in each microstructure as their outlines are indistinct. Qualitatively, however, the impression obtained from the micrographs in Fig. 18 is that the scale of the microstructures does not vary greatly with growth temperature. This implies that similar nucleation densities are developed during each heat treatment. Again the suggestion is that new nuclei are not formed at growth temperatures.

Crystallization during heat treatments at temperatures other than 1020°C were also found to produce porosity in the samples. The pore morphologies developed were the same as after the crystallization

at 1020°C. No variation in the size of the pores with crystallization temperature was observed. Measurement of the density of crystallized samples showed that, consistently, 4-5% shrinkage had occurred in all the samples by the time the crystallization reaction was complete.

Due to rapid crystal growth at higher temperatures samples of glass A could not be heated to temperatures greater than 1100°C without appreciable crystallization occurring during heating. Isothermal heat treatments could therefore not be carried out at higher temperatures. Heat treatments were however conducted at temperatures greater than 1100°C to see if any additional reactions occurred at these temperatures subsequent to the crystallization of spherulites from the glass. No further changes in microstructure could be detected even after prolonged heat treatments at temperatures up to 1300°C. From this it was concluded that the only reaction occurring in the temperature range 1000°C-1300°C was the growth of spherulites of enstatite crystals from the glass.

The structure of spherulites, along with the effect of intermediate temperature heat treatments on the phase separated microstructure of glass A, was investigated in more detail using TEM. The appearance of one of the $SiO_2$ rich droplets present in the as-cooled glass is shown in Fig. 19 after a heat treatment of 2 hours at 1020°C. The center of the droplet has been etched away during ion beam milling, but remnants of the droplet are still visible around the hole left in the foil. These appear in uniform grey contrast in the dark field image in Fig. 19 suggesting that the droplet is still glassy. The invariance of contrast in these regions and their diffuse SAD pattern confirmed this conclusion. Comparison of the shape of the droplet in

Fig. 18 with the shape of $SiO_2$ rich droplets seen in the as cooled glass (Fig. 3) shows that they remain unchanged after the intermediate temperature heat treatment. Examination of the microstructures of glass A after heat treatment at other temperatures in the temperature range 1000°C-1300°C revealed similar behavior. In contrast the MgO rich phase surrounding the droplet in Fig. 18 has crystallized indicating that the spherulites grow from this phase.

The microstructure developed in the MgO rich phase after an intermediate temperature heat treatment is shown in more detail in Fig. 20. Three distinct crystal morphologies are apparent: (1) fan like arrangements of lath shaped grains, (2) groups of well aligned elongated grains and (3) regions in which the outline of individual grains are indistinct. More detailed views of these morphologies and their corresponding electron diffraction patterns are shown in Figs. 21(a)-(c). Analysis shows that each diffraction pattern is made up of several superimposed single crystal enstatite diffraction patterns. In Fig. 21(a) lath shaped enstatite grains several microns long and about 0.1 μm across are seen. Each lath contains a high density of faults which run parallel to their long axis. The faults, which produce streaking in the corresponding diffraction pattern, (Fig. 21(b) suggest that the grains have a highly twinned clinoenstatite structure[27] in agreement with x-ray diffraction evidence. Indexing of the SAD patterns in Figs. 21(b),(d),(f) on the basis of the clinoenstatite structure shows that the three morphologies evident in the microstructure are simply sections through the same microstructure only viewed along different axes of the clinoenstatite unit cell.

Reconstruction of the microstructure from these sections shows that it consists of groups of elongated plate shaped and highly twinned clinoenstatite grains. Branching occurs from the flat surfaces of the plates such that adjacent plates are rotated with respect to each other by small angles. In Fig. 21(a) rotation between plates is about an axis perpendicular to the foil and results in an electron diffraction pattern, Fig. 21(b), consisting of several superimposed but rotated (010) clinoenstatite diffraction patterns. In this orientation the plates are seen edge on. The second orientation, Fig. 21(c),(d), lies perpendicular to that seen in Fig. 21(a).(b) so that the axis of rotation is in the plane of the foil. The plates are seen end on and grains are in a (001) orientation. In the third orientation Figs. 21(e),(f) the electron beam is parallel to the [100] clinoenstatite unit cell direction and the flat faces of the plates are seen. The superimposed diffraction patterns in Figs. 21(d),(e) are well aligned indicating that rotation between plates is predominantly about the [010] direction of the clinoenstatite unit cell. The cumulative rotation between plates results in fan-like arrangements of plates; a clear example of this morphology is shown in Fig. 22. It is these fan-like arrangmeents clinoenstatite plates that produces the distinctive "spherulitic contrast" seen in optical micrographs (for example Fig. 17).

In addition to the fibrous growth of crystals, theories of spherulitic growth suggest that individual fibers making up a spherulite will be separated by films of uncrystallized glass.[28] To see if such a glassy film existed between enstatite plates in the present microstructure dark field imaging of diffuse scattering from the

microstructure was used (see appendix II for details of this technique). It was noted that after moderate exposure to the electron beam radiation damage in the enstatite grains occurred transforming them to an amorphous structure, starting at the grain boundaries. Because of this considerable caution had to be exercised to ensure that radiation damage did not lead to an erroneous result. This was done by first setting up imaging conditions on an adjacent area and only moving to the area of interest to expose the micrograph.

A typical dark field image of an area of one of the spherulites is shown in Fig. 23. Light contrast is seen at the boundaries between most of the grains confirming the presence of films of glass between the enstatite plates. The amount of glass varied widely from boundary to boundary and in some areas the glassy phase appears to have formed pockets. The complexity of the microstructure prevents accurate assessment of the thickness of glassy films between plates but from micrographs they are estimated to be in the range 150-20Å. Attempts to analyze the composition of the residual glass in the microstructure were unsuccessful but later results suggest that it is enriched in nitrogen.

IV.3.c. High temperatures (above 1300°C)

Due to rapid crystallization of the MgO rich phase in glass A at intermediate temperatures, isothermal heat treatments at temperatures above 1300°C were not possible. It was found by x-ray diffraction that crystallization of enstatite from the MgO rich phase was complete by the time holding temperatures for high temperature

heat treatments were reached. The microstructure developed on heating was similar to that formed by isothermal heat treatments at intermediate temperatures. Fan like arrangements of enstatite grains crystallized from the MgO rich phase and porosity again formed in the sample. Density measurements indicated that shrinkage also accompanied crystallization of samples. However, unlike after holding at intermediate temperatures further changes in microstructure were observed when samples were held at temperatures above 1300°C. The microstructural changes were only apparent when thinned foils from heat treated samples were examined in the TEM.

Using the diffuse dark field imaging technique, described in detail in appendix II, isolated areas containing large amounts of residual glass were found in the microstructure. An example of one of these pockets, is shown in Fig. 24(a), from a sample of glass A heated for two hours at 1350°C. EDS spectra from the glassy regions showed that they contained only Si, suggesting they consist largely of a $SiO_2$ rich glass (see Fig. 24(b)). The distribution of the glassy pockets in the microstructure and their composition indicated that they were remnants of $SiO_2$ rich droplets formed in the as cooled glass by phase separation.

It is apparent from Fig. 24(a) that the globular shape of the $SiO_2$ rich droplets is completely lost after the high temperature heat treatment (compare with the shape of the $SiO_2$ rich droplets after intermediate temperature heat treatments, Fig. 19). The $SiO_2$ rich glass however still remains as isolated pockets in the microstructure. Apparently though the glass has softened

sufficiently for it to start to penetrate into the surrounding crystalline microstructure developed in the MgO rich phase on heating. In addition to the glass, faceted grains, which are clearly seen in dark contrast in Fig. 24, formed in these regions of the microstructure. The electron diffraction pattern shown in Fig. 24(c) identifies the faceted grains as crystals of enstatite. As the $SiO_2$ rich phase contains virtually no magnesium it is unlikely that the crystals have grown directly from this glass. It is more probable that they have developed as a result of the spherulitic microstructure surrounding the $SiO_2$ rich droplets recrystallizing to a more equilibrium microstructure.

Recrystallization was found to be limited to the regions near the $SiO_2$ rich glassy pockets even after longer heat treatments than 2 hours. In the regions away from the glassy pockets the microstructure in the crystallized MgO rich phase consisted of plate shaped enstatite grains as found after intermediate temperature heat treatments. However, unlike the microstructure after intermediate temperature heat treatments a large number of smaller crystals were observed between the enstatite plates after holding at a temperature of 1350°C for 2 hours. These are seen in Figs. 25(a),(d) with the enstatite plates in (010) and (001) orientations respectively. The corresponding electron diffraction patterns, Figs. 25(c),(f) contain extra reflections as indicated by the arrows (compare with Figs. 21(b), (d)). Dark field images taken using these reflections confirmed that they come from the crystals between enstatite plates, Figs. 25(b),(e). Using reflections from the enstatite crystals to

determine the microscope camera constant, d spacings for the extra reflections were accurately determined. The experimental d spacings were found to agree with those of $Si_2N_2O$. The extra reflections in the diffraction patterns shown in Figs. 25(c),(f) are indexed on the basis of the orthorhombic $Si_2N_2O$ unit cell found by x-ray diffraction studies.[29] In the (010) enstatite orientaion diffraction pattern, Fig. 25(c), $Si_2N_2O$ reflections are consistent with an orientation relationship of (002) $Si_2N_2O \| (400)$ clinoenstatite and (200) $Si_2N_2O \|$ (020) clinoenstatite. In the (001) orientation diffraction pattern Fig. 25(f) $Si_2N_2O$ reflections are consistent with a second orientation relationship of (002) $Si_2N_2O \| (400)$ clinoenstatite and (110) $Si_2N_2O \|$ (020) clinoenstatite.

This discrepancy is reconciled when the morphology of $Si_2N_2O$ crystals in a third orientation mutually perpendicular to the two previous orientations is examined, Fig. 26(a),(b). In this foil orientation the $Si_2N_2O$ crystals are seen as elongated grains aligned so that their long axis lies along one of three directions in the microstructure, Fig. 26(a). The three morphologies can only be accounted for if both orientation relationships described above occur and the $Si_2N_2O$ crystals grow so that they are bounded by facets which are (200) $Si_2N_2O$ planes.

The way in which the different morphologies arise can be described as follows: For the first orientation relationship the (200) $Si_2N_2O$ planes lie parallel to the (020) clinoenstatite planes. When bounded by (200) facets, $Si_2N_2O$ crystals with their long axis aligned with the [001] clinoenstatite direction form, as shown

schematically in Fig. 27(a). In the second orientation relationship either the (110) or (0$\bar{1}$0) $Si_2N_2O$ planes are matched up with the (020) clinoenstatite planes. Faceting of the $Si_2N_2O$ crystals on their (200) planes produces two sets of elongated crystals, one lying +58° from the [001] clinoenstatite direction and one lying -58° from the [001] direction. The crystallography of these two morphologies is shown schematically in Figs. 27(b),(c). Measurement of the angles between the [001] clinoenstatite direction and the long axis of the $Si_2N_2O$ crystals in Fig. 26(a) indicates good agreement with this analysis.

To further confirm these observations a detailed analysis of the diffraction patterns in Fig. 25(c),(f) was made. Schematic plots of both diffraction patterns, in which reflections from $Si_2N_2O$ in both orientation relationships are included, are shown in Figs. 28(a),(b). It can be seen that enstatite reflections will obscure many of the reflections from $Si_2N_2O$ crystals in both orientation relationships. The analysis indicates that the only $Si_2N_2O$ reflections that should be visible are those observed in Figs. 25(c) and (f). The occurrence of both orientation relationships is therefore consistent with the features of the experimental diffraction patterns. The superimposition of diffraction spots from $Si_2N_2O$ and enstatite crystals is indicative of the close matching of atomic planes in the two crystals. This suggests that by adopting the orientation relationships described above $Si_2N_2O$ crystals can form a low energy interface with enstatite crystals enabling $Si_2N_2O$ crystals to nucleate heterogeneously on enstatite crystals during crystallization.

# V. CONTROL OF CRYSTALLIZATION

## V.1. The Effect of Nucleation and Growth Heat Treatments on Microstructure

In crystallizing glasses to produce glass ceramics it is normal practice to use two stage heat treatments. The glass after melting and cooling is first heat treated for 1-2 hours at a temperature where crystal nucleation can readily occur but crystal growh is slow. This enables a high density of nuclei to develop in the glass. The nuclei are then grown by heat treating the glass at a higher temperature to produce a fine grained crystalline material.

To investigate the possibility of refining the crystallized microstructure of the present glasses by a nucleation and growth process, samples of glass A were given two stage heat treatments. The temperature range 800°C - 1000°C was selected for nucleation treatments as crystal growth was known to be slow at these temperatures (see section IV.3). Any nuclei developed were then grown by heating samples for two hours at 1020°C.

The effect of varying the nucleation temperature from 795°C to 945°C on the bulk microstructure and porosity of the crystallized glass is shown in Figs. 29(b)-(f). For comparison the microstructure of glass A given no nucleation treatment but a growth treatment of two hours at 1020°C is shown in Fig. 29(a). It is clear that the microstructure developed on crystallization is strongly influenced by the nucleation treatments and that there is an optimum nucleation temperature at about 850°C which leads to the most fine grained microstructure. Coincident with refinement of the grain size there

is a reduction in the size of the pores formed in the microstructure during crystallization.

A plot of the bulk density of the crystallized glass against nucleation temperature is shown in Fig. 30. The final density of the crystallized glass is only marginally greater for the sample given the optimum nucleation treatment. From this it is apparent that nucleation treatments have little effect on the amount of shrinkage that occurs on crystallization. It follows that although the size of pores are decreased by the optimum treatment their volume fraction remains essentially constant.

In an attempt to further refine the microstructures, samples of glass A were given longer nucleation treatments at the optimum nucleation temperature (850°C). Figure 31 shows a comparison between the microstructure of glass A after nucleation treatments of 2 hours and 4 hours at 850°C each followed by growth treatments at 1020°C. No further refinement of the microstructure is apparent after the longer nucleation treatment indicating that changes in the glass responsible for the enhanced nucleation are complete after two hours at 850°C.

A sample of glass A given a two hour nucleation treatment at 850°C and no growth treatment was examined using TEM. The sample was scrutinized for changes in the microstructure of the glass that could account for the enhanced nucleation effected by the heat treatment. No change in the microstructure of the glass could be detected. The appearance of the phase separation was the same as in the as cooled glass. Crystalline particles of silicon were again

found in the glass but it was not possible to tell if the number of particles had been increased by the nucleation treatments. No other crystalline particles were observed.

## V.2. The Effect of Composition Variations on Crystallization

In addition to the detailed study of glass A a brief study of crystallization in glasses of other compositions was made in an effort to study the way microstructural development was affected by variations in composition of the glasses. The study was necessarily limited to a few compositions because of the limited extent of the glass forming region in the Mg-Si-O-N system. Only glasses B, C and E were available in large enough samples that were reasonably bubble free for crystallization studies. Crystallization in the three glasses was found to be similar to that observed in glass A. Crystal growth was slow at temperatures below about 1000°C. Rapid crystallization of the MgO rich phase to enstatite in each glass occurred on heat treatment at temperatures greater than 1000°C, again producing a spherulitic type microstructure. The main difference in crystallization was in the nucleation of spherulites.

Optical micrographs of the microstructures developed in glasses A, B, C and E after a heat treatment of 2 hours at 1020°C are shown in Figs. 32(a)-(d) for comparison. The most striking feature of the microstructures is the large variation in the size of the spherulites that have grown from the glasses. As each spherulite grows from a single nucleation site the variation reflects differences in the nucleation densities in the glasses. Nucleation is

least efficient in glass E which has the composition poorest in $SiO_2$. Glasses B and C which have the compositions richest in $SiO_2$ also have the finest microstructures indicating more efficient nucleation in these glasses. The results suggest that nucleation efficiency increases with $SiO_2$ content of the glasses.

# VI. DISCUSSION

## VI.1. Glass Formation

An important observation of the present investigation regarding glass formation is that the melt containing no $Si_3N_4$ readily crystallized on cooling. In fact in the $MgO$-$SiO_2$ system it has been found that melts containing MgO crystallize even when rapidly quenched.[18] When additions of $Si_3N_4$ were included in the melts, glasses could be formed from melts even using moderate cooling rates. This clearly indicates that in the glasses investigated nitrogen plays an essential part in promoting glass formation.

Several authors have discussed factors which enable glasses to be formed on cooling liquids.[30-33] Generally it is felt that molecular rearrangements in the liquid must be slow so as to prevent crystallization on cooling. For oxides this requirement has led to the formulation of structural criteria which can be used to assess the glass forming ability of oxide melts.[30-32] Firstly it has been suggested that the glass structure should contain a high percentage of cations in tetrahedral or triangular coordination. The structural units should then be able to link up with each other, by sharing corners, to form long chains or extensive three dimensional networks. At least two corners of each polyhedron must be shared in order for structural units to link up in this way. When polyhedra in the glass melts form such a highly connected network, molecular rearrangements can not readily occur during cooling and so glass formation is favored.

In silica, $SiO_4$ tetrahedra join at their corners to produce an infinite three dimensional network structure. It is this structure that is responsible for the good glass forming properties of silica melts. However, if a so called network modifier is added to $SiO_2$ the three dimensional network tends to be broken up and the glass forming ability of the melt is reduced. MgO in acting as a network modifier is responsible for the ease with which MgO-$SiO_2$ melts crystallize on cooling.[34] The tendency for glass formation from MgO-$SiO_2$ melts to improve when $Si_3N_4$ is added, suggests that $Si_3N_4$ to some extend restors the network structure of melts in this system. This is consistent with the proposal of Jack[6] that silicon in oxynitride glasses as well as forming $SiO_4$ tetrahedra can coordinate with four nitrogen atoms as in the crystal structure of $Si_3N_4$,[35] to form $SiN_4$ tetrahedra in the glass network. Nitrogen can then, by bonding to three silicon atoms, link together a greater number of tetrahedral units than oxygen and so considerably enhance network formation in the glasses. Experimental evidence to support this proposal has been reported by Loehman,[7] who found that trends in the properties of Y-Si-Al-O-N glasses are consistent with Si-N bonding producing a more highly crosslinked glass structure as the nitrogen content of the glasses is increased. These observations suggest that glass formation in the present system is enchanced by the formation of a glass network structure in part bonded by Si-N bonds.

Sun has proposed[32] that as well as being able to form a network structure, a glass former must produce a network structure that is strongly bonded for glass formation to be possible. In an attempt to put the glass forming ability of various oxides on a more quantitative

basis he calculated the bond strengths for various metal oxygen bonds by dividing the heat of dissociation of the oxide by the coordination number for a metal atom in the oxides crystal structure.[36] From the calculated bond strengths he suggested that good glass formers produce a network structure linked by metal oxygen bonds with bond strengths greater than about 80 Kcal/bond . To assess the potency of $Si_3N_4$ as a glass former a similar calculation of the Si-N bond strength can be made as follows: Experimentally the enthalpy change for the reaction

$$\frac{1}{3} Si_3N_4(s) \rightarrow Si(s) + \frac{2}{3} N_2(g)$$

has been found to be on the order of 69 Kcal [37,38] Using standard values[39] for the enthalpy of dissociation of solid silicon to a gas ( 106 Kcal/bond) and dissociation of the $N_2$ molecule (112.5 K cal/atom) the heat of dissociation of $Si_3N_4$ is found to be 325 K cals for the reaction

$$\frac{1}{3} Si_3N_4(s) \rightarrow Si(g) + \frac{4}{3} N(g)$$

Taking a coordination number of four, for silicon in $Si_3N_4$, the bond strength of a Si-N bond is calculated to be 81 K cals. The strength of the Si-N bond therefore meets Sun's criteria for a glass former, but is considerably weaker than the Si-O bond which has a bond strength of 106 K cals/bond. This suggests that $Si_3N_4$ can act as a moderately good glass former in oxynitride glasses.

## VI.2. Conditions for the Formation of Bubble Free Oxynitride Glasses

Although the addition of $Si_3N_4$ allows $MgO-SiO_2$ glasses to be formed on cooling melts, decomposition of the melts severely limits the range of compositions over which bubble free glasses can be prepared, Fig. 1. In view of the importance of decomposition reactions in glass preparation in this and other oxynitride systems possible factors contributing to bubbling are examined in this section. The analysis presented is intended to give some insight into factors that are likely to be important in the preparation of oxynitride glasses. A rigorous analysis is not possible at the present time, since the thermodynamic properties of glass melts and the diffusivities of gases in the melts are not known. However, by making simplifying assumptions about the nature of the melts it is demonstrated that the furnace atmosphere used in melting can exert a strong influence on decomposition and bubbling in the melts.

The first thing to note is that for bubbles to form in a liquid the total vapor pressure of gases in equilibrium with the liquid must exceed the ambient pressure. This is necessary in order that surface tension forces tending to shrink the bubbles can be overcome and bubbles can nucleate and grow. The vapor pressure necessary for bubble formation depends on factors such as the surface tension of the liquid bubble interface and the availability of "easy" sites for heterogeneous bubble nucleation, as well as the ambient pressure. For the purposes of this discussion the critical vapor pressure for bubble formation is simply taken as any pressure greater than the total atmospheric pressure in the furnace. (1 atmosphere in the present experiments).

The next step is to consider what reactions in the melt are capable of producing such a pressure of gas. The maximum pressure of gas that a reaction can generate at a particular temperature can be calculated from the standard free energy change ($\Delta G°$) for the reaction provided the activities of reacting species are known.[40] The problem then is to identify which reactions are occurring and what the activities of reactants are. In the present calculations, reactions involving only $SiO_2$ and $Si_3N_4$ as constituents of the melt are considered and it is assumed that melts behave ideally so that activities of constituents of the melt are equal to their concentrations. For illustration calculations are performed for a melt of composition A (see table I). The activities of $SiO_2$ and $Si_3N_4$ are then 0.53 and 0.035 respectively, assuming ideal behavior. Melting experiments in this study were all carried out in nitrogen at one atmosphere pressure and so this pressure of nitrogen is used for calculations. Undoubtedly low partial pressures of oxygen were also present in the furnace atmosphere therefore oxygen is also considered as a reactant. Thermodynamic analysis of $SiO_2$-$Si_3N_4$ mixtures, at low partial pressures of oxygen has shown[41] that, at typical temperatures used in the present melting experiments (1500°C - 1900°C), SiO and $N_2$ will be the main vapor species formed by reactions. Reactions producing these gases are therefore considered in the analysis.

The first reaction to be considered is the thermal dissociation of $Si_3N_4$, which can be written as

$$Si_3N_4(\ell) \rightarrow Si(\ell) + 2N_2(g) \qquad (1)$$

$\Delta G^\circ$ for this reaction is unknown but $\Delta G^\circ$ for the dissociation of solid $Si_3N_4$ has been found experimentally to be:[37]

$$209000 - 96.8T \text{ cal/mole}$$

If this value is taken as $\Delta G^\circ$ for reaction (1) the pressure of nitrogen generated by the thermal dissociation of $Si_3N_4$ can be calculated for various activities of silicon in the melt. Using standard notation,[40] the equilibrium constant (k) for the reaction (1) is

$$k = \frac{P_{N_2}^2 \, a_{Si}^3}{a_{Si_3N_4}} = \exp\left(\frac{-\Delta G_1^\circ}{RT}\right) \qquad (2)$$

Hence the pressure of nitrogen that can be produced by reaction (1) is given by

$$P_{N_2} = \left(\frac{a_{Si_3N_4}}{a_{Si}^3}\right)^{\frac{1}{2}} \exp\left(\frac{-\Delta G_1^\circ}{2RT}\right) \qquad (3)$$

Taking the activity of $Si_3N_4$ as 0.035 the natural logarithm of the pressure of nitrogen in equation (3) is plotted against $\frac{1}{T}$, for different activities of silicon in the melt, Fig. 33. The graph indicates that the dissociation of $Si_3N_4$ can produce pressures of

nitrogen greater than one atmosphere even at moderate temperatures if the activity of silicon in the melt is low.

The amount of free silicon in the $SiO_2$ and MgO powders used to prepare glasses was negligible. However $Si_3N_4$ powders prepared by nitriding pure silicon frequently contain residual silicon, but as the present powder was prepared chemically it is thought that the concentration of silicon impurities were small in this powder too. This suggests that concentrations of silicon in the melts were initially low and that the generation of nitrogen bubbles by reaction (1) may have been contributing to decomposition of the melts (forming free Si). Evidence for the occurrence of this reaction is found in the observation made in section III.2 that certain glass melts contained particles of crystalline silicon on cooling. These may have arisen due to a concentration of silicon being built up by reaction (1) during melting. It can be seen from Fig. 33 though that once a sufficient activity of silicon in the melt is built up the equilibrium pressure of nitrogen will fall below one atmosphere and bubbling caused by reaction (1) will no longer be possible. The activity of silicon necessary for reaction (1) to be in equilibrium with a given pressure of nitrogen can be calculated by rearranging equation (3) to give

$$a_{Si} = \left( \frac{a_{Si_3N_4}}{p^2_{N_2}} \right)^{\frac{1}{3}} \exp \frac{-\Delta G^\circ_1}{3RT} \qquad (4)$$

Substituting for $\Delta G_1^\circ$ and using values of $a_{Si_3N_4} = 0.035$ and $P_{N_2} = 1$ the equilibrium activity of silicon can be calculated at different temperatures. Values in the temperature range 1400 - 1900°C are given in table III.

Silicon formed by the dissociation of $Si_3N_4$ may also react with oxygen in the furnace according to the reaction

$$Si(\ell) + O_2(g) \rightarrow SiO_2(\ell) \qquad (5)$$

$$G_5^\circ = -224665 + 47.8T \text{ cals}^{39}$$

This reaction may prevent the build up of sufficient activities of silicon in the melt for reaction (1) to reach equilibrium with nitrogen at 1 atmosphere and so enable frothing to continue. For a given activity of silicon and partial pressure of oxygen reaction (2) may occur when the partial pressure of oxygen is greater than

$$P_{O_2} > \frac{a_{Si}}{a_{SiO_2}} \exp \frac{\Delta G_5^\circ}{RT}$$

Substituting for the activity of silicon from equation (4) an expression for the partial pressure of oxygen which will allow reaction (1) to reach equilibrium with a given pressure of nitrogen is obtained.

$$P_{O_2} = \left(\frac{a_{Si_3N_4}}{P_{N_2}^2}\right)^{\frac{1}{3}} \frac{\exp\left(\frac{-\Delta G_1^\circ}{3RT}\right)\exp\frac{\Delta G_5^\circ}{RT}}{a_{SiO_2}} \qquad (7)$$

For a partial pressure of oxygen greater than this value frothing may occur by a reaction that is the sum of reactions (1) and (5):

$$Si_3N_4(\ell) + 3O_2(g) \rightarrow 3SiO_2(\ell) + 2N_2(g) \qquad (8)$$

i.e., the oxidation of $Si_3N_4$. Substituting for values of $G_1^\circ$, $G_5^\circ$ and using $a_{Si_3N_4} = 0.035$, $a_{SiO_2} = 0.53$ and $P_{N_2} = 1$ at the partial pressure of oxygen for equilibrium of reaction (8) can be calculated from equation (7); values at different temperatures are given in table III.

If partial pressures of oxygen greater than these values are present in the furnace, frothing may be favorable by reaction (8). (The ambient pressure is assumed to be one atmosphere.) When a continuous supply of oxygen is available at a fixed partial pressure above the equilibrium value the reaction may occur indefinitely consuming $Si_3N_4$. For example oxygen could be supplied by the dissociation of other oxides in the melt. The stability of oxide additions to the melt will therefore be important in determining the amount of frothing that occurs by reaction (8). If a continuous supply of oxygen is not available bubbling may be energetically favorable until the partial pressure of oxygen in the furnace is reduced to its

equilibrium value, by reaction (8) consuming oxygen. From examination of table III it is apparent that lower partial pressures of oxygen are required to maintain equilibrium at lower temperatures. Preventing frothing by the oxidation of $Si_3N_4$ (reaction (8)) is therefore likely to be more difficult at lower temperatures. It should also be noted that for partial pressures of oxygen lower than the values given in table III the reverse reaction will become favorable leading to an increase the partial pressure of oxygen in the furnace to its equilibrium value. Reaction (8) therefore serves to fix the partial pressure of oxygen in the furnace if no other supply of oxygen is available.

A further reaction that may affect activities of silicon in the melt is that of the oxidation of silicon by the reaction

$$2Si(\ell) + O_2(g) \rightarrow 2SiO(g) \qquad (9)$$

$$\Delta G^\circ_q = - 77.140 - 22.78T \text{ cals}^{39}$$

This reaction is clearly more complex as equilibrium depends on the partial pressure of SiO gas available as well as the partial pressure of oxygen. Taking the partial pressure of oxygen to be fixed by reaction (8) and the activity of silicon to be determined by reaction (1), the partial pressure of SiO that must be maintained above the melt for reaction (9) to be in equilibrium at a given pressure of nitrogen can be calculated. The net reaction that must be considered in this case is a combination of reactions (1), (5) and (9), that is

$$Si_3N_4(\ell) + 3SiO_2(\ell) \rightarrow 6SiO(g) + 2N_2(g) \qquad (10)$$

From the equilibrium constant for this reaction it is found that

$$P_{SiO} = \left(\frac{a_{Si_3N_4}}{P_{N_2}^2}\right)^{\frac{1}{6}} \left(a_{SiO_2}\right)^{\frac{1}{2}} \exp\left(\frac{-\Delta G^\circ_{10}}{6RT}\right) \qquad (11)$$

where $$\Delta G^\circ_{10} = \Delta G^\circ_1 - 3\Delta G^\circ_5 + 3\Delta G^\circ_9$$

$$\Delta G^\circ_{10} = 651575 - 308.54T \text{ cals}$$

Substituting for $\Delta G^\circ_{10}$ and again using values of $a_{Si_3N_4} = 0.035$, $a_{SiO_2} = 0.53$ and $P_{N_2} = 1$ at, the equilibrium partial pressure of SiO gas can be calculated from equation (11); values at several temperatures are given in table III.

If the partial pressure of SiO maintained in the melt is below the values given in table III, reaction (9) becomes favorable and may occur reducing the activity of silicon in the melt. This will in turn allow reaction (1) to occur producing nitrogen at pressures greater than one atmosphere. Thus frothing may again occur, the net reaction being that of reaction (10). Since SiO gas may condense on parts of the furnace cooler than about 1200°C[42] it is probable that it will be difficult to maintain the larger partial pressures of SiO necessary for equilibrium at higher temperatures. Therefore at high temperatures frothing may result from reaction (10). The temperature at which

this reaction will become important will depend on kinetic factors such as the rates of diffusion of SiO through the melt and the rate at which SiO can be removed from the melt surface. Examination of equation (11) shows that the equilibrium partial pressure of SiO is also dependent on the activities of $SiO_2$ and $Si_3N_4$ in the melt. Increasing these activities tends to increase the partial pressure of SiO necessary for equilibrium and so other things being equal frothing will be more likely in melts with higher $SiO_2$ and $Si_3N_4$ activities. Qualitatively this is in agreement with the behavior observed for melts in the present investigation.

To summarize, equilibrium thermodynamics suggests that several reactions may contribute to frothing in oxynitride melts. Initially frothing can occur by the dissociation of $Si_3N_4$ (reaction (1)). The amount of frothing that occurs by this reaction will be greater at higher temperatures. The dissociation of $Si_3N_4$ will produce a build up of silicon in the melt until an activity in equilibrium with the nitrogen above the melt is reached. At lower temperatures the build up of silicon may be prevented by oxidation of silicon to $SiO_2$ (reaction (5)) unless the partial pressure of oxygen in the furnace is very low. Towards higher temperature the oxidation of silicon to SiO gas may prevent the build up of silicon in the melt and so result in frothing.

The main limitation of the present analysis is that it neglects kinetic factors which are undoubtedly important to bubble formation. The rate at which the gases diffuse through the melt will affect the reaction rates and hence the partial pressures of gaseous species

that can build up in the melts. The rate at which bubbles can nucleate and grow may also be an important factor. In general through the analysis suggests that melting should be carried out at as low a temperature as possible and at low partial pressures of oxygen. Also maintaining a high partial pressure of SiO above the melt should help reduce frothing. Experiments in which these factors are controlled should be carried out to assess their importance in producing bubble free oxynitride glasses. From such experiments it may be possible to find optimum conditions for melting of the glasses. This will then allow more extensive regions of glass formation to be investigated in the Mg-Si-O-N and other systems. As far as the present melting experiments are concerned the analysis explains why bubbling is observed initially in some melts but dies down with longer melting times. The analysis also successfully predicts that frothing will tend to be increased in glass compositions that are richer in either $SiO_2$ or $Si_3N_4$.

## VI.3. Phase Separation

The phenomenon of phase separation in glasses has been found to be quite common[43-46], and its origin has been discussed in detail elsewhere[47-49]. In the $MgO-SiO_2$ system a stable miscibility gap is known to exiat at $SiO_2$ rich compositions.[18] At a temperature of 1695°C $MgO-SiO_2$ melts in the composition range 2 wt% MgO to 31 wt% MgO separate into two liquids of these extreme compositions and the stable miscibility gap has its maximum extent. Below 1695°C crystallization can occur and the miscibility gap becomes metastable. As crystallization cannot be suppressed in the MgO rich liquid formed on phase

separation, the shape of the metastable extension of the miscibility gap in the $MgO$-$SiO_2$ system has not been experimentally determined. The metastable portion of the miscibility gap can, however, be estimated by extrapolating the descending branches of the stable miscibility gap continuously to lower temperatures. Such extrapolation (Fig. 34) shows that the MgO rich phase will have a composition close to that of $MgSiO_3$ at a temperature of 850°C. This agrees quite well with the composition predicted for the MgO rich phase by extending the experimentally determined miscibility gap in Fig. 7 to the $MgO$-$SiO_2$ binary. From this it is concluded that phase separation in the oxynitride glasses investigated results from extension of the binary $MgO$-$SiO_2$ miscibility gap into the ternary $SiO_2$-$MgO$-$Si_3N_4$ system.

Investigation of phase separation in other ternary systems has shown that even small additions of a third component to a binary system that undergoes phase separation can have a pronounced effect on the extent of the miscibility gap[50]. For example, the extent of the miscibility gap in the $MgO$-$SiO_2$ system is greatly reduced when additions of $K_2O$ are included in melts, the miscibility gap being completely eliminated by an addition of only 4 wt% $K_2O$.[51] In contrast the addition of 10 wt% $Na_2O$ to $B_2O_3$-$SiO_2$ melts doubles the extent of the miscibility gap in the $B_2O_3$-$SiO_2$ system.[52] The large uncertainties involved in compositional analysis of phases in the present glasses make it difficult to draw firm conclusions about the effect of $Si_3N_4$ additions on the extent of the miscibility gap in the $MgO$-$SiO_2$ system. In particular the assumption made in construction of the miscibility boundary in Fig. 7, that glass compositions do not

change on melting, is not strictly valid as nitrogen is certainly lost from all the melts. However, as on melting glass compositions are shifted towards the $MgO$-$SiO_2$ binary, the miscibility gap is if anything more restricted than as shown in Fig. 7. This can be seen from the fact that points on the lines of constant Mg/Si ratio fixing the composition of the MgO rich phase in each glass move to more $SiO_2$ rich compositions as the nitrogen content of the glasses are reduced. This suggests that additions of $Si_3N_4$ tend to restrict the extent of the miscibility gap in the $SiO_2$-$MgO$-$Si_3N_4$ system. Further support for this conclusion is found in the observation that composition c shows no sign of forming two liquids on melting, even though a comparable composition on the $MgO$-$SiO_2$ binary (indicated in Fig. 34) undergoes stable phase separation on melting.

In all the glasses examined phase separation appears to have occurred on cooling from the melt. Under such conditions phase separation can occur by either a nucleation and growth or a spinodal decomposition mechanism[45,53]. During a nucleation and growth process the second liquid phase forms as isolated droplets within the initially homogeneous liquid. As phase separation proceeds the droplets grow and coarsen to produce a final microstructure that consists of discrete droplets of a minor phase dispersed in a continuous matrix phase of a different composition. Alternatively spinodal decomposition may occur when the melt is cooled into the central (spinodal) region of the miscibility gap where a homogeneous liquid becomes unstable. Phase separation can then occur by stationary composition waves developing in the liquid, the composition waves growing in amplitude

with time. Unlike a nucleation and growth process spinodal decomposition forms a microstructure that consists of two continuous and interpenetrating phases. The extent of the spinodal region in the $MgO-SiO_2$ miscibility gap is unknown, but has been found to be quite restricted in the similar $CaO-SiO_2$ system[19]. Therefore, as all the compositions investigated lie to one side of the miscibility gap, it is likely that phase separation in the present glasses occurred by a nucleation and growth mechanism. The fact that the $SiO_2$ rich phase in all the phase separated glasses formed as discrete droplets confirms this suggestion.

The origin of the unusually coarse microstructures observed in the more $SiO_2$ rich glasses (A, B and C) is not entirely clear. Slow cooling rates have been found to produce coarser phase separation in some glasses[54]. Slow cooling though cannot explain why, even though all the melts were cooled at about the same rate, coarse microstructures were observed in the more $SiO_2$ rich glasses A, B and C and not in glass E. Glasses A, B and C have compositions which lie further towards the center of the miscibility gap than glass E; thus phase separation in these glasses can start at higher temperatures than in glass E. At these higher temperatures the $SiO_2$ rich droplets can grow and coarsen more rapidly producing a coarser microstructure. Therefore it is possible that a combination of the moderate cooling rates used in the present melting experiments and high miscibility temperatures contributed to producing coarse phase separation in glasses A, B and C.

The flower-like morphology of the $SiO_2$ rich phase formed in glass A (Fig. 2) is also unusual. A similar morphology has been observed in Cu-Nb alloys cooled from the melt[55], in this case niobium "flowers" forming in a copper matrix. In an investigation of this behavior it was found that cooling rate had a pronounced effect on the morphology. Niobium spheres formed when melts were rapidly cooled while niobium flowers developed at slower cooling rates. However, it is not clear what causes this unusual microstructure to form.

## VI.4. Nucleation

Once a melt is cooled below its liquidus temperature nucleation of crystals becomes favorable. From the simple theory of homogeneous nucleation the steady state nucleation rate (I) is predicted to vary with temperature according to the relation

$$I = A \exp - \left( \frac{\Delta G^* + \Delta G_m}{KT} \right)$$

where A includes parameters such as the vibrational frequency and the number of molecules per unit volume; $\Delta G^*$ is the maximum free energy of activation for the formation of a nucleus; and $\Delta G_m$ is the activation energy for diffusion. (See references 56-59 for a review of of nucleation theory.) At temperatures just below the liquidus $\Delta G^*$ decreases rapidly with temperature and the nucleation rate increases as the degree of undercooling $\Delta T$ increases. At large

values of $\Delta T$ the term $\Delta G_m$ becomes important and the nucleation rate is limited by transport process. Kinetic factors then dominate and the nucleation rate decreases with further undercooling, the nucleation rate going through a maximum at some optimum nucleation temperature. (This can be represented by TTT or CCT diagrams.) For homogenous nucleation the important term is $\Delta G^*$ which for a spherical nucleus is given approximately by the expression (strain energy can be neglected in the present case as nucleation is occurring from a viscous liquid)

$$\Delta G^* = \frac{16\pi \gamma^3 T_o^2}{3(\Delta T)^2 H_V^2}$$

where $T_o$ is the liquidus temperature; $\Delta T$ is the undercooling $(T_o - T)$; $H_V$ is the enthalpy change per unit volume of nucleating phase; and $\gamma$ is the interfacial energy of the nucleus. Both $\Delta H_V$ and $\gamma$ depend on composition, but for small variations in the composition of the crystallizing phase the homogenous nucleation rate is not expected to vary greatly.

In considering nucleation and the effect of glass composition on nucleation in the present glasses, phase separation in the glasses must be taken into account. The microstructural studies in sections IV.3 and V.2 show that in each glass only the MgO rich phase crystallizes during heat treatments. Hence it is the composition of the MgO rich phase and not the average glass composition which influences homogenous nucleation. The composition of MgO rich and $SiO_2$ rich phases in each glass can be estimated from the experimentally

determined miscibility gap shown in Fig. 7. From examination of Fig. 7 it is apparent that in glasses A, B, C and E the MgO rich phase has approximately the same composition. Therefore it is felt that variations in the homogeneous nucleation rate caused by differences in the composition of the MgO rich phase are not responsible for the large variation in nucleation efficiency observed in these glasses.

The main effect of varying the average composition of the glasses is not to change the composition of the phases but to alter the volume fraction of the $SiO_2$ and MgO rich phases formed in each glass. The amount of each phase in a glass of given composition can be estimated by applying the lever rule to the miscibility gap in Fig. 7. Consistent with the microstructures observed in glasses A, B, C and E (Figs. 3 and 8) the lever rule predicts that the more $SiO_2$ rich glasses, B and C will have the largest volume fraction of $SiO_2$ rich phase, while glass E will have the smallest.

Harper et al. suggested[60,61] that variations in the amount of phase separation in a glass could indirectly influence homogenous nucleation from the glass. They proposed that phase separation could slow crystal growth and so permit more nuclei to become effective during crystallization. Thus enhanced nucleation should be expected in glasses with a larger volume fraction of second phase. This is consistent with the nucleation behavior observed in glasses A, B, C and E (see Fig. 32). However, this mechanism can only be operating if nucleation readily occurs at temperatures where crystal growth takes place. In glass A it was found that the number of clusters of

enstatite crystals per unit volume was approximately constant during crystallization and that the scale of the crystallized microstructures did not vary greatly with crystallization temperature. Both observations indicate that nucleation is not occurring at temperatures where crystal growth takes place in glass A. Therefore it is unlikely that phase separation enhances homogenous nucleation in the present glasses by slowing crystal growth. This suggests that in seeking an explanation for the nucleation behavior observed in the present glasses heterogenous nucleation must be considered.

In heterogenous nucleation interfaces between phases or local fluctuations in composition act to lower the barrier to forming nuclei $\Delta G^*$ below that required for homogenous nucleation. The heterogenous nucleation rate is then given by a similar expression to that for homogeneous nucleation

$$I_{het} = A \exp - \left( \frac{\Delta G^* f + \Delta G_m}{KT} \right)$$

where $f$ is a factor less than one. It has been suggested that in phase separated glasses the interface between phases may act as a heterogenous nucleation site.[62,63] This may happen if enstatite nuclei form so as to replace part of the interface of separated phases by a low energy glass/nucleus interface resulting in a net reduction in the surface energy contribution to $\Delta G^*$. However, as Ulhmann pointed out[64] this is not likely to be a strongly preferred site for nucleation because of the small values of interphase surface energy between two amorphous phases[65]. Because of this and the absence of

direct evidence for enstatite crystals nucleating at the interphase boundary it is thought that this nucleation site is not important in the present case.

Solid impurity particles have been found to cause internal nucleation in some glasses[66], and it is possible that the crystalline silicon and impurity rich particles observed in the present glasses act as heterogenous nucleation sites for enstatite crystals. Silicon particles were found in the glasses which showed high nucleation densities (A, B, and C), but not in glass E which crystallized with a very coarse microstructure. Circumstantial evidence, therefore, supports this suggestion. If in the as-quenched melts silicon exists as a supersaturated solution, further precipitation of silicon from the glasses may occur during subsequent nucleation treatments. The resulting increase in the number of silicon particles would then account for the effectiveness of nucleation treatments in refining the microstructures of crystallized glasses. As once all silicon had precipitated from the glass no new nucleation sites could develop, nucleation treatments would necessarily have only a limited effect on microstructure. This is again consistent with the results of nucleation experiments carried out in this investigation. In view of these observations it is felt that the heterogenous nucleation of enstatite crystals on silicon particles is the most likely mechanism for internal nucleation in the present glasses.

The origin of silicon particles in the glasses is not clear. It is possible that the silicon comes from dissociation of $Si_3N_4$ during melting as discussed in section VI.2. If this is the case, differences

in the decomposition behavior of melts may be responsible for the variation in the number of silicon particles found in the glasses. It is also possible that phase separation indirectly influences precipitation of silicon from the melts. Silicon is known to be highly immiscible with $SiO_2$,[67] and so the rejection of silicon from the $SiO_2$ rich phase as the glasses phase separate may concentrate silicon in the MgO rich phase. More silicon particles would then be expected to form in glasses which have a larger volume fraction of $SiO_2$ rich phase. Qualitatively this is in agreement with the present observations and also explains the enhanced nucleation observed in more $SiO_2$ rich glass compositions. However, further experimental work is needed to confirm these ideas.

## VI.5. Microstructural Development

### VI.5.a. Structure of spherulites

Interpretation of crystallization behavior in the present glasses is some what complicated by the fact that enstatite can undergo several phase transformations on cooling from high temperatures. Three polymorphs of enstatite have been identified but the conditions under which enstatite transforms from one structure to another are still controversial[68-71]. At temperatures above 1000°C the orthorhomgic form of enstatite, protoenstatite, is believed to be the stable form[68]. This temperature range also corresponds to the temperature range where crystallization occurred in the glasses investigated. X-ray diffraction, though indicated that on cooling to room temperature crystallized glasses consisted mainly of the monoclinic polymorph

of enstatite, clinoenstatite. While it is possible that clinoenstatite crystallizes metastably from the glasses, it has also been found that protoenstatite even on rapid cooling transforms to clinoenstatite by a displacive transformation[68,71]. As it is not normally possible to suppress this transformation the possibility that protoenstatite is the polymorph crystallizing from the glasses on heat treatment must also be considered. A further complicating factor is that clinoenstatite once formed can slowly transform to the third polymorph of enstatite, orthoenstatite. Evidence for this transformation is seen in the highly faulted appearance of enstatite grains in Fig. 20(a) which analysis has shown is caused by an intimate mixture of clino and orthoenstatite[72].

Because of the variety of transformations that can occur on cooling samples it is unlikely that the microstructures observed in this investigation at room temperature are representative of the "as crystallized" structure of enstatite grains. Fortunately a simple relationship exists between the crystal structures of the different polymorphs of enstatite, the main difference being in their stacking sequence in the a unit cell direction. Therefore the crystallographic analysis of enstatite plates made in section IV.3.a still serves to define the relationship between the shape of the plates and main crystallographic axes of the enstatite structure. Because of this it is also felt that the essential features of crystallized microstructures were preserved during cooling from heat treatment temperatures.

The observed microstructures show the main features of spherulitic growth i.e., fibrous crystal growth with repeated low angle branching of the fibers. Of the several theories advanced to explain the development of spherulitic microstructures,[28,73-75] the theory of Keith and Padden[28] is the only one that adequately accounts for the main features of this kind of microstructure. Their model requires that impurities in the glass be rejected at the crystal glass interface to form an impurity rich layer around growing crystals. Spherulitic growth may then be initiated as a result of the impurity rich layer producing an unstable growth front in a manner similar to constitutional supercooling.[76] This Keith and Padden suggest occurs when crystal growth rates are fast compared to the rate of diffusion of solute from the interface and if the rejected solute tends to slow down crystal growth. As a result of the instability a fibrous crystal morphology develops, a layer of uncrystallized melt enriched in the rejected solute separating fibers.

In the present glasses enstatite crystals grow from the MgO rich phase in each glass and at least at lower temperatures, the $SiO_2$ rich phase remains essentially inert during crystallization. In glass A the MgO rich phase has a composition that lies close to the $MgSiO_3$ - $Si_2N_2O$ tie line in the $SiO_2$-MgO-$Si_3N_4$ phase diagram as can be seen from Fig. 7. If it is assumed that the solubility of nitrogen in enstatite is small, as enstatite crystals grow from the MgO rich phase. $SiO_2$ and $Si_3N_4$ components of the glass will be rejected ahead of the growing crystals. Consequently a diffusion layer enriched in $SiO_2$ and $Si_3N_4$ may initially form around enstatite crystals. As discussed earlier, $SiO_2$ and $Si_3N_4$ are both believed to be glass network

formers and so an enrichment in the glass of these components is likely to slow crystal growth. Therefore, following Keith and Padden's model the formation of an "impurity layer" enriched in $SiO_2$ and $Si_3N_4$ around growing enstatite crystals may be responsible for the fibrous growth habit of enstatite crystals in the present glasses.

Microstructural evidence supports this view of crystallization. In agreement with predicted microstructures, Fig. 23, shows that a layer of uncrystallized glass separates the fibrous enstatite plates that make up the spherulitic microstructures. If all the MgO in the MgO rich phase of glass A combines with $SiO_2$ to form enstatite crystals it is expected that the residual glass separating enstatite plates will have a composition on the $Si_3N_4$-$SiO_2$ binary tie line. The exact point representing the composition of the residual glass will depend on the original composition of the MgO rich phase. The proximity of the composition of the MgO rich phase in glass A to the $MgSiO_3$-$Si_2N_2O$ tie line indicates that the residual glass (neglecting the $SiO_2$ rich phase) should have a composition close to that of $Si_2N_2O$. The observation that $Si_2N_2O$ crystals form between enstatite plates after high temperature heat treatments agrees very well with this prediction. This strongly suggests that the rejection of $SiO_2$ and $Si_3N_4$ ahead of growing enstatite crystals is responsible for the initiation of spherulitic growth in the present microstructures.

A second important feature of spherulitic crystallization is the tendency of the fibers (or in this case elongated plates of enstatite) to branch non-crystallographically. It is branching in this manner that produces the characteristic morphology of diverging arrangements of fibrous crystals. Keith and Padden suggested that

branching could arise from growth of misaligned nuclei that form on existing fibers,[28] but the reasons for the formation of such nuclei are not clear. In the present investigation a direct relationship between branching of the enstatite plates and the crystallography of the plates was observed. This suggests that branching in the present spherulites may be directly related to the structure of the growing crystals. Unfortunately identification of which form of enstatite is growing from the glasses at crystallization temperatures is complicated by the phase transformations that may occur on cooling samples to room temperature. Hence futher conclusions regarding the connection between the structure of plates and small angle branching in the spherulites cannot be drawn.

VI.5.b. Recrystallization

The recrystallization of spherulites to faceted crystals observed after high temperature heat treatments is similar to reactions found in spherulitic microstructures in other systems[77-79]. The transformation is believed to be promoted by instability of spherulites caused by their large interfacial area and disordered structure. A peculiarity of the reaction in the present microstructures is that recrystallization initiated only in regions close to the pockets of $SiO_2$ rich glass. This and the coincidence of the start of recrystallization with softening of the $SiO_2$ rich phase suggests that the $SiO_2$ rich phase plays an important part in the reaction.

A possible explanation for this behavior is that recrystallization is occurring by a mechanism of solution of enstatite plates

in the $SiO_2$ rich phase and reprecipitation of enstatite as faceted grains in the pockets of $SiO_2$ rich glass. This would mean that the $SiO_2$ rich glass is necessary to act as a rapid transport path for MgO and $SiO_2$ in the reaction. The reaction would therefore be expected to start when diffusion becomes rapid in the $SiO_2$ rich phase, i.e., when the glassy phase softens. The annealing point of fused $SiO_2$ lies in the temperature range 1020°C - 1200°C[80] (the exact annealing point depends on the impurity content of the glass). At first sight therefore it is surprising that recrystallization does not start at a temperature lower than 1300°C. However Elmer and Nordberg have shown[1] that the annealing point of fused $SiO_2$ is considerably raised by the presence of nitrogen in the glass. Thus, the small amounts of nitrogen detected in the $SiO_2$ rich phase of glass A may account for the high temperature needed to initiate recrystallization in this glass. It is also probable that nitrogen slows rates of diffusion in the glassy phase and so is in part responsible for the sluggishness of the reaction. Once the $SiO_2$ rich phase softens recrystallization can start. Recrystallization though is necessarily confined to localized regions in the microstructure as the $SiO_2$ rich phase remains in isolated pockets in the microstructure even after softening.

As a result of recrystallization, faceted grains of enstatite are formed in the pockets of $SiO_2$ rich glass. The x-ray diffraction evidence that protoenstatite as well as clinoenstatite crystals develop in partially recrystallized microstructures suggests that the faceted grains are protoenstatite crystals that remain untransformed on cooling. This is surprising in view of the displacive nature of the inversion of protoenstatite to clinoenstatite. However, work on

steatite ceramics has shown that the transformation of protoenstatite to clinoenstatite can be suppressed when crystals are smaller than about 7 μm[81]. In the recrystallized microstructures faceted grains were generally less than 1 μm across (see Fig. 24). Therefore the faceted grains may have been stabilized as protoenstatite by their small size.

VI.5.c. Porosity

A feature common to all the glass samples in which an appreciable amount of crystallization had occurred was the formation of coarse porosity throughout the samples. Density measurements indicated that crystallization was also accompanied by shrinkage of the samples. This suggests that volume changes on crystallization may be responsible for the formation of porosity.

As cooled glass A has a density of 2.663 grams/cc. Assuming that the $SiO_2$ rich phase in the as cooled glass has the density of fused silica (2.2 grams/cc) and estimating the weight fraction of this phase in glass A as 0.1 from the miscibility gap determined in section III.2 the density of the MgO rich phase in glass A is estimated to be about 2.73 grams/cc. On crystallization the MgO rich phase transforms almost completely to enstatite which has a density of 3.209 grams/cc. The MgO rich phase therefore decreases in volume by about 15% on crystallization. Allowing for the $SiO_2$ rich phase an overall volume decrease of about 13% should occur on crystallization of glass A if no pores are formed in the sample. Bulk densities of crystallized samples of glass A were found to be consistently on the order of 2.80 grams/cc indicating that only 4-5% shrinkage occurs.

The remaining 8% change in volume must then be accounted for by porosity in the samples. The experimentally determined volume fraction of porosity in fully crystallized samples (10% porosity) is in reasonble agreement with this calculated vlaue. Therefore volume changes on crystallization of the MgO rich phase are large enough to entirely account for both shrinkage and the formation of porosity in the samples of glass A.

Porosity formation in the samples is envisaged as occurring in the following way: Crystallization starts from isolated nucleation sites in the bulk of the glass. Spherulites of enstatite grow from these nucleation sites, but in the early stages of crystallization are completely surrounded by glass which can accommodate volume changes by viscous flow. Consequently crystallization initially occurs without forming pores and produces uniform shrinkage of the samples. At a later stage of crystallization the spherulites start to impinge on each other forming a rigid network of crystallized material enclosing regions of uncrystallized glass. Further shrinkage of the sample is then prevented by the restraining effect of the crystalline network. As a result when the remaining glass crystallizes pores nucleate to accommodate the accompanying volume decrease. As crystallization proceeds the pores grow, until finally coarse porosity is formed throughout the microstructure and crystallization is complete.

The final size of the pores formed will depend on the size of pockets of glass left in the microstructure at the stage where spherulites start to form a rigid network of crystals. This in turn depends on the number of active nucleation sites in the glass. The

higher the density of nuclei the smaller spherulites will be before they start to impinge, hence the smaller pockets of uncrystallized glass will be at this stage. Consequently increasing the number of nuclei in the glass is expected to decrease the size of pores as was indeed observed after nucleation and growth treatments. It is not clear though what effect further refinement of the microstructure would have on the formation of pores. It is possible that if sufficiently high crystal nucleation densities could be obtained in the glasses the nucleation of pores could be prevented. All the volume change on crystallization would then be accommodated by shrinkage of the samples. However, from the point of view of forming glass ceramics this is also undesirable. A more satisfactory way of eliminating the porosity would be to reduce the volume change accompanying crystallization. It may be possible to do this by making suitable additions (such as $Al_2O_3$) to the base Mg-Si-O-N glass compositions.

## VI.6. Formation of Glass Ceramics from Oxynitride Glasses

The glasses investigated show promise as starting materials for the formation of glass ceramics insofar as crystals nucleated internally from the glasses and two stage heat treatments were effective in refining the microstructures of crystallized samples. Nucleation treatments however had only a limited effect and further refinement of the microstructures would be needed to produce a useful material. The addition of a nucleating agent may be able to bring acout the necessary increase in nucleation efficiency in the glasses.

In other glasses both $TiO_2$ and $ZrO_2$ have been found to be effective nucleating agents[82]. Both these catalysts form stable nitrides and in oxynitride glasses may react with $Si_3N_4$ according to the reactions

$$3TiO_2 + Si_3N_4 \rightarrow 3TiN + 3SiO_2 + \frac{1}{2} N_2$$

and

$$3ZrO_2 + Si_3N_4 \rightarrow 3ZrN + 3SiO_2 + \frac{1}{2} N_2$$

As these reactions are likely to contribute to decomposition during melting of oxynitride glasses is is felt that $TiO_2$ and $ZrO_2$ are unlikely useful nucleating agents in these glasses. Other catalysts that have proved effective in developing fine grained glass ceramics are $P_2O_5$, noble metals such as Au or Pt and certain other oxides[81]. The effect of these nucleating agents on the crystallization behavior in Mg-Si-O-N glasses should be examined in future work.

An alternative route to that of the normal nucleation and growth process used to produce glass ceramics has recently been suggested.[78,79] In this technique a relatively coarse crystalline microstructure of spherulites is first developed in the glass at a low temperature. The spherulites are then converted to a fine grained microstructure by recrystallization at a higher temperature. The occurrence of recrystallization reactions in the present microstructures suggests that this method may also be of use in producing glass ceramics from Mg-Si-O-N glasses.

# VII. SUMMARY AND CONCLUSIONS

A qualitative study was made of the crystallization behavior of oxynitride glasses prepared in the Mg-Si-O-N system. $Si_3N_4$ was found to be a necessary component of melts for glass formation in this system and the production of bulk glass samples was mainly limited by decomposition reactions which occurred on melting. Except for the compositions richest in MgO, melts in the glass forming region phase separated on cooling. Phase separation resulted in glass microstructures which consisted of discrete droplets of a $SiO_2$ rich phase dispersed in a continuous matrix of MgO rich glass. Both phases were found to contain nitrogen, but more nitrogen was concentrated in the MgO rich phase. Quantitative compositional analysis showed that phase separation occurred as a direct consequence of liquid immiscibility in the $SiO_2$-MgO system.

Glass formation was found to be most successful for a melt of composition 59 wt% $SiO_2$, 32 wt% MgO and 9 wt% $Si_3N_4$. In a detailed investigation of crystallization in this glass the following behavior was observed:

1. On heating to above the glass transition temperature ($\approx$ 800°C) crystals nucleated in the MgO rich phase of the glass. However, at temperatures below 1000°C slow rates of crystal growth prevented extensive crystallization of the glass from occurring.

2. At temperatures above 1000°C rapid crystallization of the MgO rich phase to enstatite crystals occurred.

The crystals grew with a spherulitic morphology consisting of fan like arrangements of plate shaped enstatite grains. Individual plates in the spherulites were found to be separated by thin films of uncrystallized glass in agreement with theories of spherulitic growth.

3. Heat treatments in the temperature range 1000°C-1300°C had no apparent effect on the $SiO_2$ rich phase.

4. Above 1300°C softening of the $SiO_2$ rich phase initiated recrystallization of the spherulites to a more equilibrium microstructure of faceted grains of enstatite. Recrystallization was limited to regions surrounding the $SiO_2$ rich droplets. In the reaction the $SiO_2$ rich phase appears to act as a rapid transport path for $SiO_2$ and MgO enabling recrystallization of the spherulites to occur by a solution reprecipitation mechanism.

5. Also at temperatures above 1300°C it was found that $Si_2N_2O$ crystallized from the residual glass separating enstatite plates in the spherulites, $Si_2N_2O$ crystals nucleating heterogenously on the enstatite crystals.

6. Large volume changes that accompanied crystallization of the MgO rich phase caused porosity to form throughout glass samples on crystallization.

The effect of selected heat treatments and variations in glass composition on crystallization behavior were investigated. Two stage nucleation and growth heat treatments were found to have a pronounced effect on the microstructures developed in the glasses on crystallization. Holding at temperatures in the range 800°C-1000°C resulted in enhanced nucleation in the glasses and produced fine grained microstructures when nuclei were grown at higher temperatures. The finest grained microstructure was achieved using a nucleation treatment of 2 hrs. at 850°C. Longer heat treatments at this temperature produced no further refinement of the microstructure. A survey of crystallization behavior in other glass compositions showed that nucleation efficiencies varied widely from glass to glass. Circumstantial evidence suggests that nucleation in the glasses occurs heterogenously on silicon crystals precipitated from the melts on cooling.

From the results of crystallization experiments it is concluded that glasses in the Mg-Si-O-N system show promise as starting materials for the preparation of glass ceramics of new compositions.

# ACKNOWLEDGEMENTS

It is a pleasure to express my appreciation to Professor G. Thomas for his encouragement and support throughout the course of this investigation. I would also like to thank Professors A. G. Evans and A. Portis for their time and effort in reading and commenting on the thesis.

Special thanks are due to R. Loehman for his cooperation in preparing materials for this study and for allowing unpublished results from his investigations to be used in this study. My thanks are extended to O. L. Krivanek for his assistance in compositional analysis of the materials.

The great measure to which my friends and colleagues have contributed to the completion of this work is also gratefully acknowledged. In particular I would like to thank D. R. Clarke for his guidance and active interest in this research.

Finally I thank my wife, Linda, for her constant companionship and understanding when most needed.

This research was supported by the National Science Foundation grant #DMR-77-24022. Technical staff and facilities were provided by the Director, Office of Energy Research, Office of Basic Energy Sciences, Division of Materials Sciences of the U.S. Department of Energy under Contract No. W-7405-ENG-48.

# APPENDIX I

## DENSITY MEASUREMENT BY A SINK FLOAT TECHNIQUE

Several methods for determining the density of solids have been proposed.[83] The most commonly used technique used for ceramics is that based on Archimedes principal in which the apparent loss in weight of the sample on immersion in a liquid is measured. From the weight change the volume of the sample is found and hence the density of the sample measured. However, errors in the measurement of the weight of the sample immersed and unimmersed in the liquid make this an unreliable technique when accurate density measurements are to be made on small samples. For this reason a sink float technique was adopted for all bulk density measurements in the present investigation.

The method relies on the fact that a solid will neither sink nor float when immersed in a liquid of the same density. The liquid medium of appropriate density can be made up by mixing two miscible liquids one of density greater than the sample and one of density less than the sample. (In the present experiments diiodemethane $\rho$ = 3.3 gm/cc and carbon tetrachloride $\rho$ = 1.59 gm/cc were used.) The sample is immersed in the liquid taking care to ensure that complete wetting of the surface of the sample occurs. If the sample floats more of the lower density liquid is added and if it sinks more of the high density liquid is added. After each addition the liquid is thoroughly mixed and the behavior of the sample again noted. The procedure is repeated until the sample is supended in the liquid. The density of the liquid is then measured by pouring the liquid into a pycnometer of previously determined volume and weight. Weighing the

bottle plus liquid then gives the density of the liquid and hence the bulk density of the sample.

For density measurements of glass samples in the present study a slightly modified technique to the one just described was used to obtain greater accuracy. A liquid mixture of approximately the same density as the sample was first found at room temperature. The liquid plus sample were poured into a pycnometer which was fitted with a thermometer. By slowly heating and cooling the pycnometer the density of the liquid could be finely controlled until the sample was just suspended in the liquid. Liquid was either removed or added to the pycnometer to compensate for volume changes in the liquid. The weight of the full bottle ($W_F(T)$) was then measured and the temperature noted. The volume of the bottle as a function of temperature ($V(T)$) was calibrated using distilled water and the weight of the empty bottle measured ($W_e$). The density of the sample was then calculated from

$$P = \frac{V(T)}{W_F(T) - W_e}$$

Using this technique bulk density measurements of 0.5 gram samples which were reproducible to within ± 0.001 grams/cc (± 0.04%) were obtained.

# APPENDIX II

## TRANSMISSION ELECTRON MICROSCOPY TECHNIQUES FOR THE CHARACTERIZATION OF GLASSY PHASES IN CERAMIC MICROSTRUCTURES

The presence of even small amounts of a glassy phase in a polycrystalline material can have a dramatic effect on its properties. In addition the materials properties are also frequently dependent on the way in which the glass is distributed in the microstructure. For example intergranular films of glass result in loss in strength at high temperatures in materials such as glass ceramics[84,85] and $Si_3N_4$ based "alloys"[9]. For assessment of the properties of ceramic materials containing glass a reliable method for the location of the glassy phases is required. Several TEM techniques have been developed to examine microstructures for the presence of glassy phases. The advantages and disadvantages of these techniques are considered in this appendix. A new technique, developed by the author in which the glassy phase can be directly imaged is also described and compared to other techniques.

When glass is present as large pockets in the microstructure conventional imaging is often sufficient to locate the glass. Advantage can be taken of the fact that contrast in an amorphous specimen does not change on tilting, to distinguish glassy regions from those that are crystalline. In some materials the glassy phase may also undergo cavitation due to radiation damage in the electron beam making glassy regions easily identifiable. If the glassy pockets are sufficiently large ($\approx 1$ μm) they can also be identified by their diffuse diffraction pattern. Frequently however glass is present in

only small amounts in ceramic materials: Unambiguous identification of glassy regions then requires more sophisticated techniques.

A technqiue first used by Clarke[86] makes use of lattice imaging to examine grain boundaries for the presence of an intergranular phase. Here lattice fringes are imaged in adjacent grains by allowing strong bragg reflections from crystal planes in each grain to interfere with the transmitted beam. As fringes will only be imaged from the crystalline regions the presence of a gap between the fringes from adjacent grains implies the presence of a grain boundary phase, as shown schematically in Fig. 35. Similarly grain boundary phases can be detected by high resolution dark field imaging[87], again as gaps between the images of crystalline grains whose bragg reflections have been admitted through the objective aperture. Both these techniques image the phase indirectly and therefore suffer from the disadvantage that an existing boundary phase will become invisible if the boundary is not exactly edge on. Also as no direct information is obtained from the boundary phase using these methods it is not possible to say whether the phase is amorphous or crystalline, only that the phase is not contributing to the image. In the case of lattice imaging it has been shown[88] that a further limitation is that image shifts with microscope focus can obscure a grain boundary film at focus values other than the Scherzer defocus condition. In spite of these disadvantages both techniques are capable of revealing grain boundary phases as thin as 10Å and so offer a considerable improvement over conventional imaging techniques.

Many of the disadvantages of the indirect methods for detecting amorphous phases described above can be overcome by directly imaging glassy regions in the microstructure.[88,89] This can be done by excluding all Bragg beams from the objective aperture and allowing only part of the diffuse diffraction rings from amorphous phases to contribute to the image. With this diffraction geometry amorphous regions in the microstructure appear in light contrast in the image and so can be readily identified. The technique is shown schematically in Fig. 35. In practice the diffuse rings from glassy regions are generally too weak to be seen in the microscope, but as in most glasses the first diffraction rings is at a distance of about $3.5\text{Å}^{-1}$ from the transmitted beam the objective aperture can be simply placed at this position for imaging.

The performance of bright field, lattice imaging and diffuse dark field techniques, in imaging a thin intergranular film at a planar grain boundary in a $Si_3N_4$ ceramic, are compared in Fig. 36. The 15Å wide glassy phase is almost identifiable from the bright field image, Fig. 36(a), by virtue of the strong Bragg contours seen in the adjacent $Si_3N_4$ grains. A direct confirmation of the glasses' presence is, however, only obtained from the dark field and lattice images, Figs. 36(b),(c). Only the diffuse dark field image provides direct evidence that the grain boundary phase is amorphous. A further advantage of the diffuse dark field technique is that observation of the glass does not depend on the boundary being edge on. This is illustrated in Fig. 37 where a grain boundary, again in a $Si_3N_4$ material, is seen to twist away from being edge on. Where the boundary is not edge on the bright line from the glassy boundary phase simply becomes broader and

weaker as illustrated by the microdensitometer traces taken along A-A' and B-B'. Similarly the dark field technique is relatively insensitive to microscope focus the bright line from a boundary phase only broadening in a defocused image.

Although the dark field technique offers several advantages over indirect imaging techniques precautions used to be exercised to prevent a false impression of the amount of glass in a microstructure from being obtained. Firstly weak reflections from crystalline grains which are not apparent when the diffraction pattern is viewed in the microscope can result in bright contrast at grain boundaries even in the absence of a glassy phase. Recording of the diffraction conditions used for imaging is therefore essential to avoid misinterpretation of this phenomenon. An additional factor that may contribute to image contrast is the filling of grooves or hollows in the surface of thin foils, formed by preferential etching during ion beam milling, with the carbon evaporated on ceramic specimens to prevent charging in the electron beam. This problem can generally be avoided by using only the minimum thickness of carbon on specimens necessary to prevent charging or coating specimens with gold instead of carbon. A more severe problem is encountered when the crystalline phases in the material to be examined are sensitive to ionization damage in the electron beam. Ionization damage can convert crystalline phases to an amorphous structure. Damaged regions in a foil then appear in light contrast in a diffuse dark field image giving a false impression of the amount of glass in the microstructure. Figure 38 shows an example of this in the microstructure of a cordierite glass ceramic. In the dark field

image shown in Fig. 38(a) light contrast is seen at grain boundaries and in the interior of some of the grains giving the impression of large amounts of glass in the microstructure. After a further exposure to the electron beam of 1 minute the amorphous regions have increased in size, (Fig. 38(b)), indicating that it is not an intrinsic feature of the microstructure but results from ionization damage of the cordierite grains. The damage has nucleated preferentially at grain boundaries giving the appearance of an intergranular film of glass between grains. The severity of this problem varies from material to material and is generally worst in silicates. The use of higher accelerating voltages for the electron beam can reduce the rate of damage but not eliminate it. When the rate of damage is not too rapid though an idea of the true amount of glass in the microstructure can be obtained by setting up imaging conditions in an adjacent region and only moving to the region of interest to record the micrograph.

In conclusion the diffuse dark field technique provides a versatile and accurate method for surveying microstructures for the presence of glassy phases. The technique is not only useful for examining grain boundaries for thin intergranular films but is also sufficiently convenient to be used as a general method for examining the morphology of glassy regions throughout the microstructure. For this reason the diffuse dark field technique was used throughout the present investigation to examine glassy regions in the partially crystallized glasses.

# REFERENCES


1. Elmer, T. H., and Nordberg, M. E., "Nitrided Glasses," Paper No. 30, Proc. VII International Congress on Glass, Brussels, Belgium, 1965, Instuit National du Verre Charleroi, Belgium,(1965).

2. Elmer, T. H., and Nordberg, M. E., "The Effect of Nitriding on Electrolysis and Devitrification of High Silica Glasses," J. Amer. Ceram. Soc., 50, 275-279.

3. Mulfinger, H. O., "The Physical and Chemical Solubility of Nitrogen in Glass Melts," J. Amer. Ceram. Soc., 49, 462-467 (1966).

4. Wild, S., Grieveson, P., Jack, K. H., and Latimer, M. J., "The Role of Magnesia in Hot-Pressed Silicon Nitride," Special Ceramics, 5, 377-384, Ed. P. Popper, published British Ceramic Research Association (1970).

5. Kossowsky, R., "The Microstructure of Hot-Pressed Silicon-Nitride," J. Mat. Sci., 8, 1603-1615 (1973).

6. Jack, K. H., "Sialon Glasses," in Nitrogen Ceramics, Proc. NATO Advanced Study Institute, ed. F. L. Riley, 257-261, Noordhoff (1977).

7. Lochman, R. E., "Preparation and Properties of Yttrium-Silicon-Aluminum Oxynitride Glasses," J. Amer. Ceram. Soc., 62 (9-10), 491-494 (1979).

8. Evans, A. G., and Wiederhorn, S. M., "Crack Propagation and Failure Prediction in Silicon Nitride at Elevated Temperatures," J. Mat. Sci., 9, 270-278 (1974).

9. Lange, F. F., "High-Temperature Strength Behavior of Hot-Pressed $Si_3N_4$, Evidence for Subcritical Crack Growth," J. Amer. Ceram. Soc., 57, 84-87 (1974).

10. Kossowsky, R., Miller, D. G., and Diaz, E. S., "Tensile and Creep Strengths of Hot-Pressed $Si_3N_4$," J. Mat. Sci., 10, 983-997 (1975).

11. Iskoe, J. L., Lange, F. F., and Diax, E. S., "Effect of Selected Impurities on the High Temperature Mechanical Properties of Hot-Pressed Silicon Nitride," J. Mat. Sci., 11, 908-912 (1976).

12. Clarke, D. R., and Lange, F. F., "Oxidation of Silicon Nitride Alloys: Relationship to Phase Equilibria in the $Si_3N_4$-$SiO_2$-MgO System," to be published.

13. Wusirika, R. R., and Chyung, C. K., "Oxynitride Glasses and Glass-Ceramics," J. Non Cryst. Solids, 39, 39-44 (1980).

14. Lange, F. F., "Phase Relations in the System $Si_3N_4$-$SiO_2$-MgO and Their Interrelation with Strength and Oxidation," J. Amer. Ceram. Soc., 61, 53-56 (1978).

15. Lange, F. F., "Silicon Nitride Alloy Systems: Fabrication, Microstructure and Properties," to be published.

16. Levin, E. M., Robbins, C. R., and McMurdie, H. F., "Phase diagrams for Ceramists," ed. M. K. Reser, The American Ceramic Society, Inc., Columbus, Ohio (1964).

17. Prochazka, S., and Greskovich, C. D., "Development of Sintering Process for High Performance $Si_3N_4$," General Electric Report SRD-77-178 (AMMRC, TR 78-32), July 1978.

18. Greig, J. W., "Immiscibility in Silicate Melts," Amer. J. of Science, XIII, 1-44 and 132-154 (1927).

19. Tewhey, J. D., and Hess, P. C., "The Two Phase Region in the CaO-$SiO_2$ System Experimental Data and Thermodynamic Analysis," Phys. and Chem. Glasses, 20 (3), 41-53 (1979).

20. Drew, P., and Lewis, M. H., "The Microstructures of Silicon Nitride Ceramics During Hot-Pressing Transformations," J. of Mat. Sci., 9, 261-269 (1974).

21. Lavel, J. Y., and Westmacott, K. H., "The Mechanism of Ionization Damage in Glassy Ceramics," to be published in J. Amer. Ceram. Soc.

22. Cliff, G., and Lorimer, G. W., "The Quantitative Analysis of Thin Specimens," J. of Microscopy, 103, 203-207 (1975).

23. Masing, G., "Ternary Systems," Translated by B. A. Rogers, Dorer, New York (1960).

24. ASTM Powder diffraction data file.

25. Richardson, J. H., "Optical Microscopy for the Materials Sciences," published Marcel Dekker, Inc., N. Y. (1971).

26. Morse, H. W., and Donnary, J. D. A., "Optics and Structure of Three-Dimensional Spherulites," Amer. Mineral, 21 (7), 391-426 (1936).

27. Buseck, P. R., and Iijima, S., "High Resolution Electron Microscopy of Silicates," Amer. Mineral, 59, 1-21 (1974).

28. Keith, H. D., and Padden, F. J. (Jr.), "A Phenomenological Theory of Spherulitic Crystallization," J. Appl. Physics, 34 (8), 2409-2420 (1963).

29. Idrestedt, I., and Brosset, C., "Structure of $Si_2N_2O$," Acta Chem. Scand., 18, 1879-1886 (1964).

30. Zachariasen, W. H., "Atomic Arrangement in Glass," J. Amer. Chem. Soc., 54 (10), 3841-3851 (1932).

31. Stanworth, J. E., "Oxide Glass Formation from the Melt," J. Amer. Ceram. Soc., 54, 61-63 (1971).

32. Sun, K. H., "Fundamental Condition of Glass Formation," J. Amer. Ceram. Soc., 30, 277-281 (1947).

33. Uhlmann, D. R., "A Kinetic Treatment of Glass Formation," J. Noncryst. Solids, 7, 337-348 (1972).

34. Dormemus, R. H.. "Glass Science," John Wiley and Sons (1973).

35. Wild, S., Grieveson, P. and Jack, K. H., "The Crystal Structure of Alpha and Beta Silicon and Geramanium Nitrides," Special Ceramics, 5, 385-393, ed. P. Popper, published British Ceramic Research Association (1970).

36. Pauling, L., "Nature of the Chemical Bond," p. 83, 3rd edition, Cornell University Press (1960).

37. Wild, S., Grieveson, P., and Jack, K. H., "The Thermodynamics and Kinetics of Formation of Phases in the Ge-N-O and Si-N-O Systems," Special Ceramics, 5, 271-287, ed. P. Popper, published British Ceramic Research Association (1970).

38. Blegen, K., "Equilibria and Kinetics in the Systems Si-N and Si-N-O," Special Ceramics, 6, BCRA, P. Popper, ed. (1974).

39. JANAF Thermochemical tables, 2nd edition (Dow Chem. Co.) (1971).

40. Swalin, R. A., "Thermodynamics of Solids," Chapter 7, John Wiley and Sons (1962).

41. Singhal, S. C., "Thermodynamic Analysis of High Temperature Stability of Silicon Nitride and Silicon Carbide," Ceramurgia International, 2 (3), 123-129 (1976).

42. Brewer, L., and Edwards, R. K., "The Stability of SiO Solid and Gas," J. Phys. Chem., 58, 351-358 (1954).

43. Levin, E. M., "Liquid Immiscibility in Oxide Systems," in Phase Diagrams, 3, 143, ed. A. M. Alper, Academic Press (1964).

44. Zarzyki, J., "Phase Separated Systems," Discussions of Faraday Soc., No. 50, 122-133 (1971).

45. James. P. F., "Liquid-Phase Separation in Glass Forming Systems," J. Mat. Sci., 10, 1802-1825 (1975).

46. Uhlmann, D. R., and Kolbeck, A. G., "Phase Separation and the Revolution in Concepts of Glass Structure," Phys. Chem. Glasses, 17 (5), 146-158 (1976).

47. Levin, E. M., and Block, S., "Structural Interpretation of Immescibility in Oxide Systems I Analysis and Calculation of Immiscibility, J. Amer. Ceram. Soc., 40, 95-106 (1957).

48. Charles, R. J., "The Origin of Immiscibility in Silicate Solutions," Phys. Chem. Glasses, 10 (5), 169-178 (1969).

49. Haller, W., Blackburn, D. H., and Simmons, J. H., "Miscibility Gap in Alkali Silicate Binaries Data and Thermodynamic Interpretation," J. Amer. Ceram. Soc., 57 (3), 120-126 (1974).

50. Nakagawa, K., and Izumitani, T., "Effect of a Third Component upon the Immiscibility of Binary Glass," Phys. Chem. Glasses, 13 (3), 85-90 (1972).

51. Roedder, E. W., "The System $K_2O$-MgO-$SiO_2$," Amer. J. Sci. 249 (2), 81-130 (1951).

52. Haller, W., Blackburn, D. H., Wagstaff, F. E., and Charles, R. J., "Metastable Immiscibility Surface in the System $Na_2O$-$B_2O_3$-$SiO_2$," J. Amer. Ceram. Soc., 53, 34-39 (1970).

53. Cahn, J. W., and Charles, R. J., "The Initial Stages of Phase Separation in Glasses," Phys. Chem. of Glasses, 6 (5), 181-191 (1965).

54. Moriya, Y., Warrington, D. H., and Douglas, R. W., "A Study of Metastable Liquid Immiscibility in Some Binary and Ternary Alkali Silicate Glasses," Phys. Chem. Glasses, 8, 19-25 (1967).

55. Fihey, J. L., Nguyen-Duy, P., and Roberge, R., "On the Solidification of Copper Rich Niodium Alloys," J. Mat. Sci., 11, 2307-2311 (1976).

56. Hammel, J. J., "Nucleation in Glass - A Review," p. 1-9, in Advances in Nucleation and Crystallization in Glasses, ed. L. L. Hench and S. W. Freiman, published Amer. Ceram. Soc. (1971).

57. Kingerey, W. D., Bowen, H. K., and Uhlmann, D. R., "Introduction to Ceramics," p. 328, 2nd Edition, published John Wiley and Sons (1976).

58. Christian, J. W., "The Theory of Transformations in Metals," Part I, published Pergamon Press (1975).

59. Fine, M. E., "Phase Transformations in Condensed Systems," published MacMillan (1965).

60. Harper, H., James, P. F., and McMillan, P. W., "Crystal Nucleation in Lithium Silicate Glasses," Discuss Faraday Soc., 50, 206-213 (1970).

61. Harper, H., and McMillan, P. W., "The Formation of Glass - Ceramic Microstructures," Physics Chem. Glasses, 13 (4), 97-101 (1972).

62. Ohlberg, S. M., Golob, H. R., and Strickler, D. W., "Crystal Nucleation by Glass in Glass Separation," p. 55-62, Symposium on Nucleation and Crystallization of Glass and Melt, ed. M. K. Reser, published Amer. Ceram. Soc. (1962).

63. Tomozawa, M., "Liquid Phase Separation and Crystal Nucleation in $Li_2O$-$SiO_2$ Glasses," Physics Chem. Glasses, 13 (6), 161-166 (1972).

64. Uhlmann, D. R., "The Vitreous State," (general discussion), Discussions of the Faraday Soc., 50, 233-234 (1970).

65. Hammel, J. J., "Direct Measurements of Homogeneous Nucleation Rates in a Glass-Forming System," J. Chem. Phys., 46 (6), 2234-2244 (1967).

66. Doremus, R. H., and Turkalo, A. M., "Crystallization of Lithium Disilicate in Lithium Silicate Glasses," Physics Chem. Glasses, 13 (1), 14-15 (1972).

67. Johnson, R. E., and Muan, A., "Phase Diagrams for the Systems Si-O and Cr-O," J. Amer. Ceram. Soc., 51, 430-433 (1968).

68. Smyth, J. R., "Experimental Study on the Polymorphism of Enstatite," American Mineralogist, 59, 345-352 (1974).

69. Foster, W. R., "High-Temperature X-ray Diffraction Study of the Polymorphism of $MgSiO_3$," J. Amer. Ceram. Soc., 34 (9), 255-259 (1951).

70. Sarver, J. F., and Hummel, F. A., "Stability Relations of Magnesium Metasilicate Polymorphs," J. Amer. Ceram. Soc., 45 (4), 152-156 (1962).

71. Sadanaga, R., Okamura, F. P., and Takeda, H., "X-ray Study of the Phase Transformations of Enstatite," Minerological J., 6, 110-130 (1969).

72. Iijima, S., and Buseck, P. R., "High Resolution Electron Microscopy of Enstatite I: Twinning, Polymorphism and Polytypisin," Amer. Mineralogist, 60, 758-779 (1975).

73. Sears, G. W., "The Origin of Spherulites," J. Phys. Chem., 65 (10), 1738-1741 (1961).

74. Price, F. P., "Spherulite Growth Rates in Polyethylene Cross-Linked with High Energy Electrons," J. Phys. Chem., 64 (1), 169-170 (1960).

75. Morgan, L. B., "Crystallization Phenomena in Polymers II: The Course of Crystallization," Phil. Trans., A247 (921), 12-22 (1954).

76. Chadwick, G. A., "Metallography of Phase Transformations," p. 94, Butterworths (1972).

77. Freiman, S. W., Onoda, G. Y. (Jr.), and Pincus, A. G., "Controlled Spherulitic Crystallization in 3 BaO-5 $SiO_2$ Glass," J. Amer. Ceram. Soc., 55, 354-359 (1972).

78. Lewis, M. H., and Smith, G., "Spherulitic Growth and Recrystallization in Barium Silicate Glasses," J. Mat. Sci., 11, 2015-2026 (1976).

78. Lewis, M. H., Metcalf-Johansen, J., and Bell, P. S., "Crystallization Mechanisms in Glass Ceramics," J. Amer. Ceram. Soc., 62, 278-288 (1979).

80. Dambaugh, W. H. (Jr.), Molinendier, J. W., "Refractory Glasses," p. 1-12 in High Temperature Oxides, Vol. 5-IV, ed. A. M. Alper, Academic Press.

81. Bloor, E. C., "Conversion in Steatite Ceramics," J. Brit. Ceram. Soc., 1-2, 309-316 (1964).

83. Muller, L. D., In Physical Methods in Determinative Minerology, ed. J. Zussman, p. 459-466, Academic Press (1967).

84. James, K., and Ashbee, K. H. G., "Plasticity of Hot Glass-Ceramics," Progress in Mat. Sci., 21, 1-58 (1975).

85. Barry, T. I., Lay, L. A., and Morrell, R., "High Temperature Mechanical Properties of Cordierite Refractory Glass Ceramics," Proc. Brit. Ceram. Soc., 25, 67-84 (1975).

86. Clarke, D. R., and Thomas, G., "Grain Boundary Phases in a Hot-Pressed MgO Fluxed Silicon Nitride," J. Amer. Ceram. Soc., 60, 491-495 (1977).

87. Lou, L. K. V., Mitchell, T. E., and Henev, A. H., "Impurity Phases in Hot-Pressed $Si_3N_4$," J. Amer. Ceram. Soc., 61, 392-396 (1978).

88. Krivanek, O. L., Shaw, T. M., and Thomas, G., "Imaging of Thin Intergranular Phases by High-Resolution Electron Microscopy," J. Appl. Phys., 50 (6), 4223-4227 (1979).

89. Kirn, M., Ruhle, M., Schmid, H., and Gauckler, L. J., "Transmission Electron Microscopy of Si-Al-O-N Alloys," Proc. 9th Int. Congress on Electron Microscopy, Toronto, ed. J. M. Sturgess, Imperial Press (1978).

TABLE I. MELTS PREPARED IN THE Mg-Si-O-N SYSTEM

| Melt | Composition Wt% | | | Melting Conditions | | Appearance of Melt on Cooling |
|---|---|---|---|---|---|---|
| | $SiO_2$ | MgO | $Si_3N_4$ | Temperature | Time Hours | |
| A | 59.1 | 31.81 | 9.09 | 1700°C | 4 1/2 | Gray opaque glass |
| B | 65.0 | 26.0 | 9.00 | 1650°C | 1 | Gray opaque glass, some bubbles |
| C | 67.0 | 24.0 | 9.00 | 1650°C | 1 | Gray opaque glass, some bubbles |
| D | 61.91 | 33.33 | 4.76 | 1650°C | 1 | Gray opaque glass |
| E | 55.0 | 35.0 | 10.0 | 1650°C | 1 | Clear blueish clored glass |
| F* | 52.5 | 37.5 | 10.0 | 1600°C | 1 | Clear glass |
| G | 70.0 | 21.0 | 10.0 | 1650°C | 1 | Frothy glass |
| H | 54.2 | 29.0 | 16.8 | 1600°C | 1 | Frothy glass |
| I | 65.0 | 35.0 | 0 | 1700°C | 1 | Crystalline opaque |
| J* | 55.0 | 40.0 | 5.00 | 1600°C | 1 | Partly crystalline |
| K | 40.0 | 40.0 | 10.0 | 1650°C | 1 | Crystalline opaque |
| L | 45.0 | 45.0 | 10.0 | 1600°C | 1 | Crystalline opaque |

*Melts prepared using Centor furnace

TABLE II

Mg/Si RATIOS IN $SiO_2$ AND MgO RICH PHASES

IN PHASE SEPARATED MgOSi-O-N GLASSES

| Glass | Mg/Si Ratio in $SiO_2$ Rich Phase | Mg/Si Ratio MgO Rich Phase |
|---|---|---|
| A | $1.6 \times 10^{-2}$ | 0.796 |
| B | - | 0.785 |
| C | - | 0.764 |
| D | - | 0.906 |

TABLE III

CALCULATED EQUILIBRIUM ACTIVITIES OF SILICON AND PARTIAL PRESSURES OF OXYGEN AND SiO FOR $Si_3N_4$-$SiO_2$ MELTS

1 atmosphere of nitrogen  activity of $Si_3N_4$ = 0.035

activity of $SiO_2$ = 0.53

| T°C | $a_{Si}$ in melt | $P_{O_2}$ above melt | $P_{SiO}$ above melt |
|---|---|---|---|
| | Reaction 1 | Reaction 8 | Reaction 10 |
| 1400 | 0.00292 | $2.26 \times 10^{-17}$ | 0.00047 |
| 1500 | 0.00953 | $3.14 \times 10^{-16}$ | 0.00296 |
| 1600 | 0.02738 | $3.291 \times 10^{-15}$ | 0.0153 |
| 1700 | 0.0707 | $2.717 \times 10^{-14}$ | 0.0674 |
| 1800 | 0.1666 | $1.829 \times 10^{-13}$ | 0.256 |
| 1900 | 0.3629 | $1.033 \times 10^{-12}$ | 0.863 |
| 2000 | 0.7381 | $5.02 \times 10^{-12}$ | 2.609 |

FIGURE CAPTIONS

Figure 1 - $SiO_2MgO$-$Si_3N_4$ phase diagram after Lange[14,15] shown in wt% representation. The circles mark the composition of melts prepared for this investigation and the dotted line indicates the approximate extent of the glass forming region found.

Figure 2 - Bright field image of the phase separated microstructure of glass A in the as quenched condition. Droplets of the minor phase appear in light contrast due to preferential etching of this phase during foil preparation. The EDS spectrum (b) indicates that the minor phase contains mainly silicon while the spectrum (c) shows that the matrix phase contains nearly equal amounts of magnesium and silicon.

Figure 3 - (a), (b) and (c) are low magnification bright field images of thin foils of phase separated glasses A, B and C respectively. The $SiO_2$ rich minor phase, in each case, has been etched from the foil during foil preparation. The general morphology of phase separation in the glasses, however, is apparent from the holes left in the foils.

Figure 4 - The appearance of a region of the MgO rich matrix phase in glass C after exposures of 0 (a), 100 (b), 200 (c) and 300 (d) seconds to an electron probe. Cavities nucleate and grow in the foil due to ionization damage of the glass induced by the high intensity electron probe.

Figure 5 - Graph of Mg/Si count ratio against time of exposure to the electron beam, from a region of the matrix phase of glass C. Magnesium is rapidly lost from the exposed region when a high intensity beam is used but the Mg/Si count ratio stays nearly constant when a low intensity beam is used.

Figure 6 - Electron energy loss spectra from minor (a) and matrix (b) phases in glass A. Oxygen K edges are prominent in both spectra but nitrogen K edges are only revealed after background stripping. The relative areas of nitrogen edges, shown in black beneath each spectrum magnified 20X, indicate there is approximately twice as much nitrogen in the matrix phase as in the minor phase.

Figure 7 - $SiO_2$ rich portion of the $SiO_2$-MgO-$Si_3N_4$ phase diagram in wt% representation showing the experimentally determined position of the miscibility boundary in this sytem at 850°C. The boxed region is shown in more detail below.

Figure 8 - Bright field images of the microstructures of glasses E and F in the as quenched condition. Glass E whose composition lies within the experimentally determined miscibility gap has phase separated (a). No evidence of phase separation is seen in glass F with a composition outside the miscibility boundary.

Figure 9 - Typical bright field image of a crystalline particle in glass B (a). The inset diffraction pattern indicates that the particle is elemental silicon. This is confirmed by the EDS spectrum from the particle (b) which contains only a silicon peak. The EDS spectrum from the dark particle, indicated by the arrow, shows that it contains a high concentration of Ti, Cr, and Fe impurities.

Figure 10 - Typical bright field (a) and dark field (b) images of a small silicon particle found in glass A on cooling from the melt.

Figure 11 - Differential thermal analysis traces from coarse (a) and fine (b) powders of glass A. The glass transformation temperature is indicated by a small endothermic peak at about 800°C in both traces. Exothermic peaks indicate the occurrence of reactions on the surface and in the bulk of the glass.

Figure 12 - Polarized light micrographs revealing the surface microstructure of samples of glass A crystallized by heat treatments of: (a) 2 hours at 945°C, (b) 2 hours at 1070°C and (c) 2 hours at 1350°C. The surface of the sample appears at the top of each micrograph.

Figure 13 - Dark field image of forsterite dendrites grown from the surface of glass A during a heat treatment of 2 hours at 1070°C. Glass between the dendrite branches appears in light contrast. The inset electron diffraction pattern

indicates that each dendrite is a single crystal of forsterite.

Figure 14 - Transmitted polarized light micrograph showing internally nucleated crystals that have grown from glass A during a heat treatment of 2 hours at 945°C.

Figure 15 - Transmitted polarized light micrographs of the bulk microstructure of glass A after heat treatments of 0 (a), 10 (b), 20 (c), 50 (c) and 120 (e) minutes at 1020°C. Spherulites have grown from internal nucleation sites in the glass and extended throughout the microstructure after holding for 120 minutes at temperature.

Figure 16 - Reflected light micrograph of porosity developed in a sample of glass A crystallized at 1020°C for 2 hours.

Figure 17 - Transmitted polarized light micrograph of glass A after crystallization at 1020°C. Cross like contrast is evident in several regions indicating a spherulitic type microstructure.

Figure 18 - Transmitted polarized light micrographs of "spherulites" grown from glass A at temperatures of 1000°C (a), 1020°C (b), 1070°C (c), and 1100°C (d). Similar microstructures are developed at each temperature.

Figure 19 - Dark field image showing the appearance of one of the $SiO_2$ rich droplets found in glass A after a heat treatment of 2 hours at 1020°C. Remnants of the droplet around the

hole formed in the foil by etching away the $SiO_2$ rich phase are seen in uniform grey constant indicating that the $SiO_2$ rich phase is still glassy. The surrounding MgO rich phase has crystallized during the intermediate temperature heat treatment.

Figure 20 - Dark field image showing the crystalline microstructure developed in the MgO rich phase of glass A during an intermediate temperature heat treatment of 2 hours at 1020°C. Different crystal morphologies are evident in the regions labeled 1, 2 and 3.

Figure 21 - (a), (c) and (d) show more detailed views of the morphologies seen respectively in regions 1, 2 and 3 of Fig. 20. Indexing of their corresponding diffraction patterns (b) (d)(f) shows that the morphologies are sections through the same microstructure of enstatite crystals only viewed along different axes of the enstatite unit cell.

Figure 22 - Bright field image of the fan like arrangements of enstatite plates crystallized from glass A during an intermediate temperature heat treatment of 2 hours at 1020°C.

Figure 23 - Part of an enstatite spherulite crystallized from glass A during an intermediate temperature heat treatment of 2 hours at 1020°C. The lath shaped enstatite crystals shown in the bright field image (a) are seen to be separated by thin films of uncrystallized glass in the diffuse dark

field image (b). The corresponding diffraction geometry for (b) is shown in (c).

Figure 24 - Dark field image (a) showing the appearance of one of the $SiO_2$ rich droplets found in glass A after a heat treatment of 2 hours at 1350°C. The $SiO_2$ rich phase, seen in grey contrast, has remained glassy during the heat treatment but has apparently softened to the extent that it dissipated into the surrounding microstructure. An EDS spectrum from the glassy region is shown in (b). Facted grains evident in several regions of the micrograph are identified as crystals of enstatite by their corresponding diffraction pattern (c).

Figure 25 - $Si_2N_2O$ crystals crystallized from glass between enstatite plates during a high temperature heat treatment of 2 hours at 1350°C. The enstatite grains are in an (010) orientation in Figs. (a), (b) and (c) and in an (100) orientation in Figs. (d), (e) and (f). Dark field images taken using one of the $Si_2N_2O$ reflections indicated by arrows in the corresponding electron diffraction patterns (c) and (f) are shown in (b) and (e).

Figure 26 - Bright field image (a) of $Si_2N_2O$ crystals developed in a sample of glass A heated for 2 hours at 1350°C. The enstatite plates in this micrograph are in an orientation perpendicular to both orientations shown in Fig. 27. In this orientation the $Si_2N_2O$ crystals are seen as elongated

grains with their long axis lying along one of three directions as shown. The corresponding diffraction pattern is shown in (b).

Figure 27 - Schematic drawing of the crystallography of $Si_2N_2O$ crystals seen in Fig. 26. (a) (200) $Si_2N_2O \| 001$ clinoenstatite, (b) (110) $Si_2N_2O \| 001$ clinoenstatite and (c) $(1\bar{1}0)$ $Si_2N_2O \| 001$ clinoenstatite.

Figure 28 - (a) and (b) show an anslysis of the diffraction patterns shown in Figs. 25(c) and (f) respectively. Reflections from $Si_2N_2O$ crystals in both orientation relationships described in the text are included. It can be seen that many of the $Si_2N_2O$ reflections superimpose on reflections from the enstatite grains.

Figure 29 - The effect on the microstructure of glass A of a prior nucleation treatment of 2 hours at the temperature indicated followed by a growth treatment of 2 hours at 1020°C (b)-(f). For each heat treatment a transmitted polarized light micrograph of crystals grown in the sample is shown on top and a reflected light micrograph of porosity in the sample is shown below. For comparison the microstructure of glass A given no nucleation treatment but crystallized at 1020°C for 2 hours is shown in (a).

Figure 30 - A plot of the density of samples of glass A given two stage treatments versus temperature of the nucleation treatment. The density of the samples is only marginally greater for the optimum treatment of 2 hours at 850°C.

Figure 31 - Effect of nucleation treatments of 2 hours (a) and 4 hours (b) at 850°C on the final crystallized microstructure of glass A. No further refinement in the microstructure is apparent after the longer nucleation treatment, indicating that nucleation is complete after the 2 hours heat treatment.

Figure 32 - Transmitted polarized light micrographs of "spherulites" grown from glasses E (a), A (b), B (c), C (d) during a heat treatment of 2 hours at 1020°C. The micrographs are arranged in order of increasing $SiO_2$ content of the glasses. It is apparent that the more $SiO_2$ rich glasses develop a higher density of nuclei resulting in finer scaled microstructures.

Figure 33 - Calculated equilibrium pressures of nitrogen for the thermal dissociation of $Si_3N_4$ plotted against $\frac{1}{T}$, for various activities of silicon and an assumed activity of $Si_3N_4$ of 0.035. For low activities of silicon the reaction can produce nitrogen pressures greater than one atmosphere, even at moderate temperatures.

Figure 34 - $SiO_2$ rich portion of the $SiO_2$-MgO phase diagram in wt% representation showing the stable miscibility gap in the system extrapolated to temperatures of 850°C. Also marked on the phase diagram is a composition with the same $SiO_2$-MgO ratio as glass C. It is apparent that such a composition would separate into two immiscible liquids on melting.

Figure 35 - Schematic illustration of lattice imaging (on the left) and dark field (on the right) techniques for detecting amorphous intergranular films.

Figure 36 - Comparison of (a) bright field, (b) dark field, and (c) lattice imaging techniques in imaging of a thin grain boundary phase in a polycrystalline $Si_3N_4$ material. The corresponding diffraction geometries are shown in (d)-(f).

Figure 37 - Dark field image of a twisting grain boundary in a $Si_3N_4$ material (a). The microdensitometer traces taken along A-A' (b) and B-B' (c) show that for boundaries not edge on, their images simply become more diffuse.

Figure 38 - Dark field images taken from a corderite glass ceramic. After a short exposure to the electron beam significant areas of amorphous material are detected in the microstructure (a). The amorphous regions have increased in size after a further exposure to the electron beam of 1 minute (b), indicating that they are formed by ionization damage of the crystalline grains.

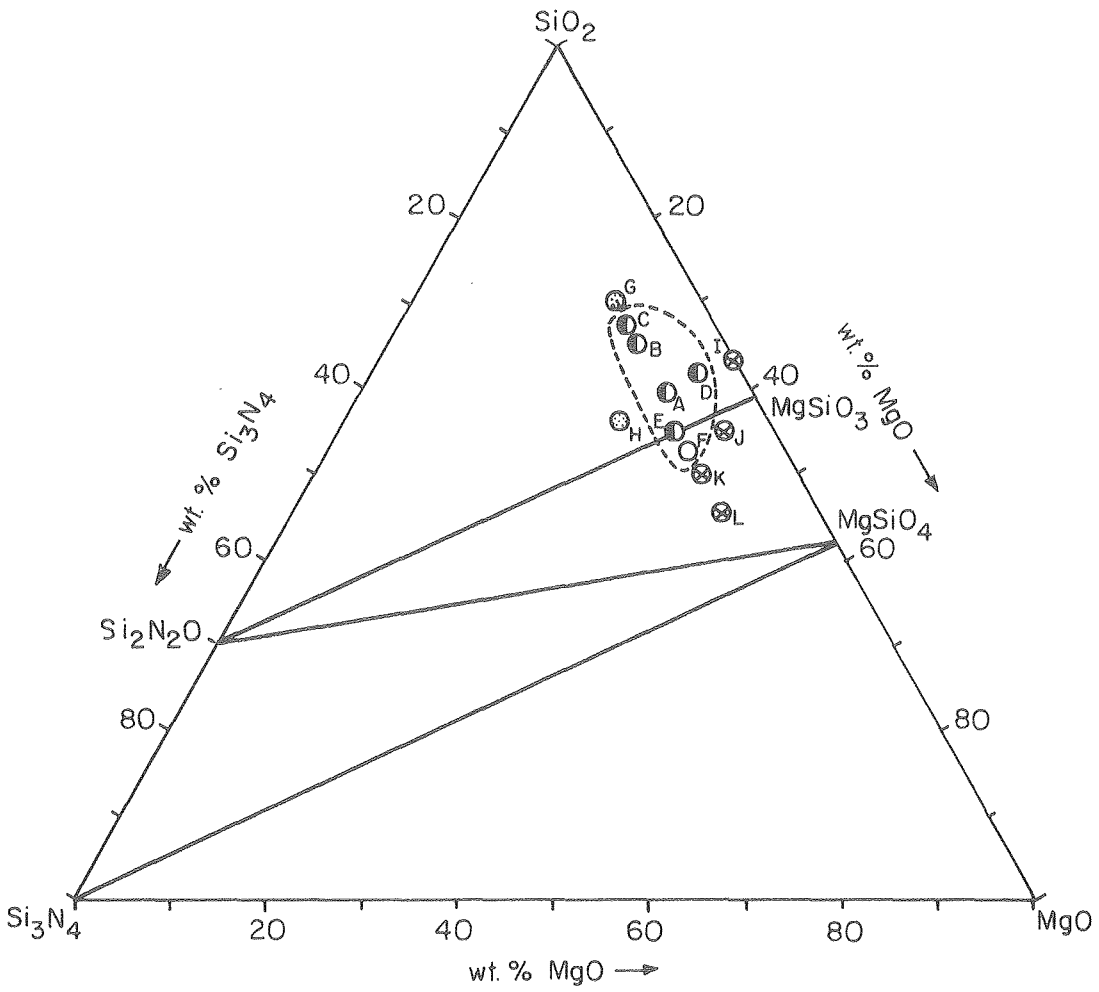


XBL 809-11708

Figure 1

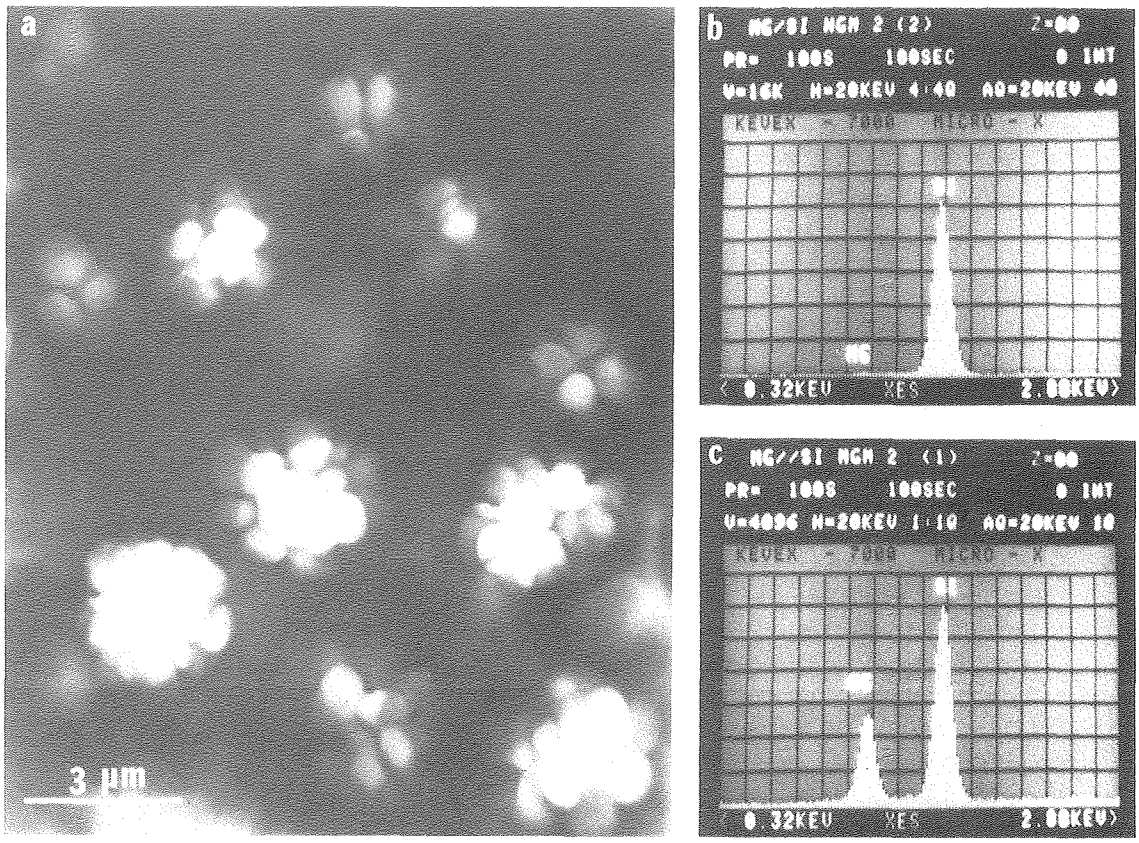


XBB 802-1977

Figure 2

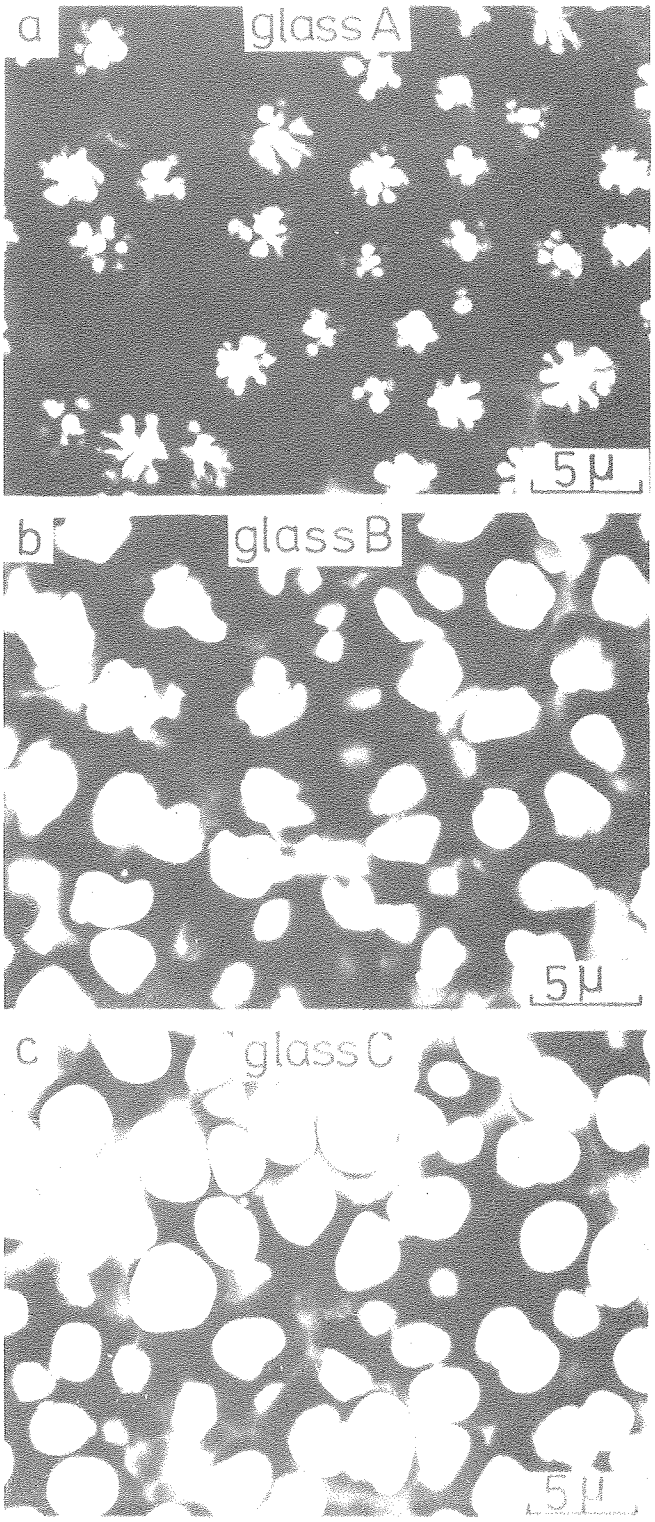


XBB 809-10369

Figure 3

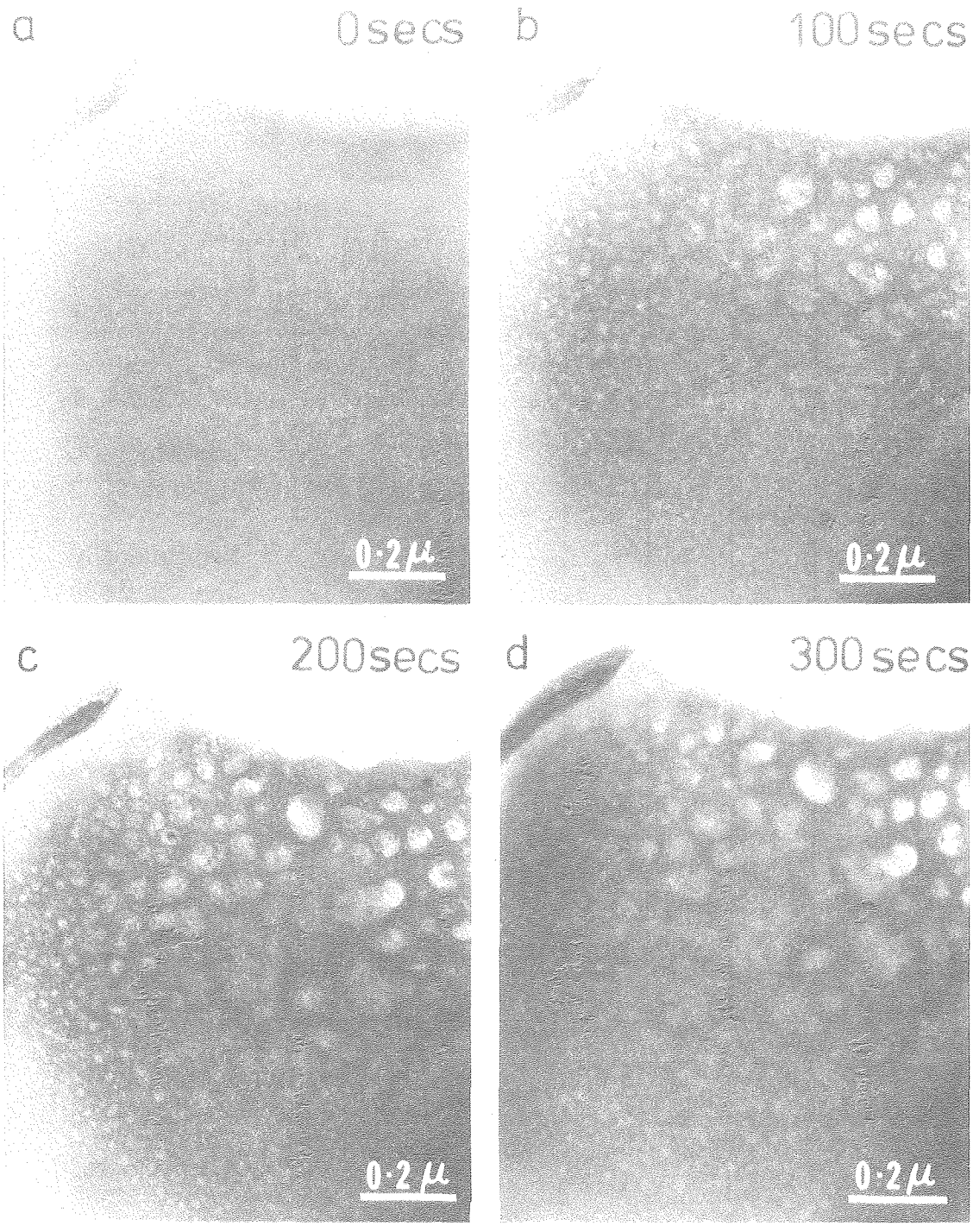


XBB 809-10370

Figure 4

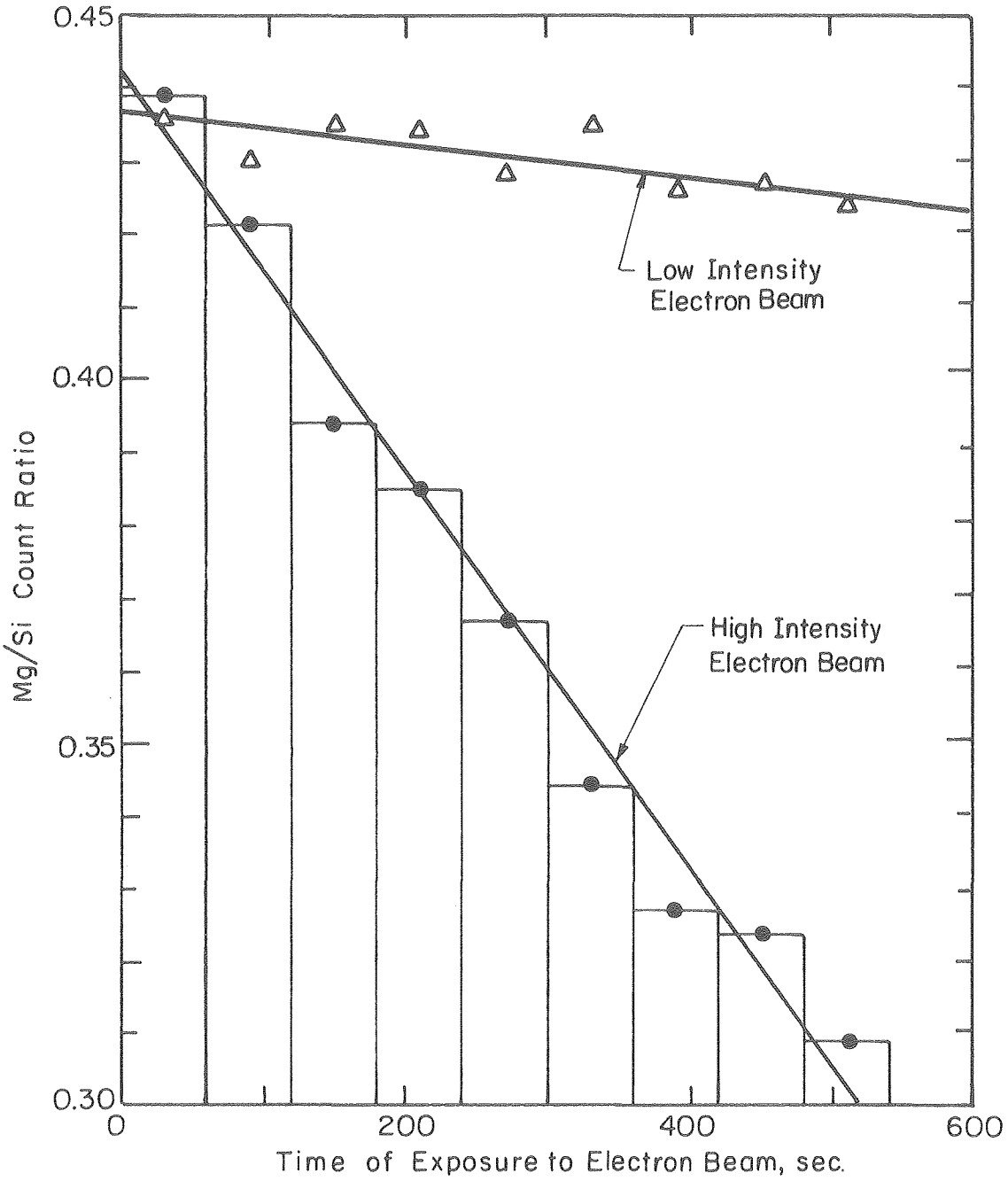


XBL 809-11712

Figure 5

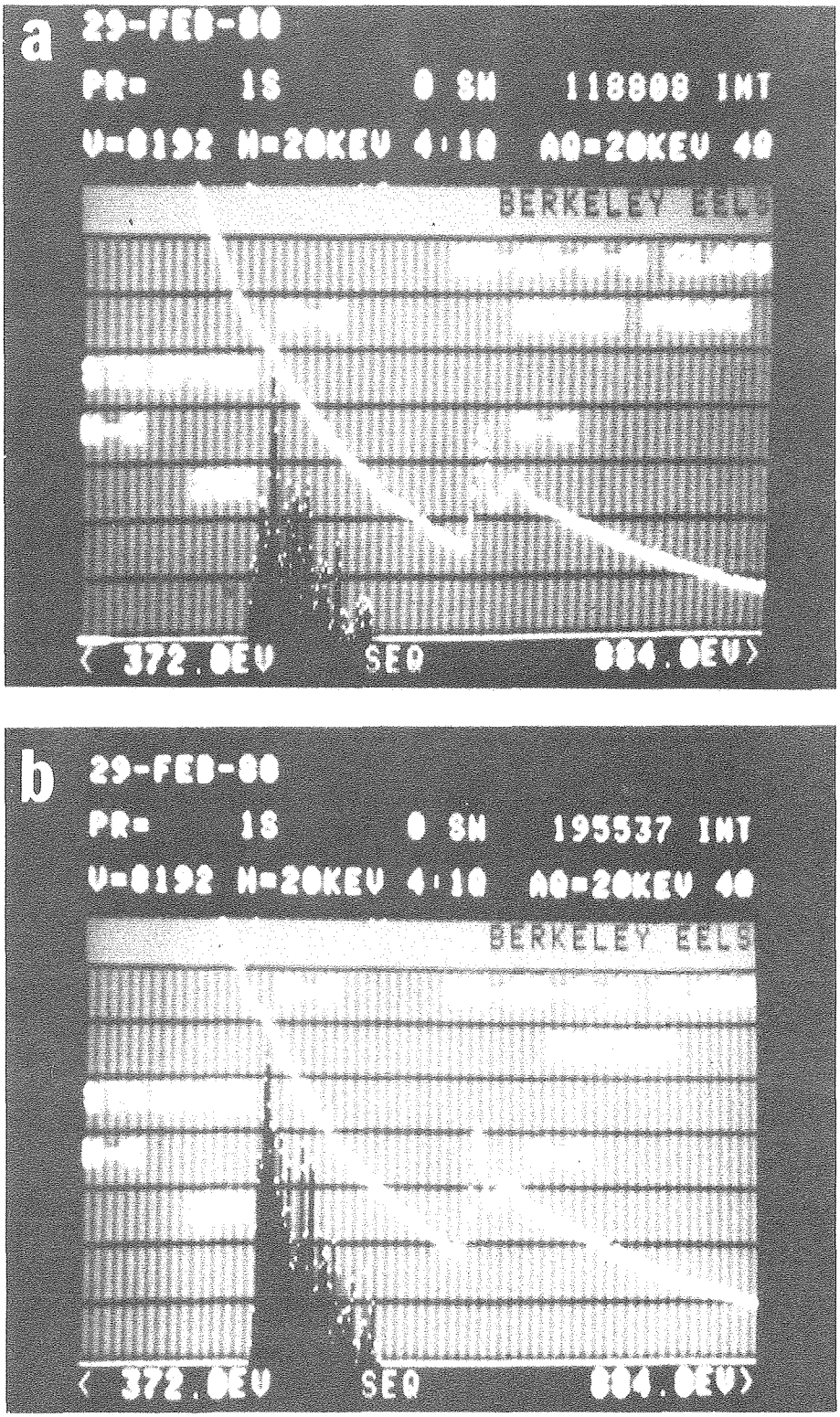


XBB 806-7159

Figure 6

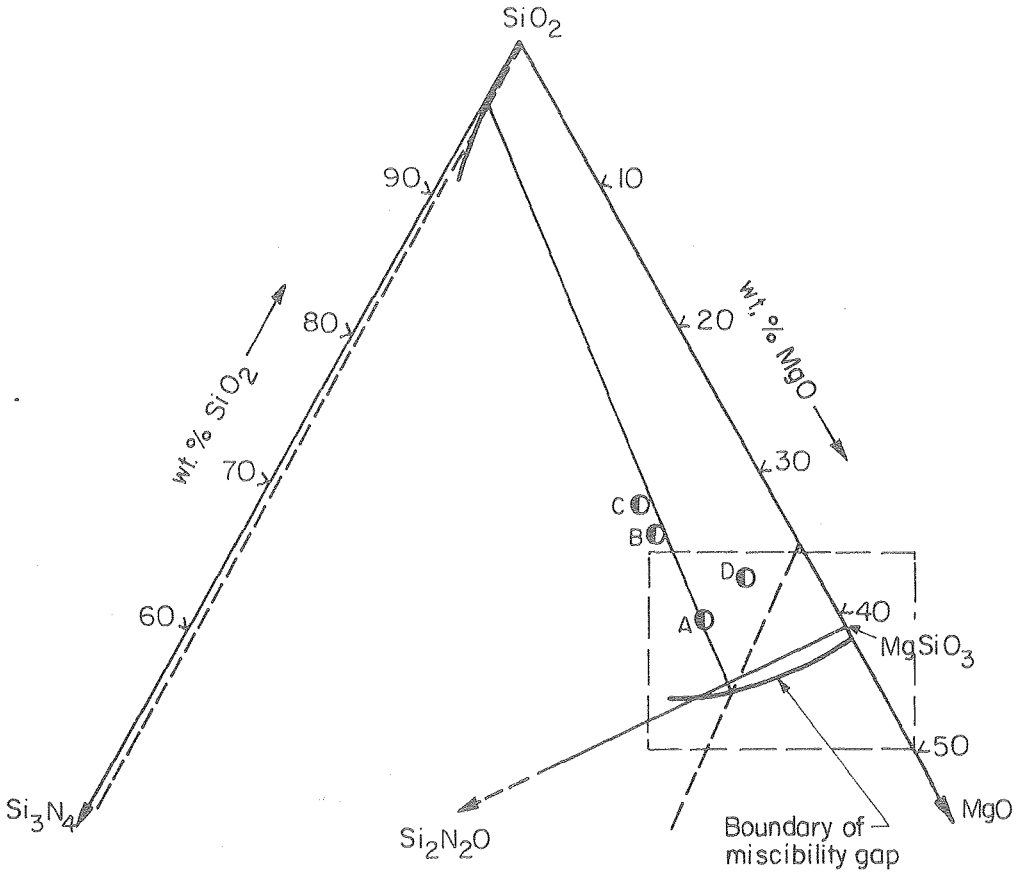


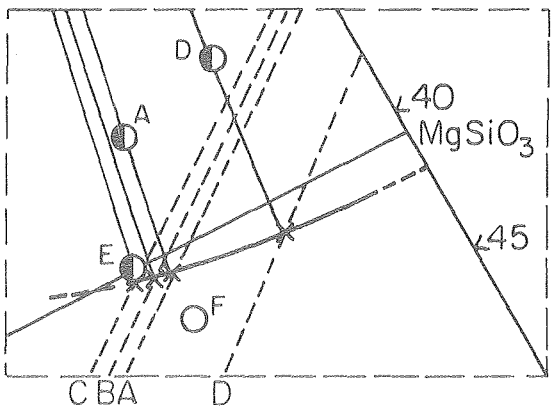


◐ Phase separated glass
○ Clear glass (no phase separation)
—— Tie lines
- - - Line of constant Mg/Si ratio

XBL 809-11714

Figure 7

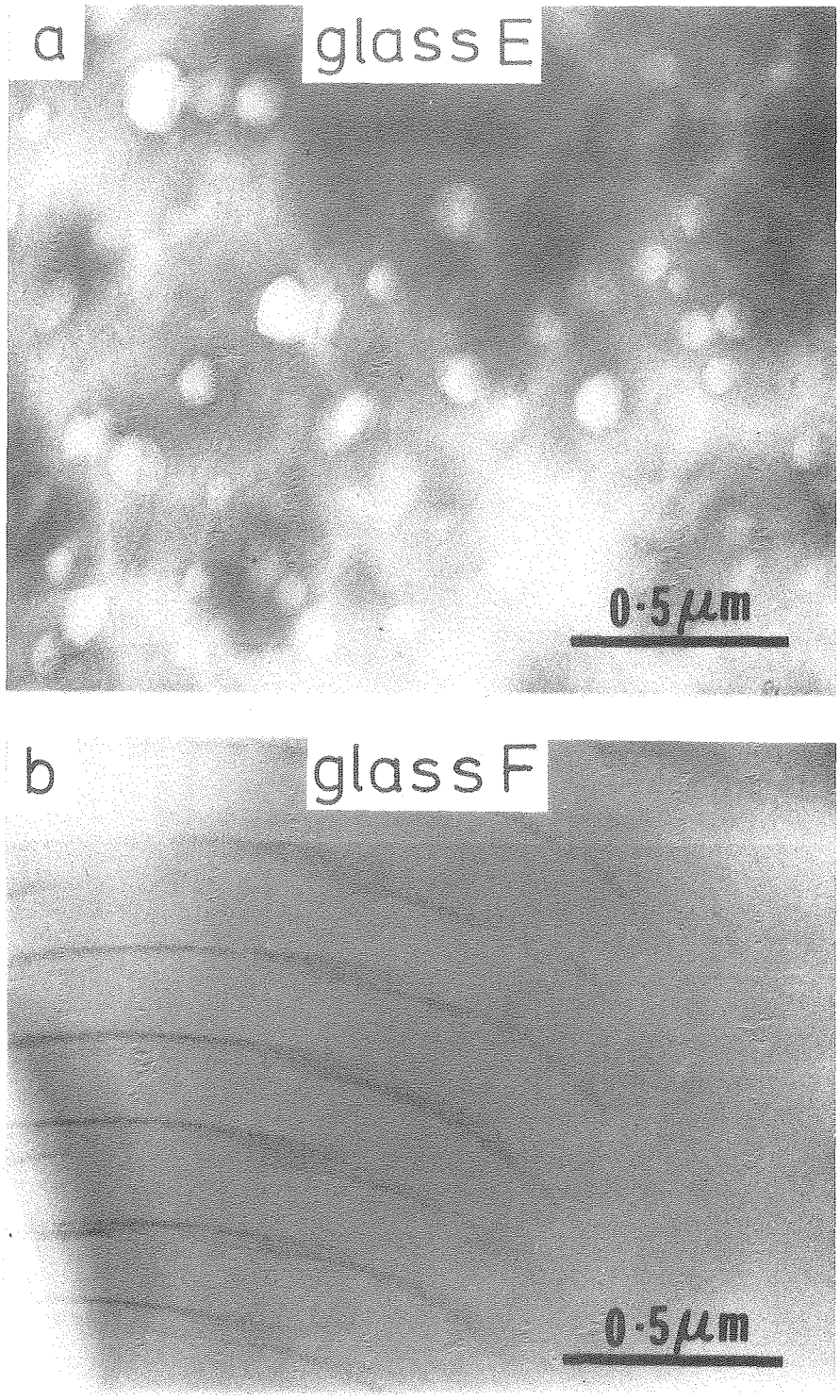


XBB 809-10365

Figure 8

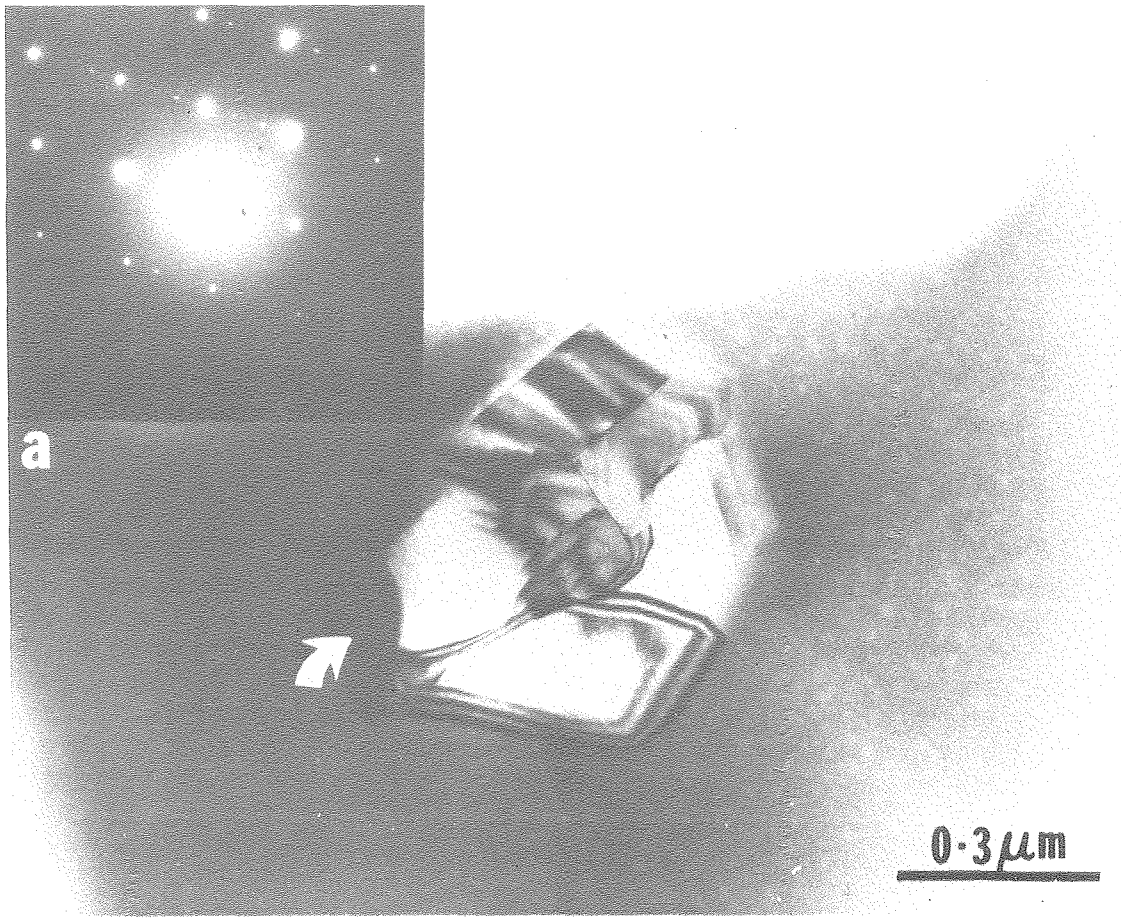


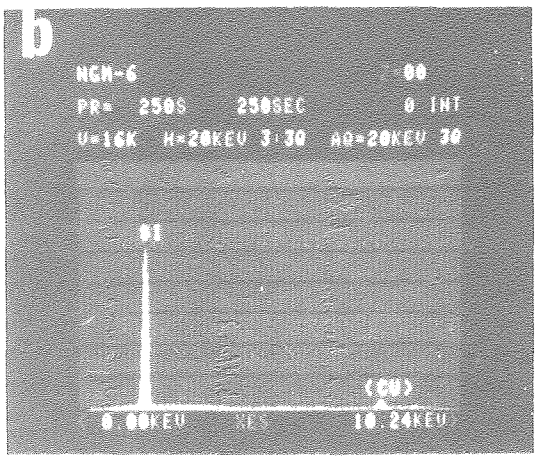


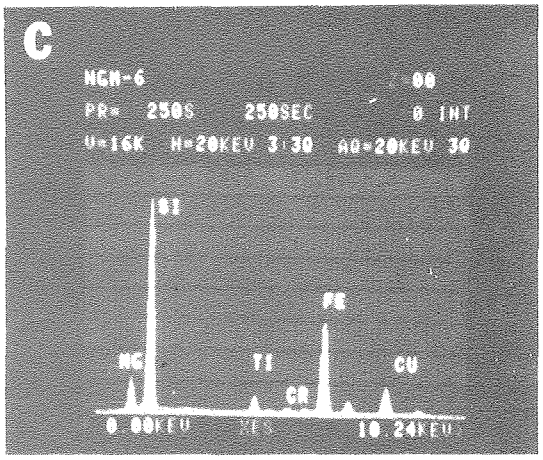


CBB 809-10379

Figure 9

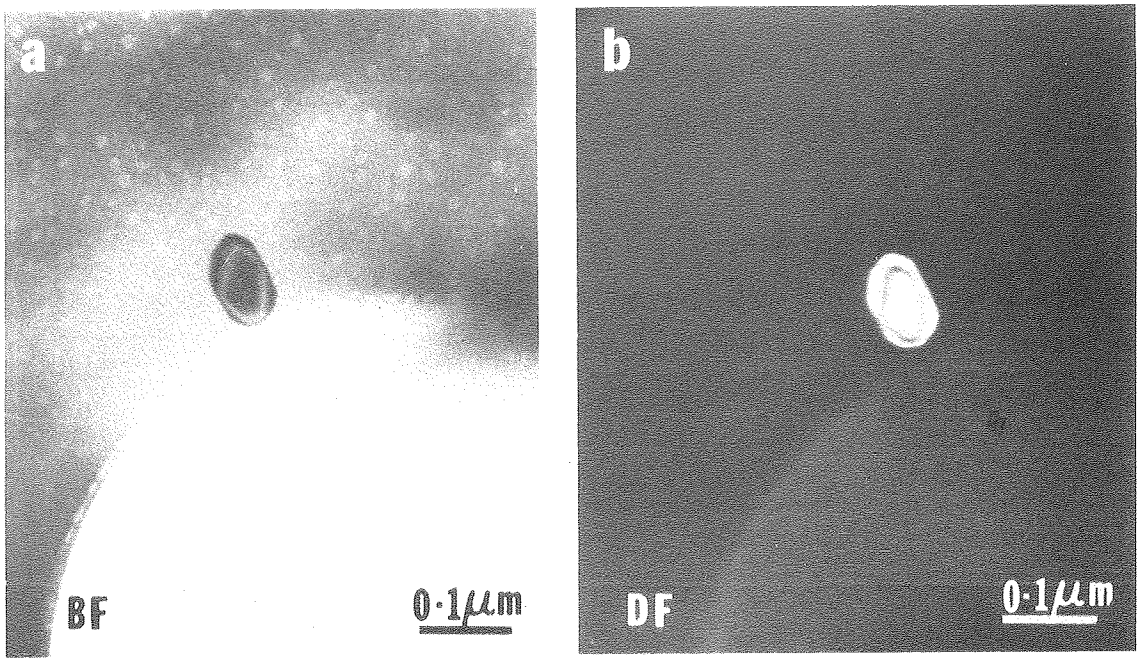


XBB 809-10363

Figure 10

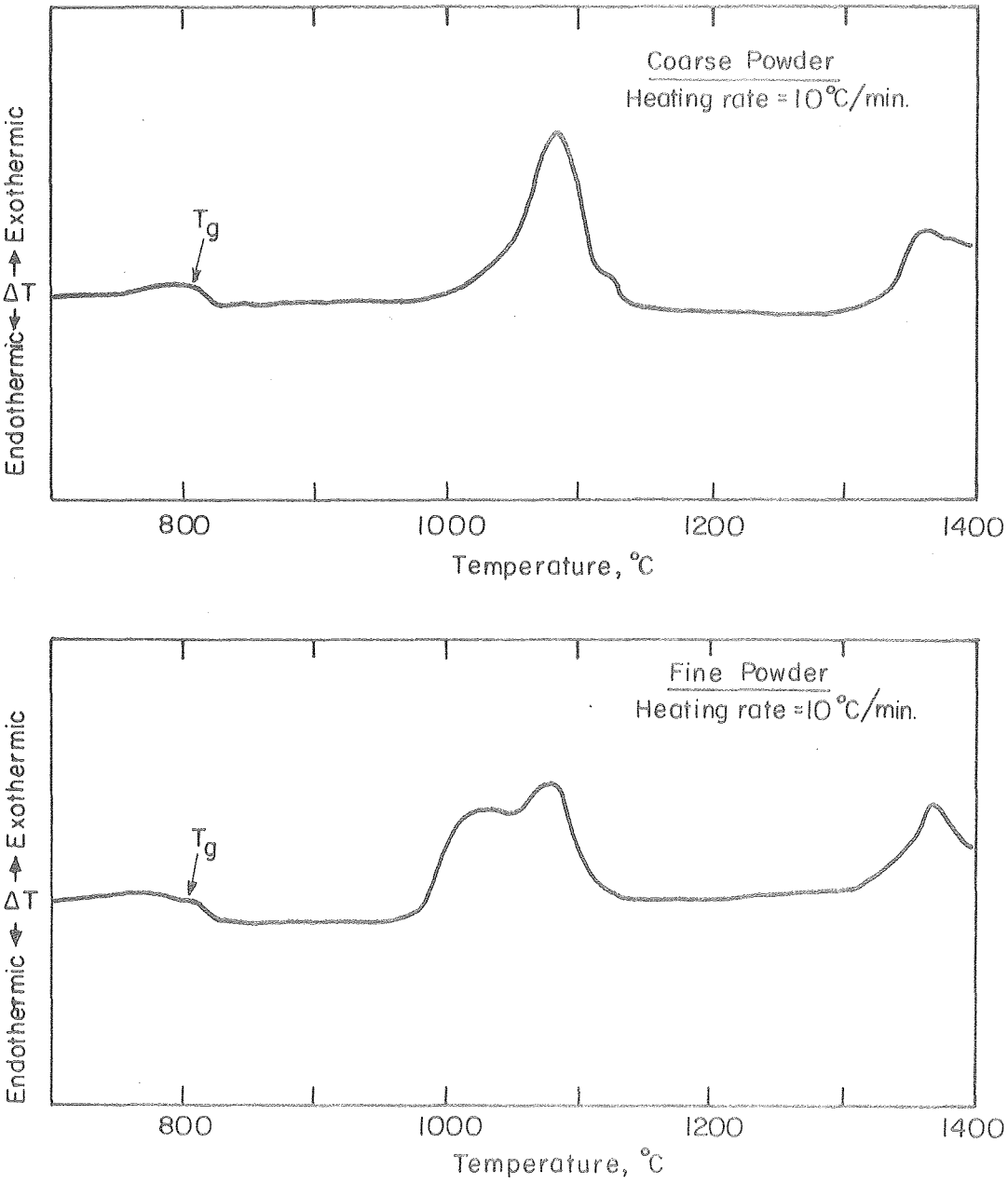


XBL 809-11711

Figure 11

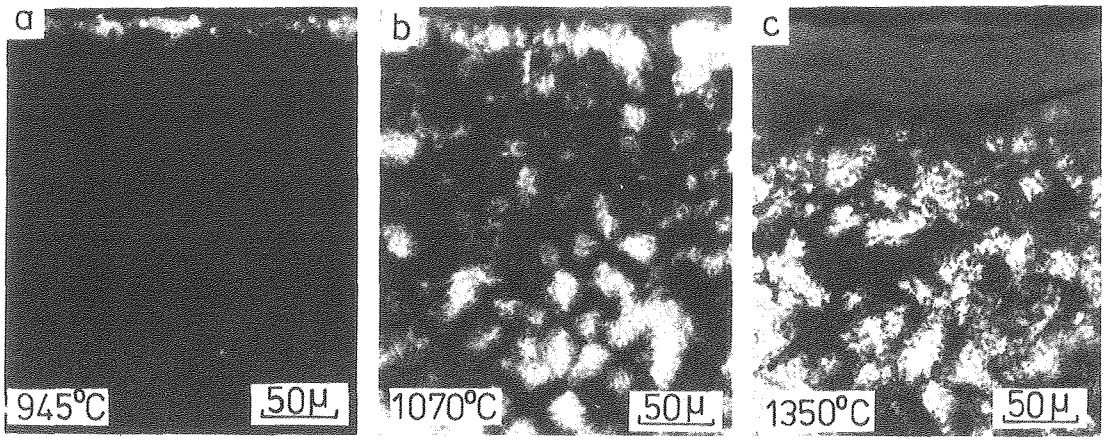


XBB 809-10368

Figure 12

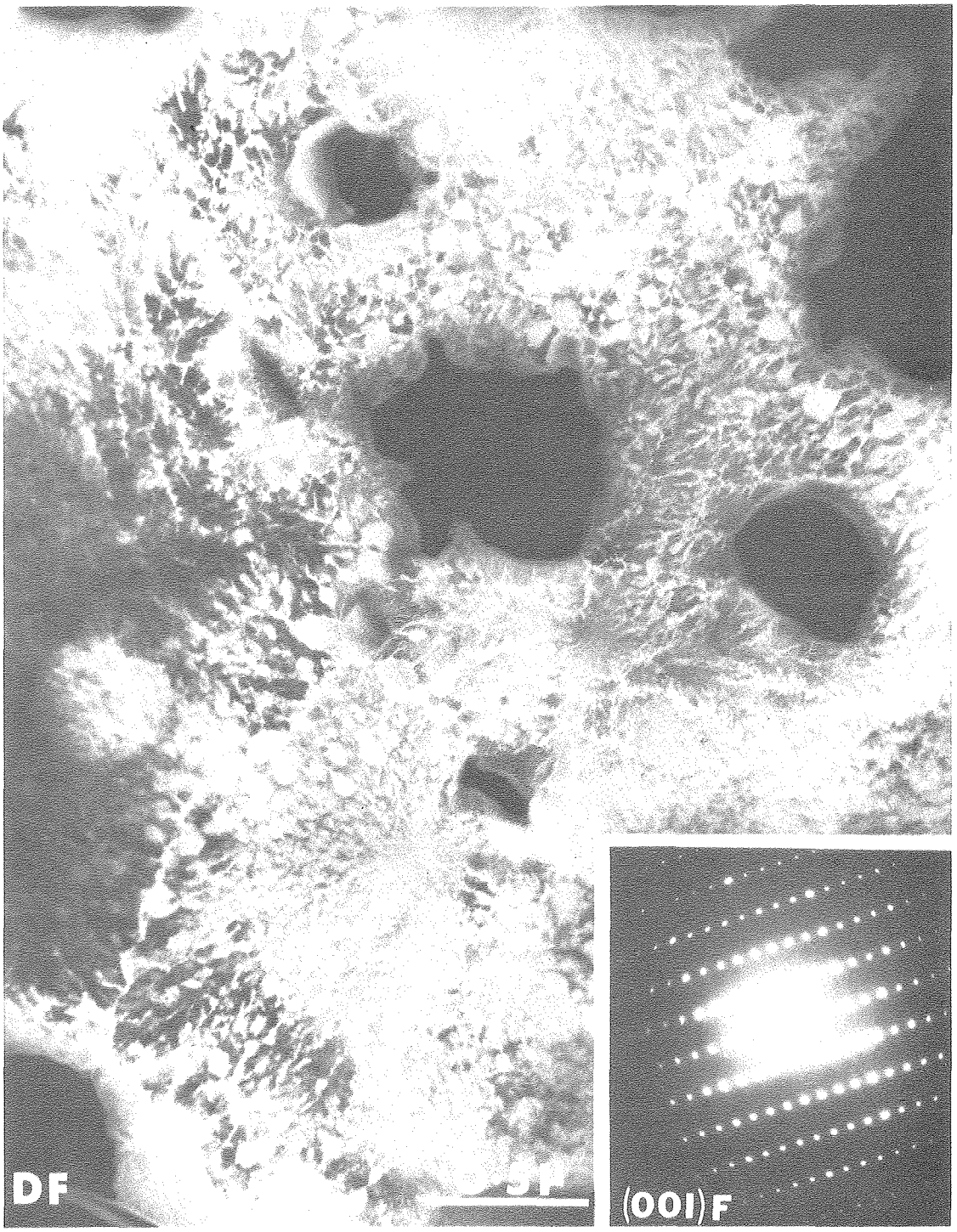


XBB 799-11622

Figure 13

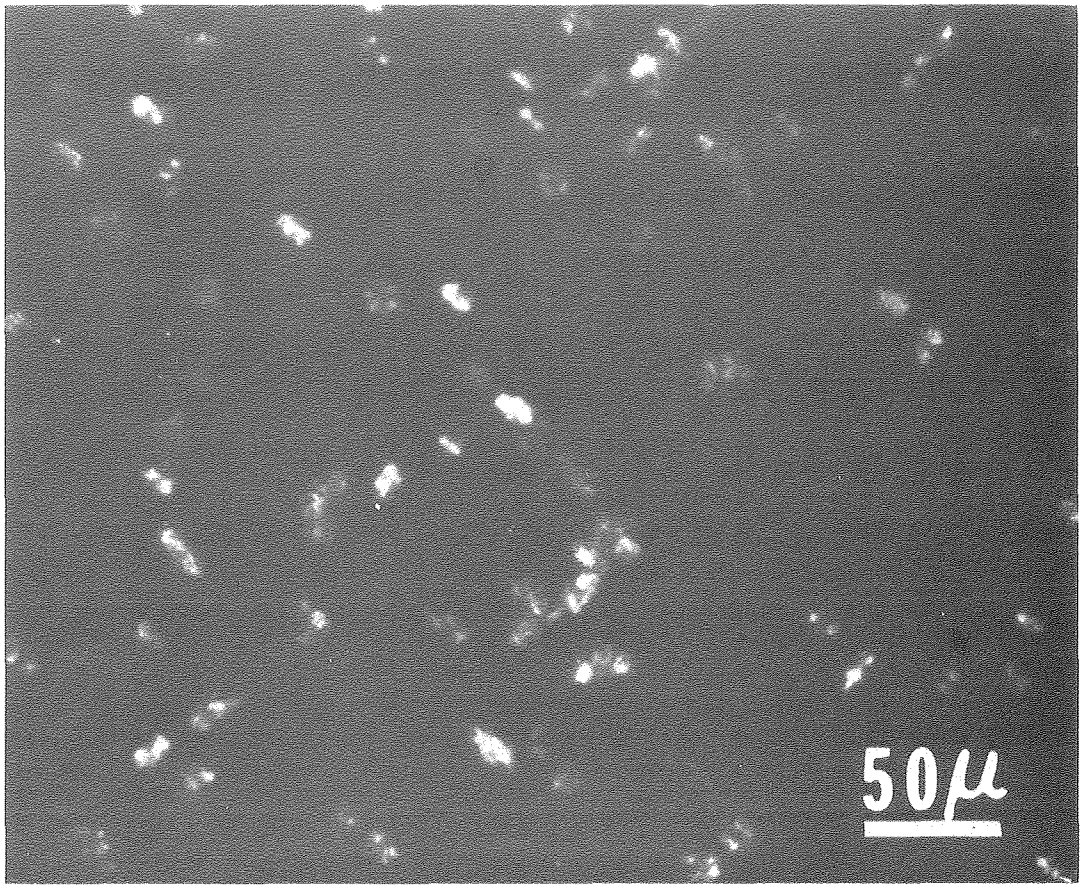


XBB 809-10362

Figure 14

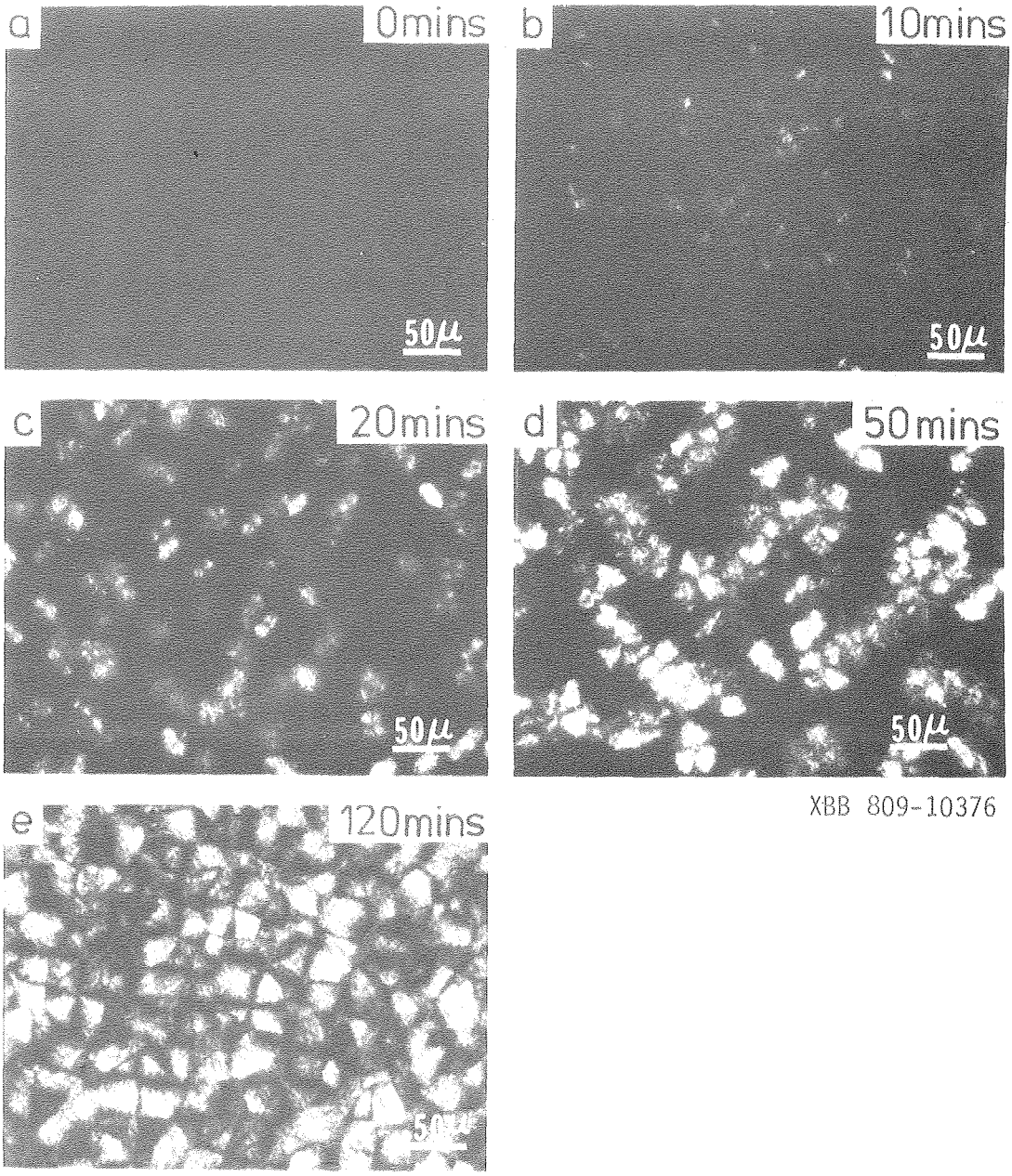


XBB 809-10376

Figure 15

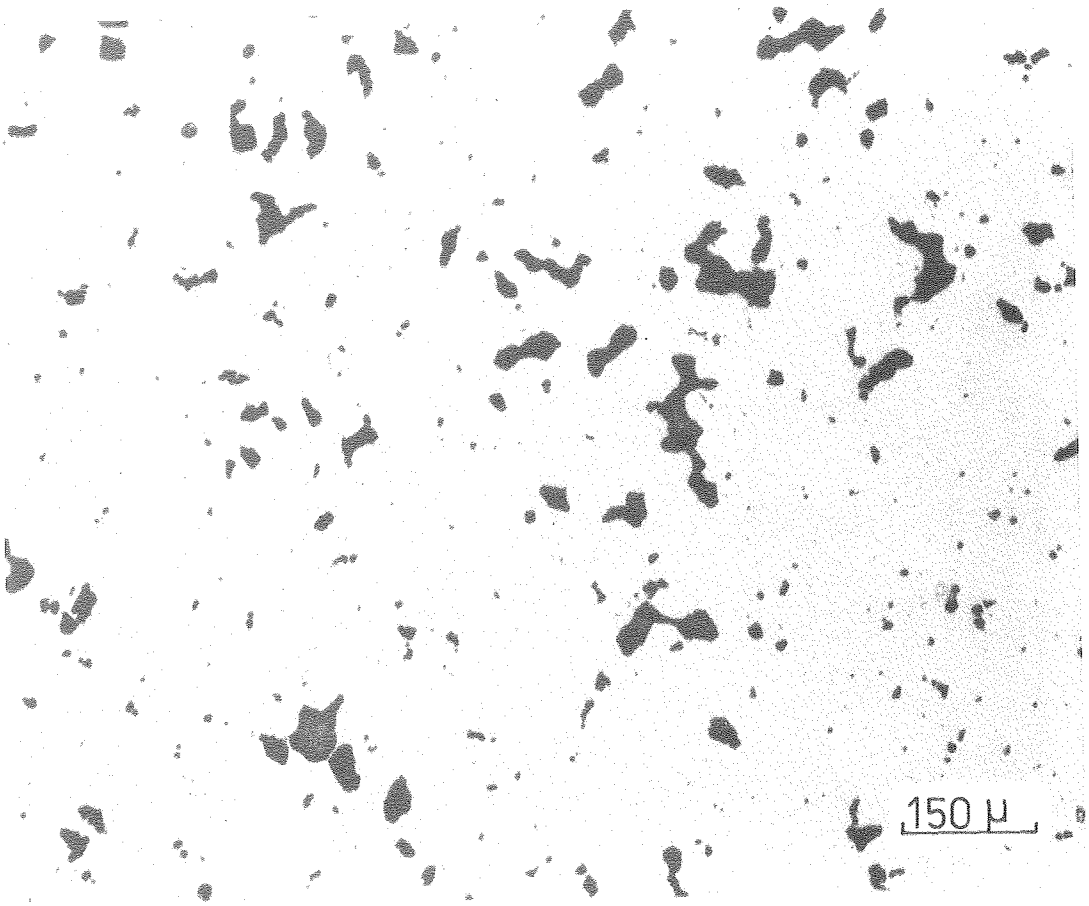


XBB 809-10371

Figure 16

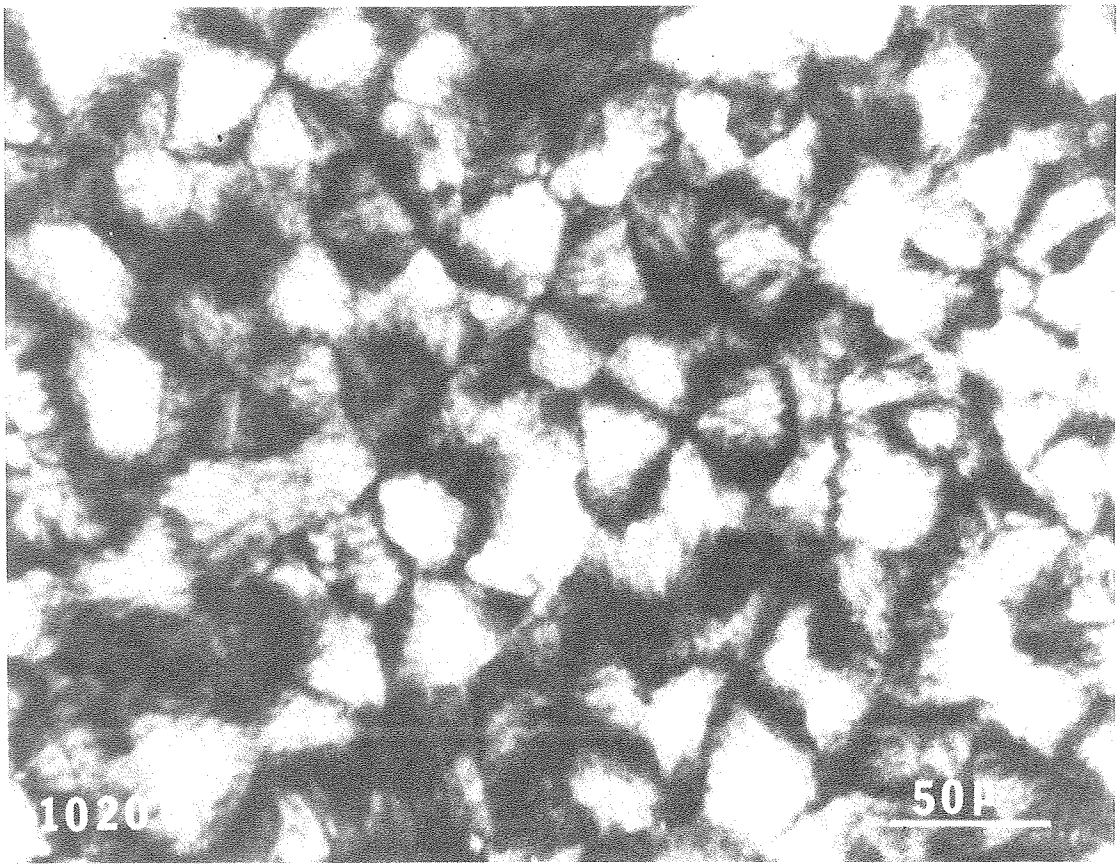


XBB 806-7155

Figure 17

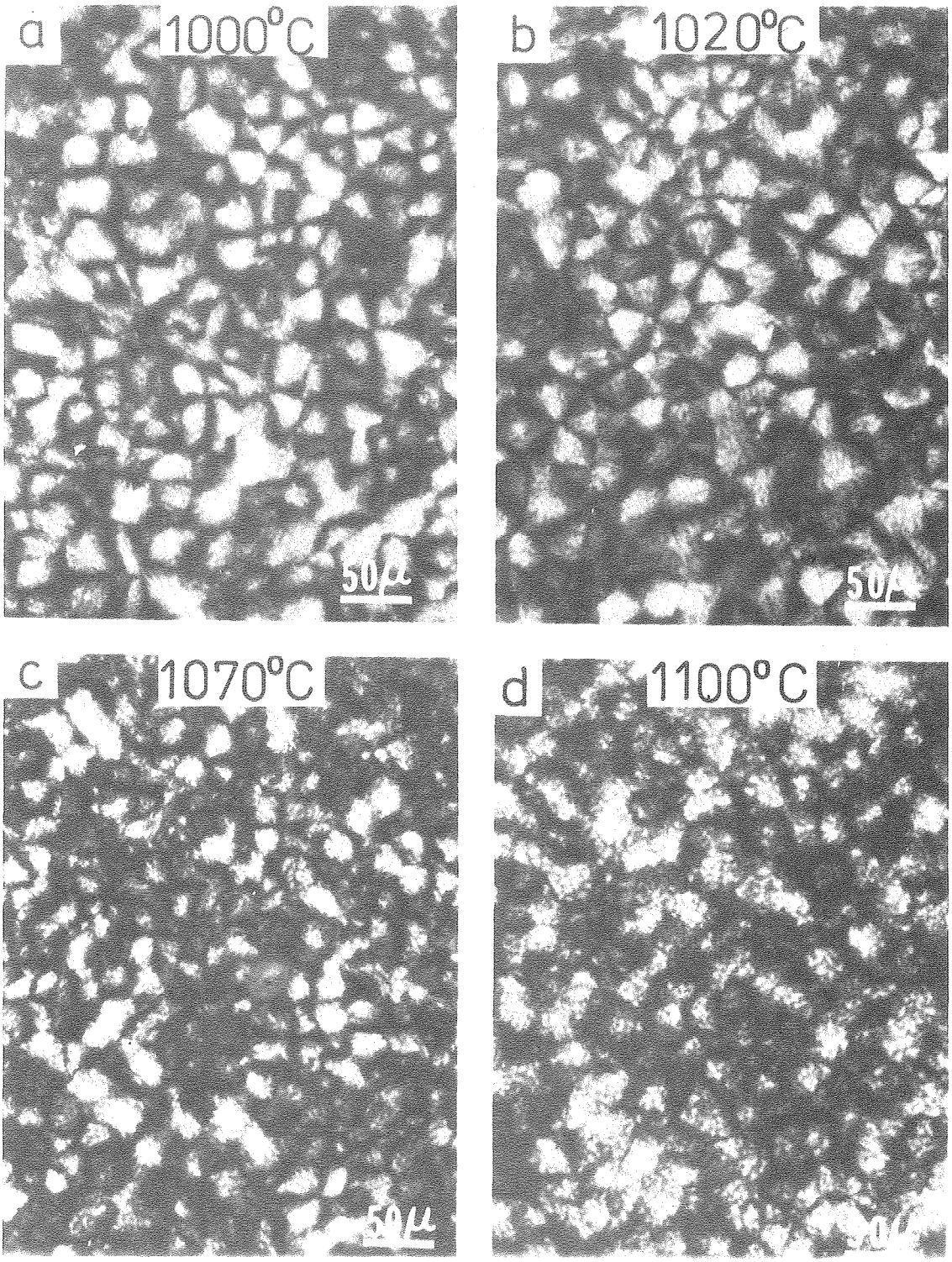


XBB 809-10372

Figure 18

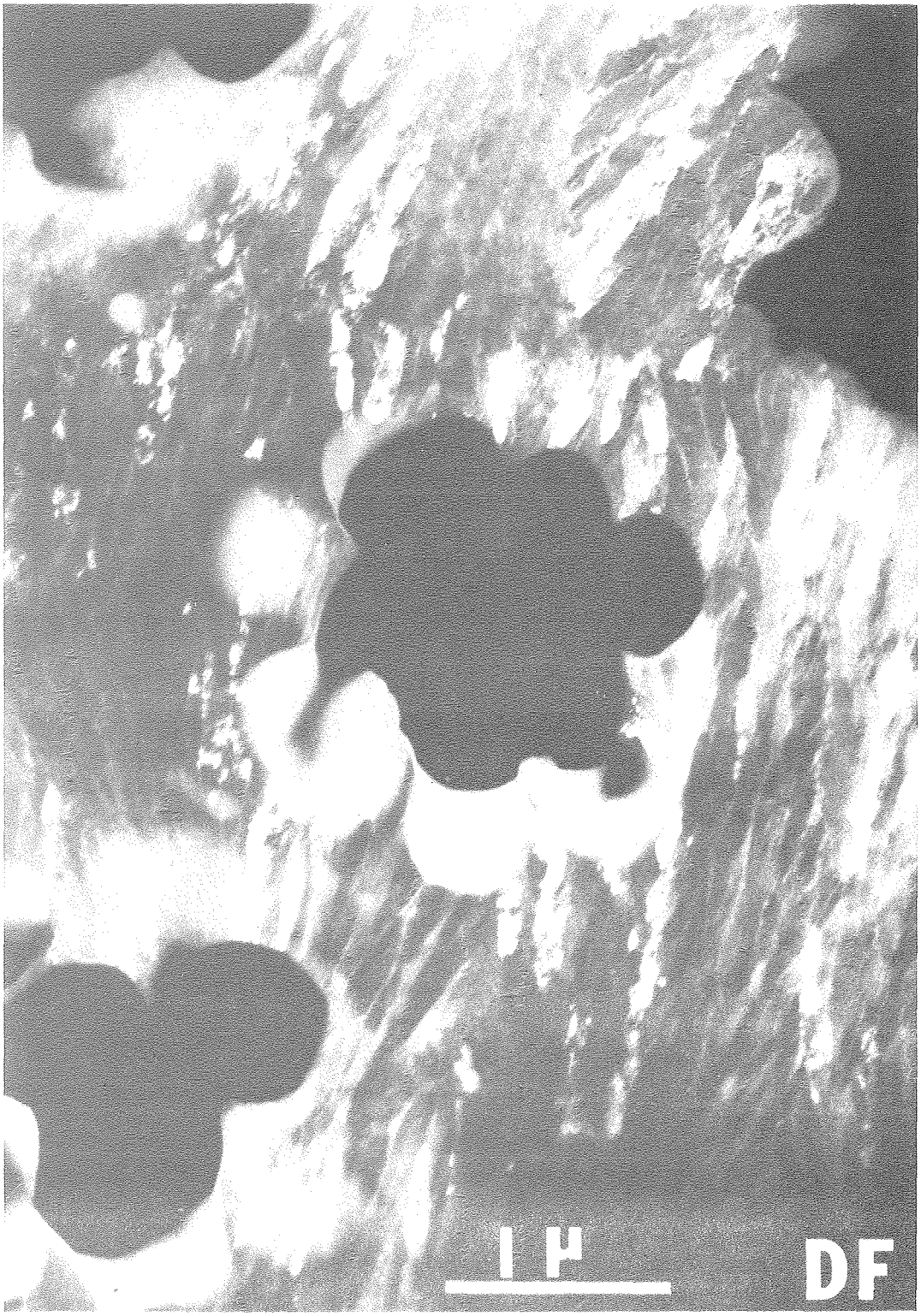


XBB 799-11618

Figure 19

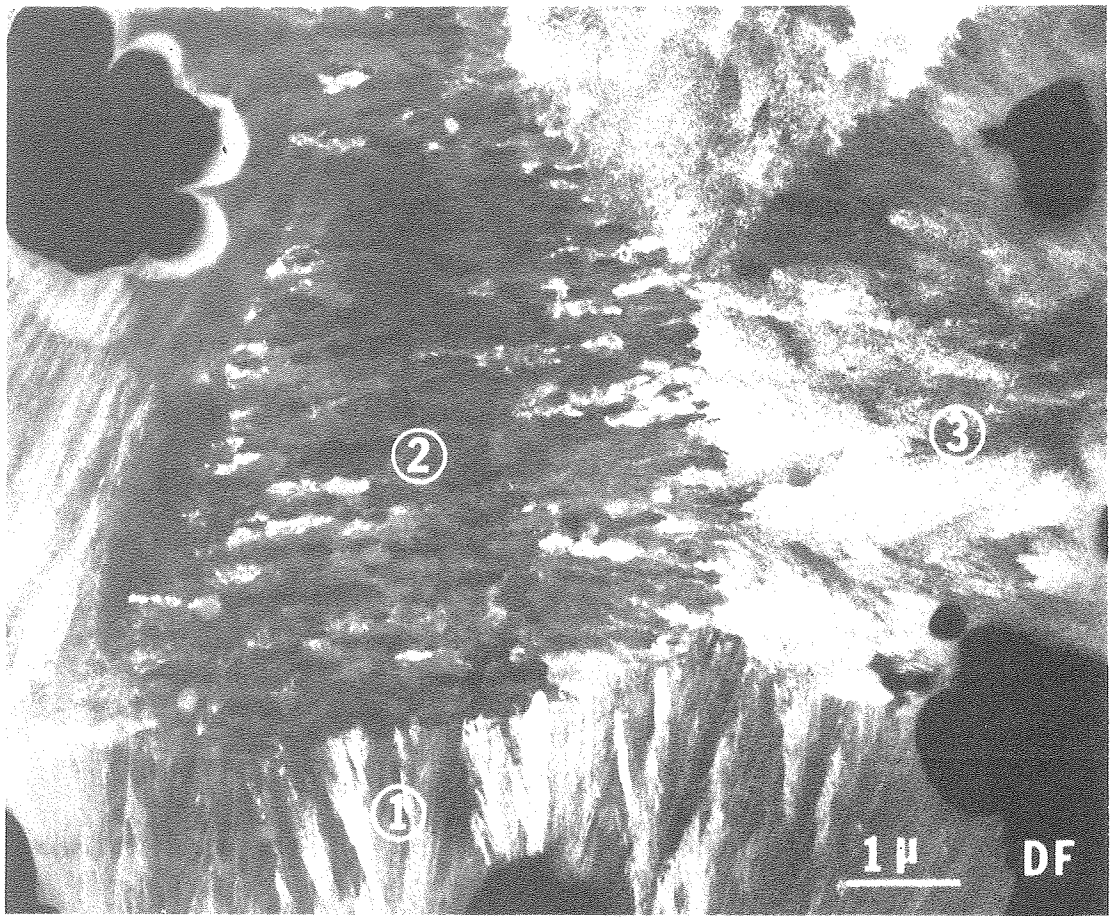


XBB 799-11625A

Figure 20

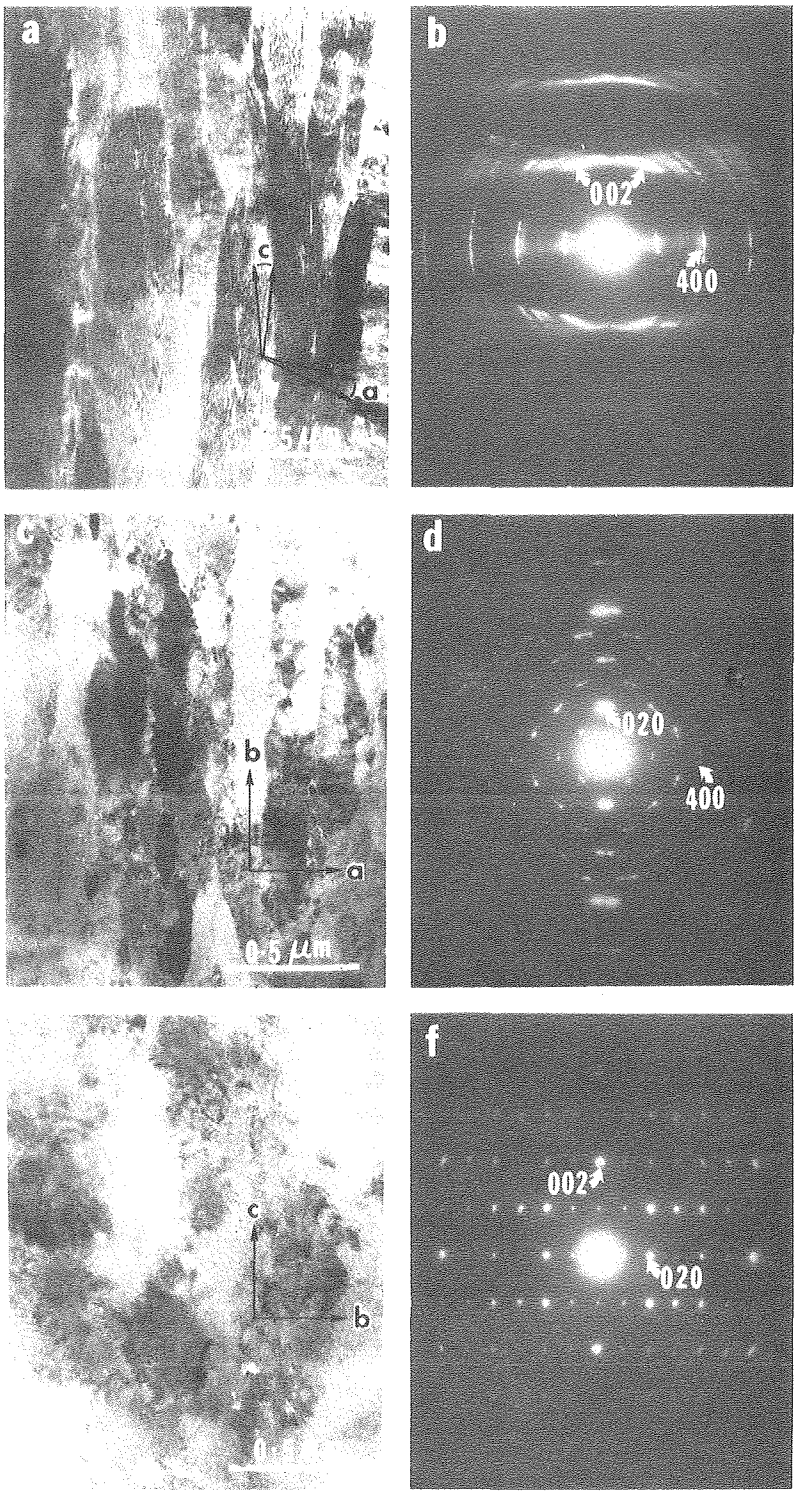


XBB 809-10377

Figure 21

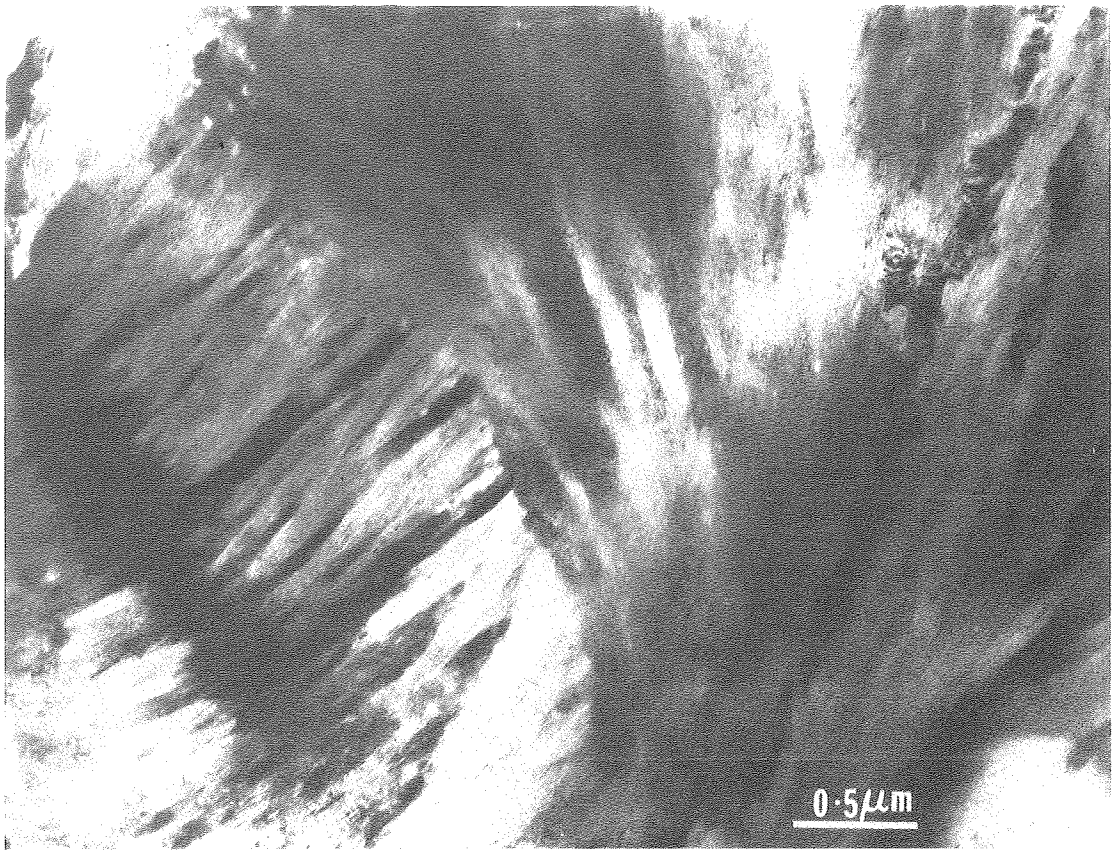


XBB 809-10374

Figure 22

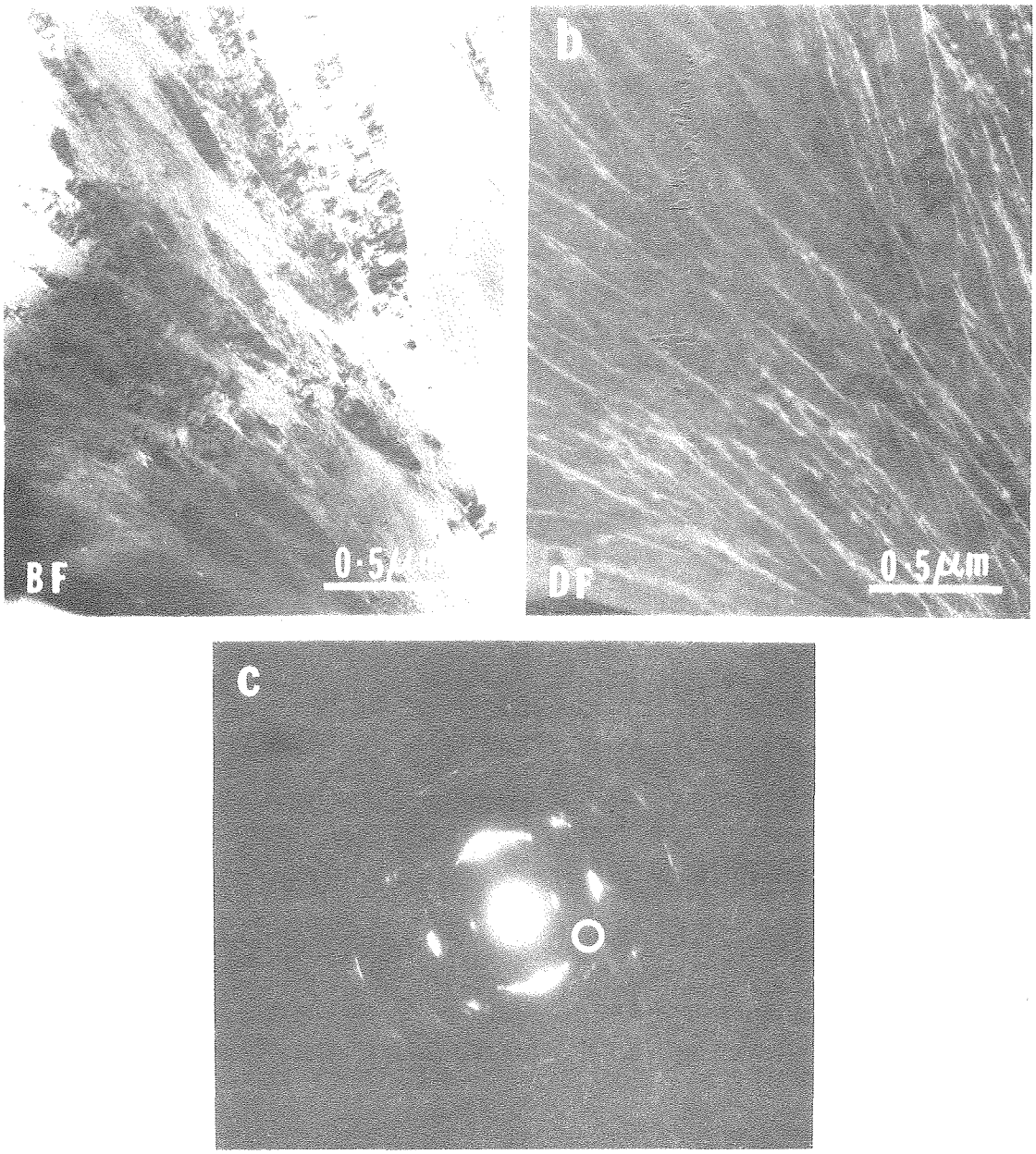


XBB 809-10373

Figure 23

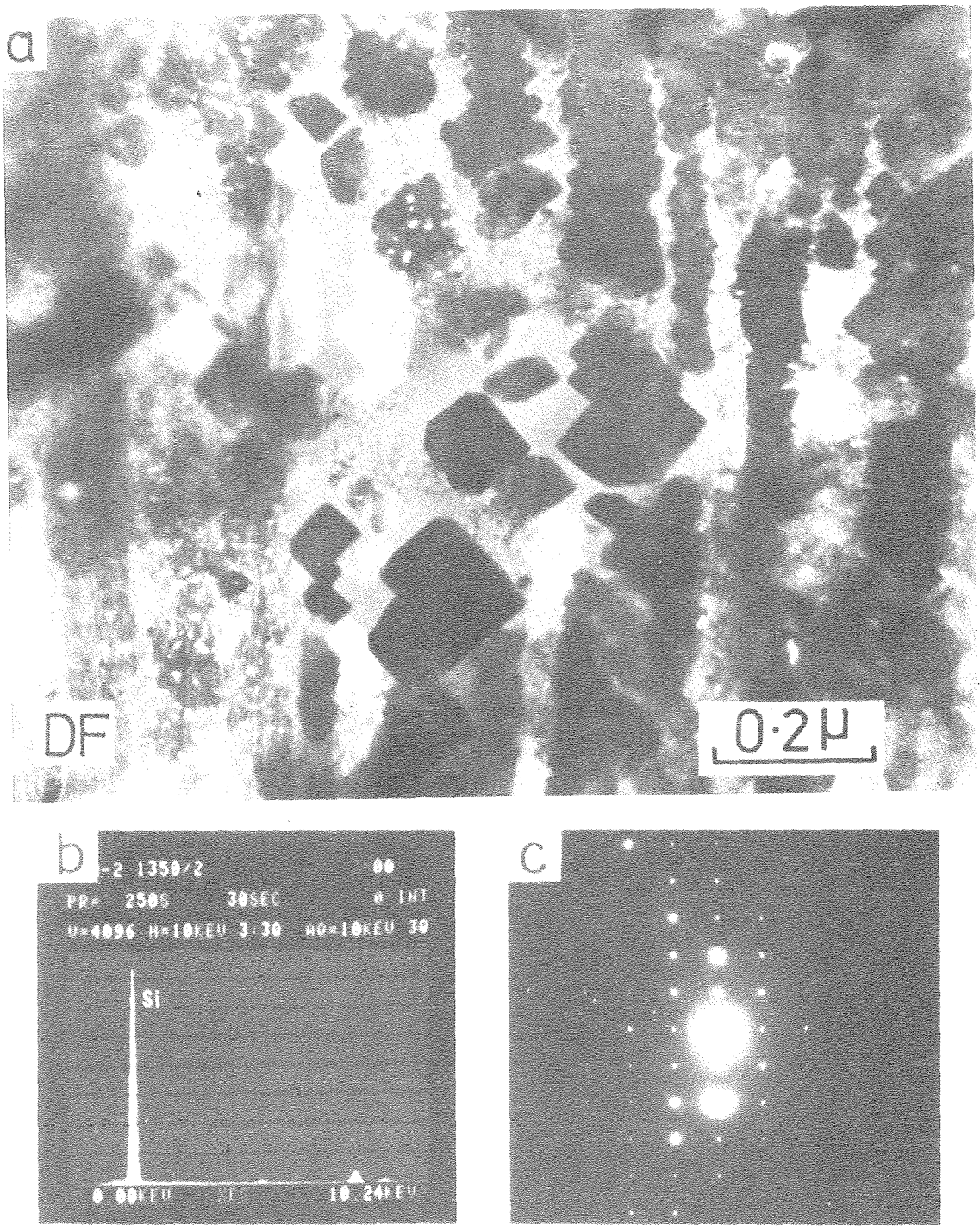


CBB 809-10381

Figure 24

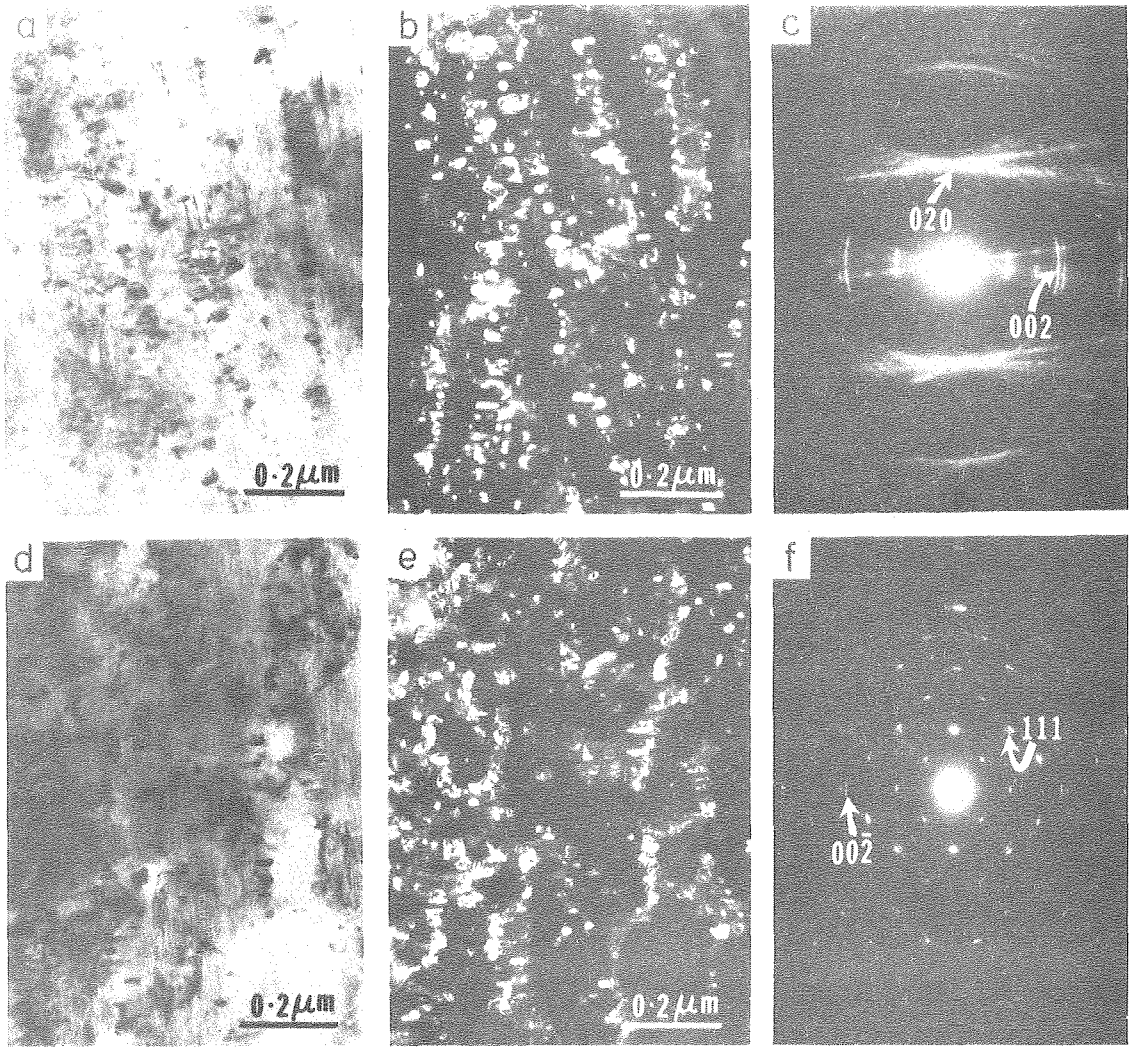


XBB 809-10375

Figure 25

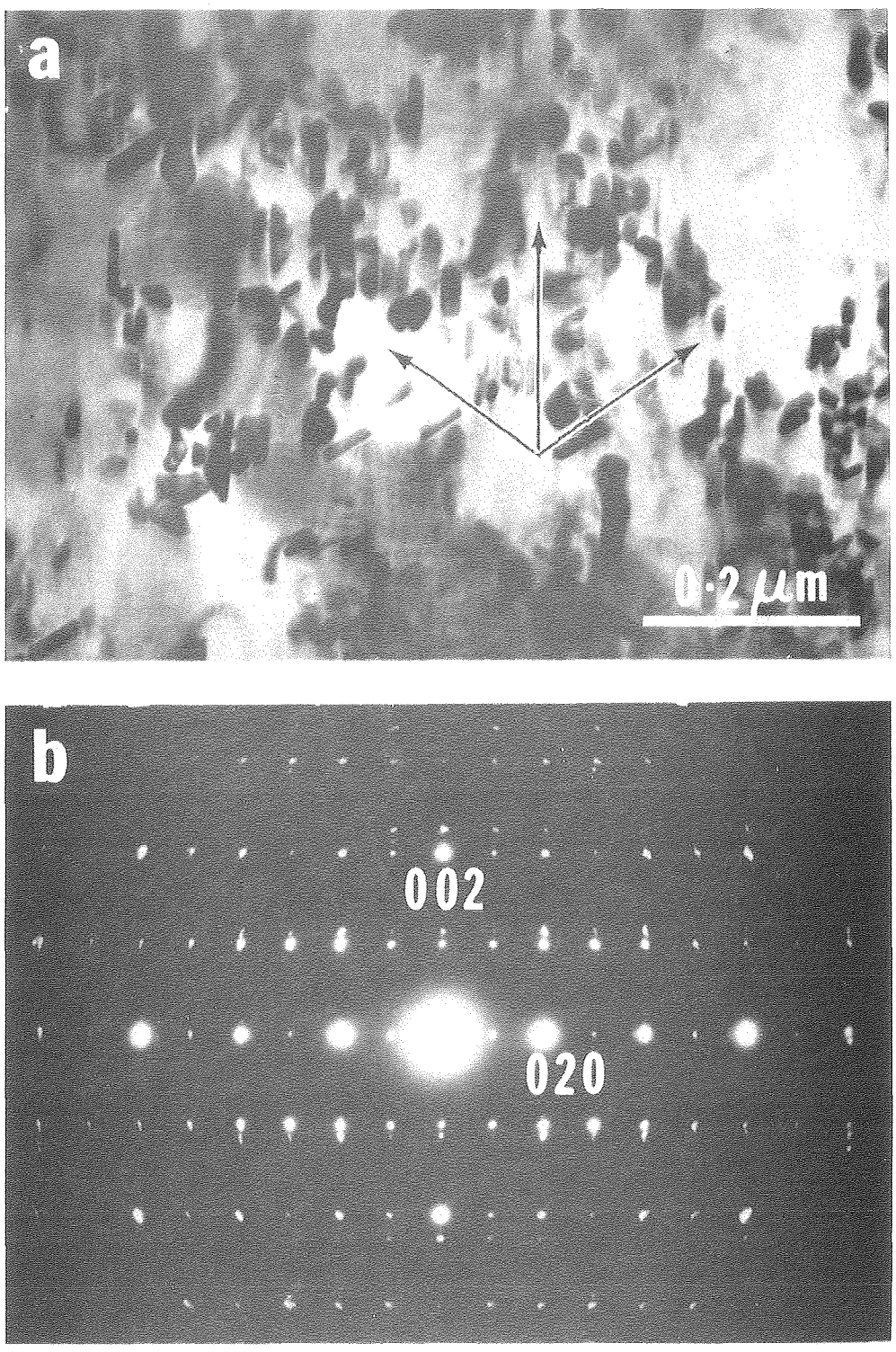


XBB 809-10366

Figure 26

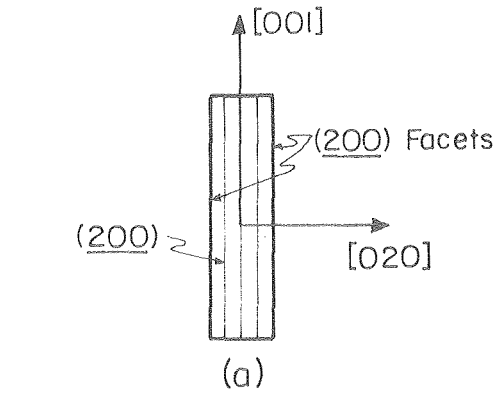


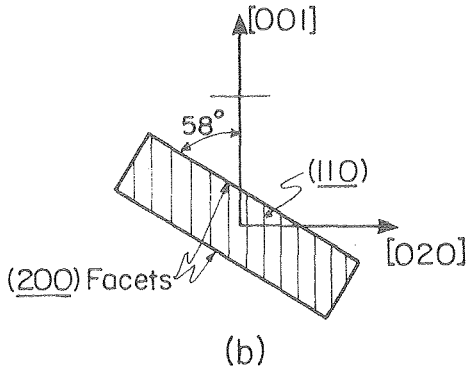


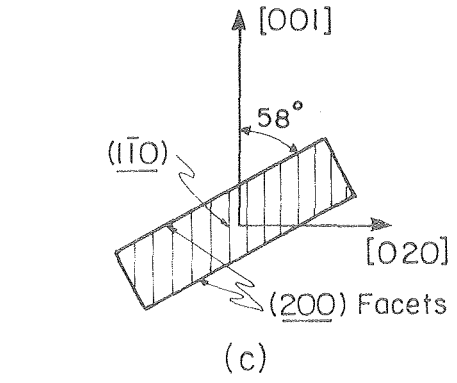


(200) $Si_2N_2O$ [020] CLEN

XBL 809-11715

Figure 27

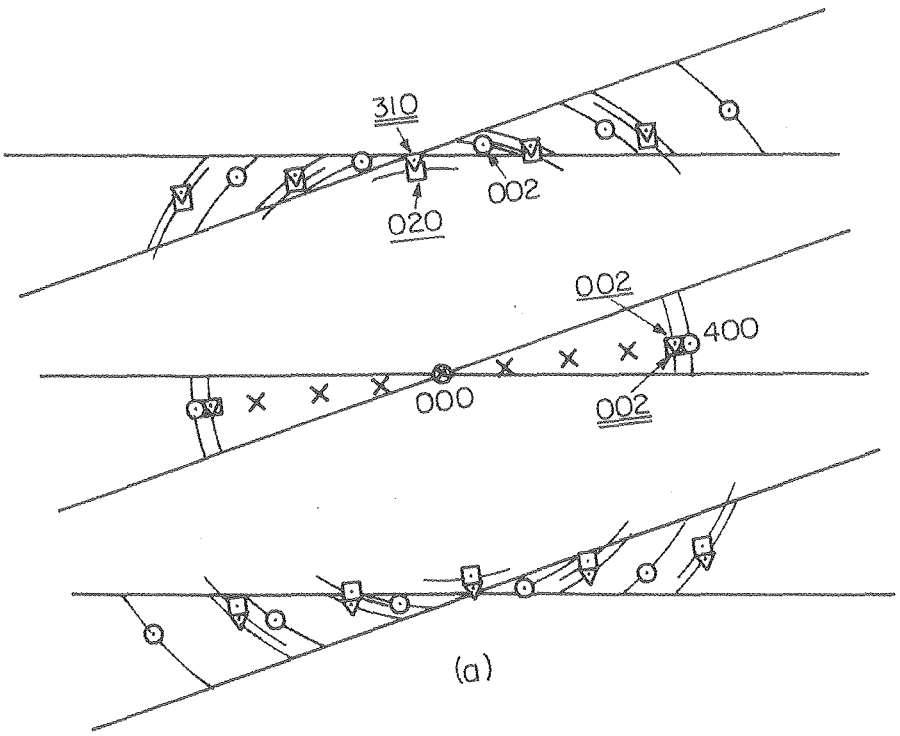


(a)

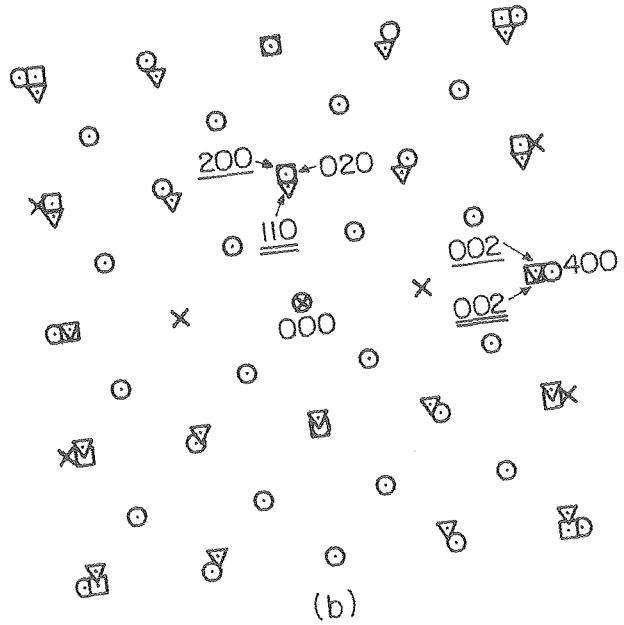


(b)

⊙400 Clinoenstatite

× Double diffraction

⊡020 $Si_2N_2O$ orientation 1

▽310 $Si_2N_2O$ orientation 2

XBL 809-11716

Figure 28

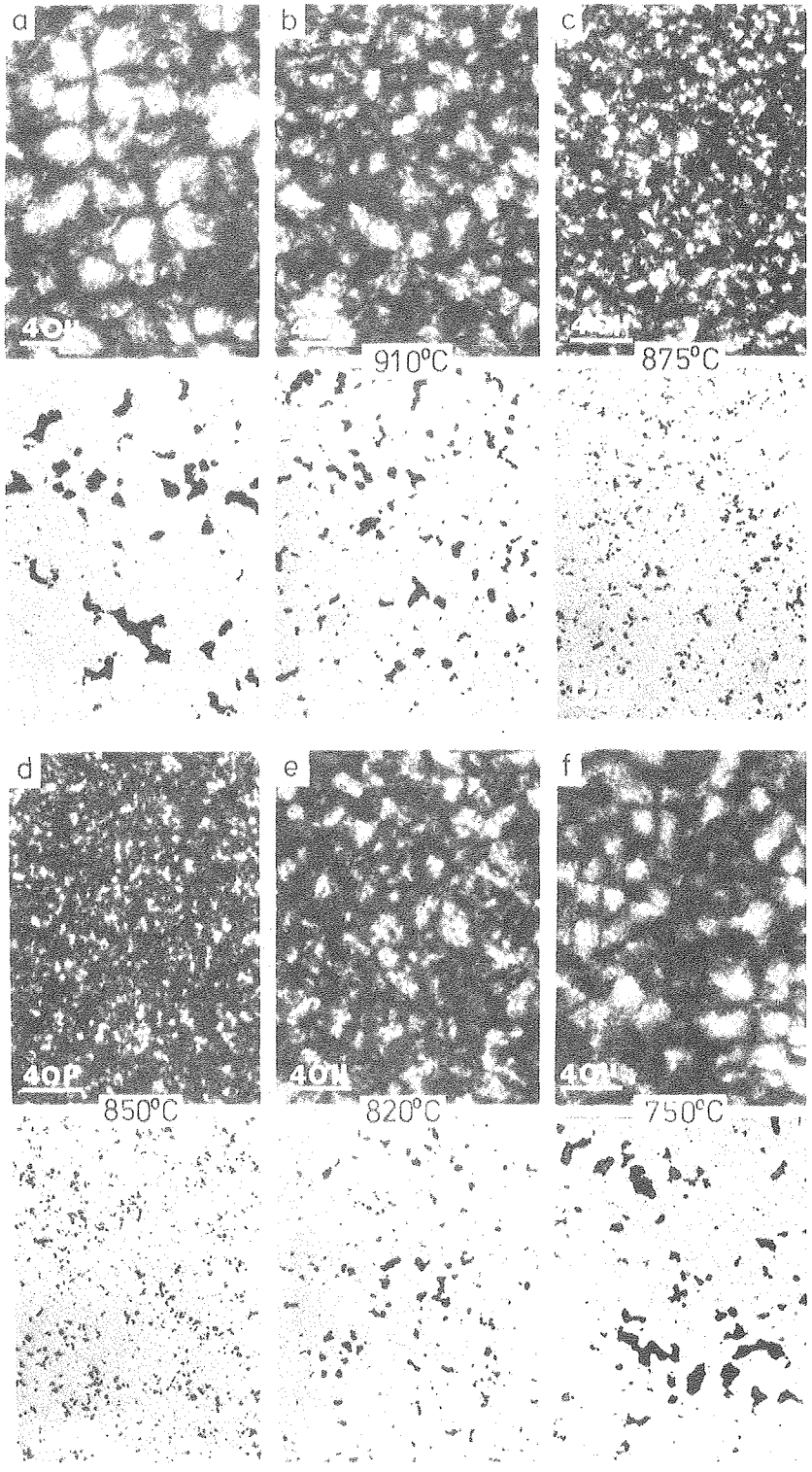


XBB 809-10738

Figure 29

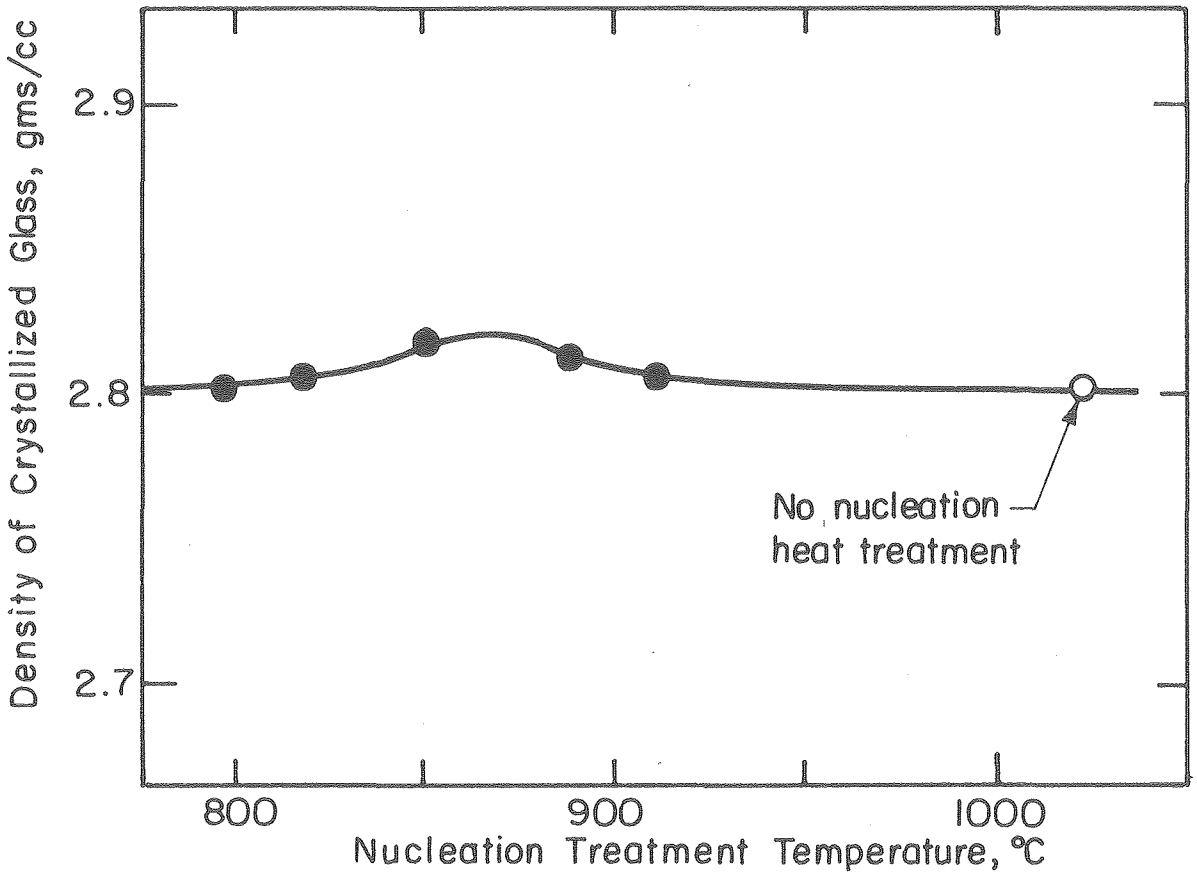


XBL 809-11713

Figure 30

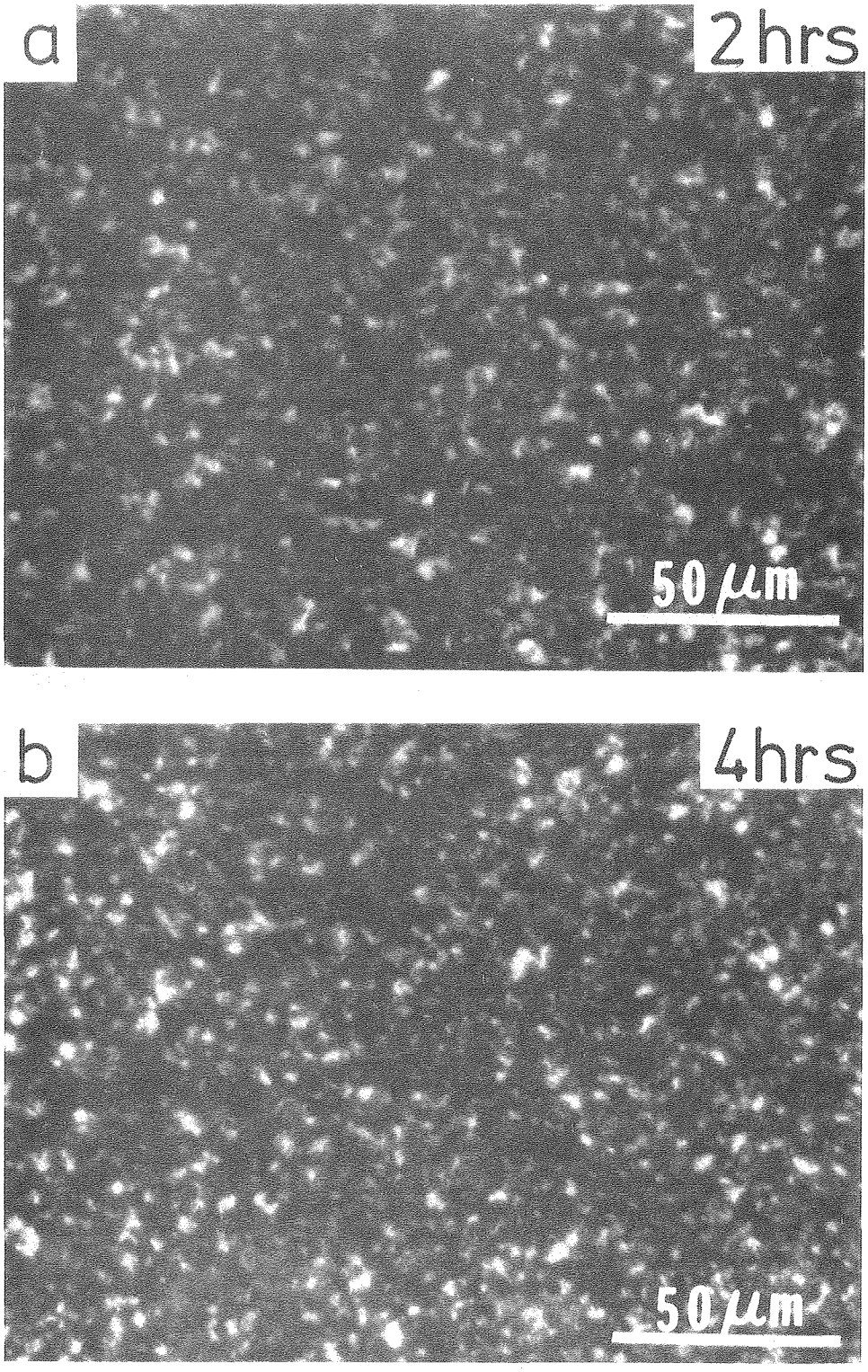


XBB 809-10364

Figure 31

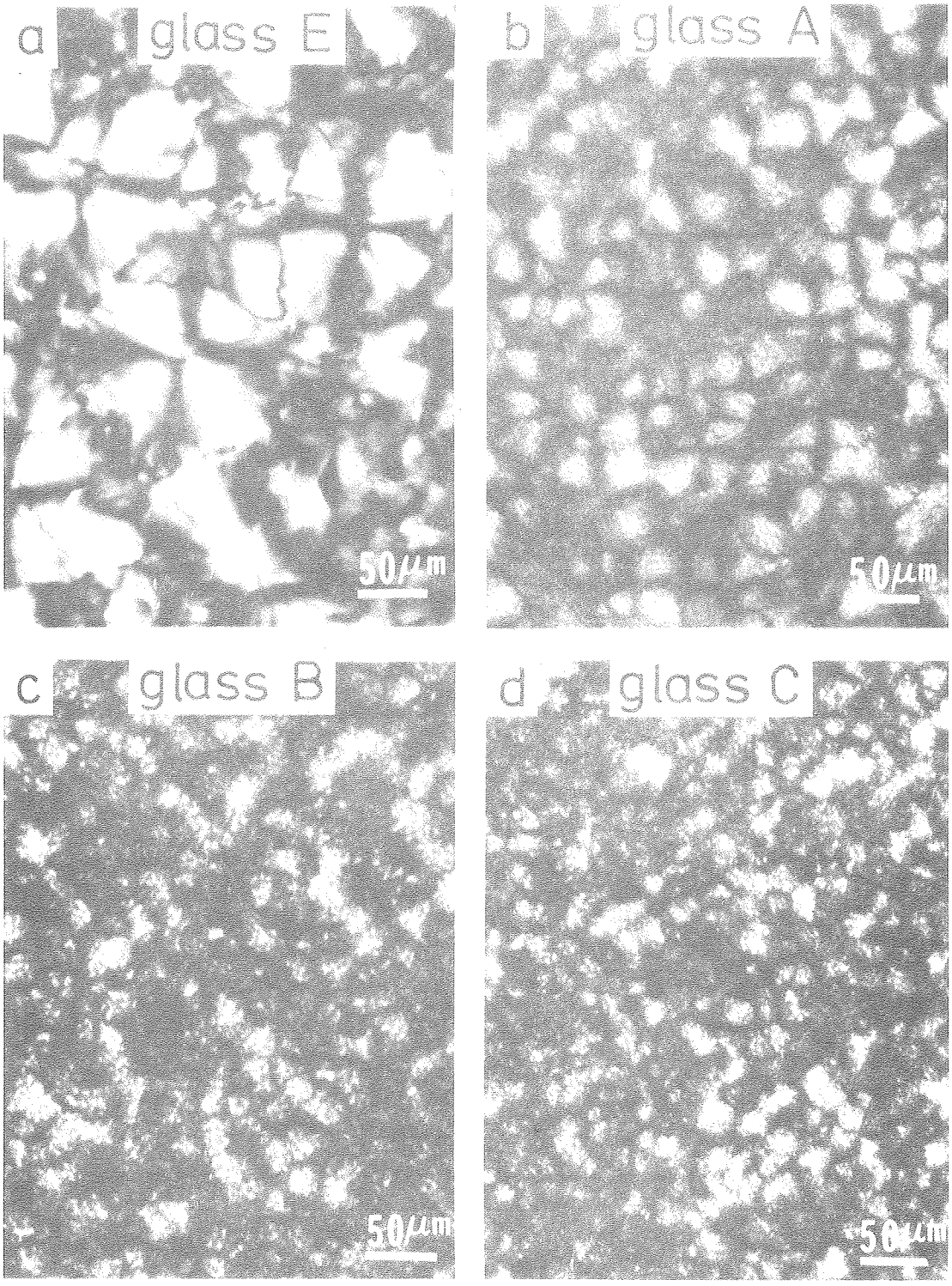


XBB 809-10367

Figure 32

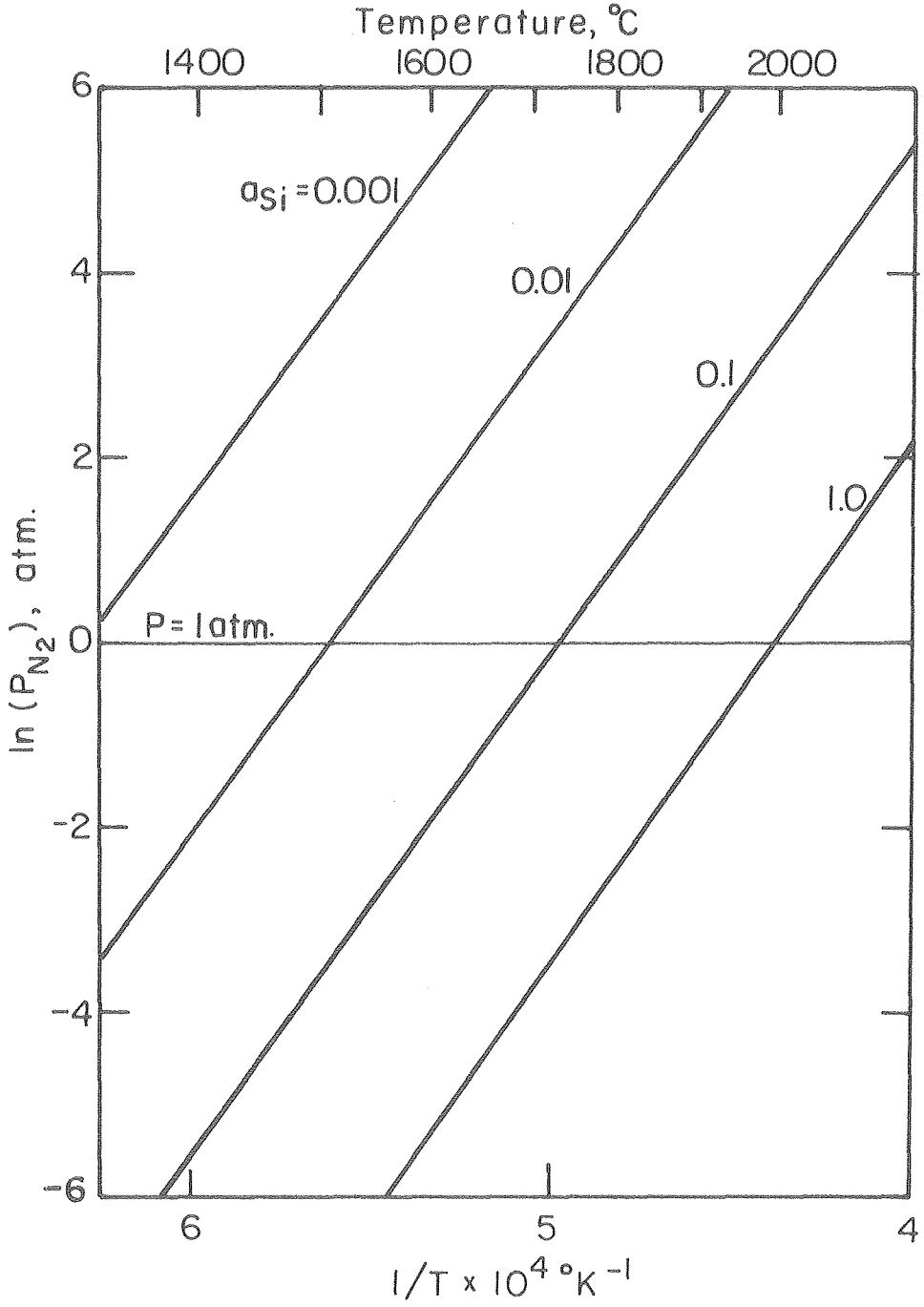


XBL 809-11710

Figure 33

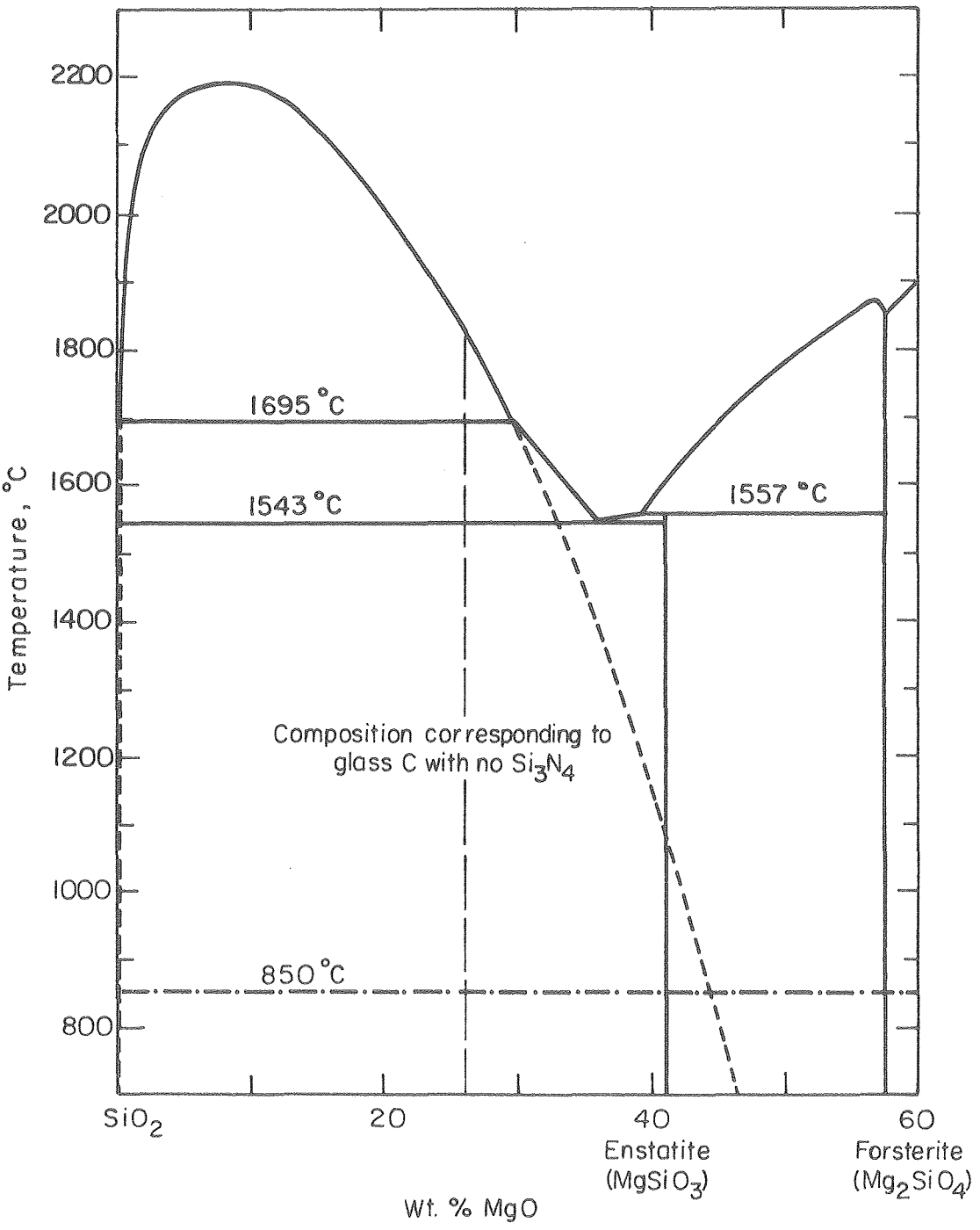
2200
2000
1800
1600
1400
1200
1000
800
Temperature, °C
1695 °C
1543 °C
1557 °C
850 °C
Composition corresponding to glass C with no $Si_3N_4$
$SiO_2$
20
40
60
Enstatite ($MgSiO_3$)
Forsterite ($Mg_2SiO_4$)
Wt. % MgO
XBL 809-11709

Figure 34

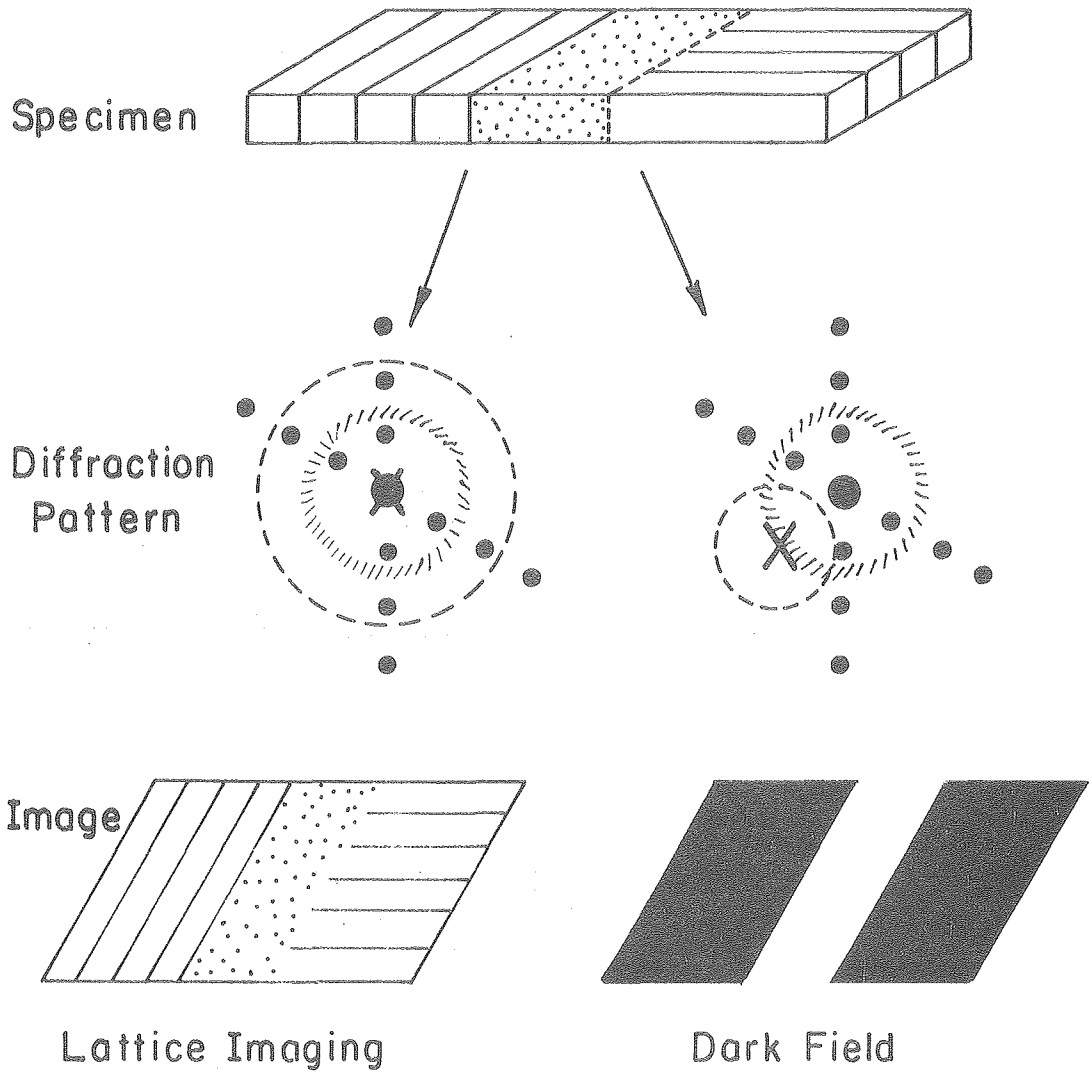
Specimen
Diffraction Pattern
Image
Lattice Imaging
Dark Field
Main beam
Optic axis
Diffuse ring (very weak)
Objective aperture
XBL786-5135

Figure 35

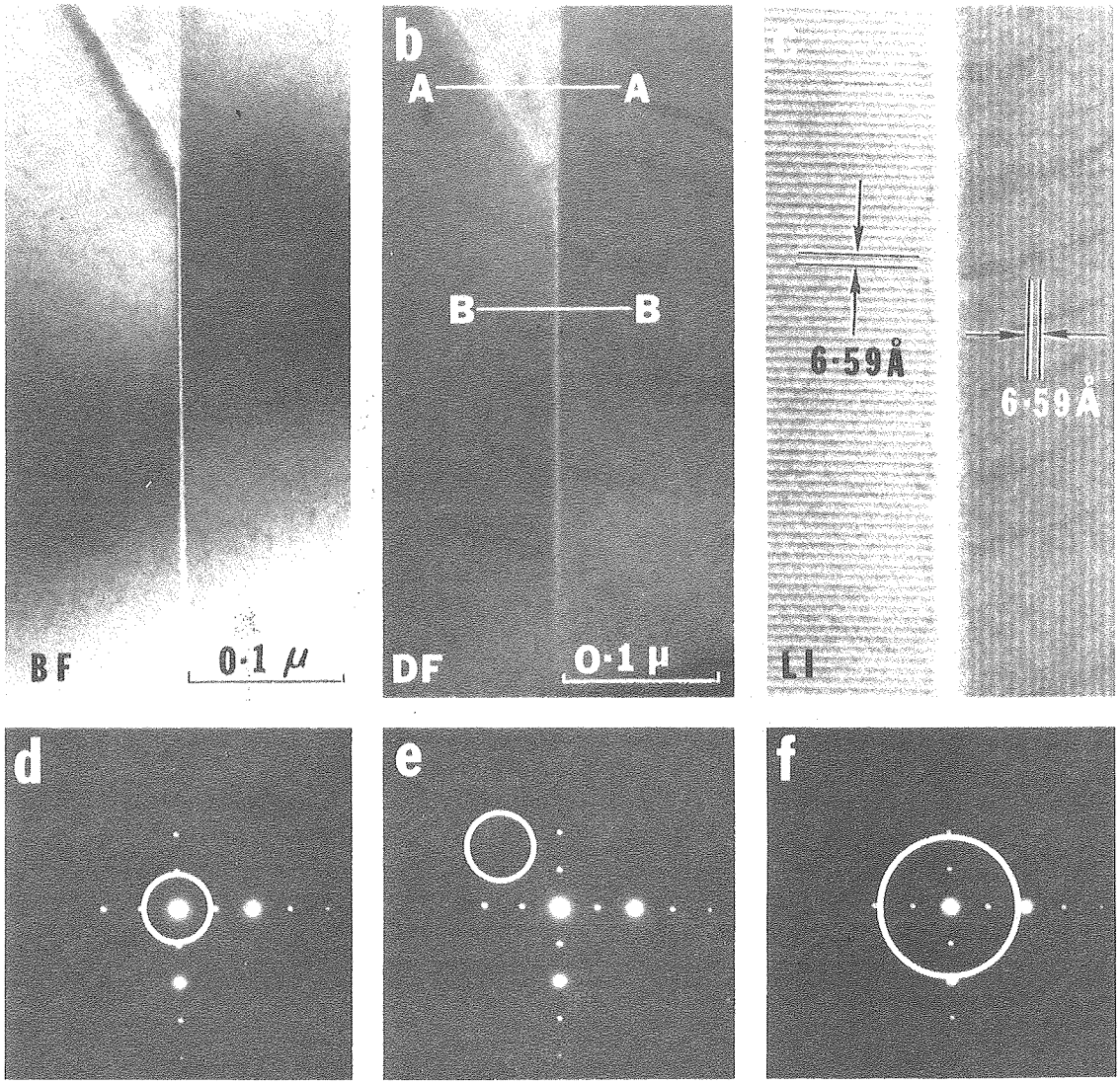


XBB 787-8787

Figure 36

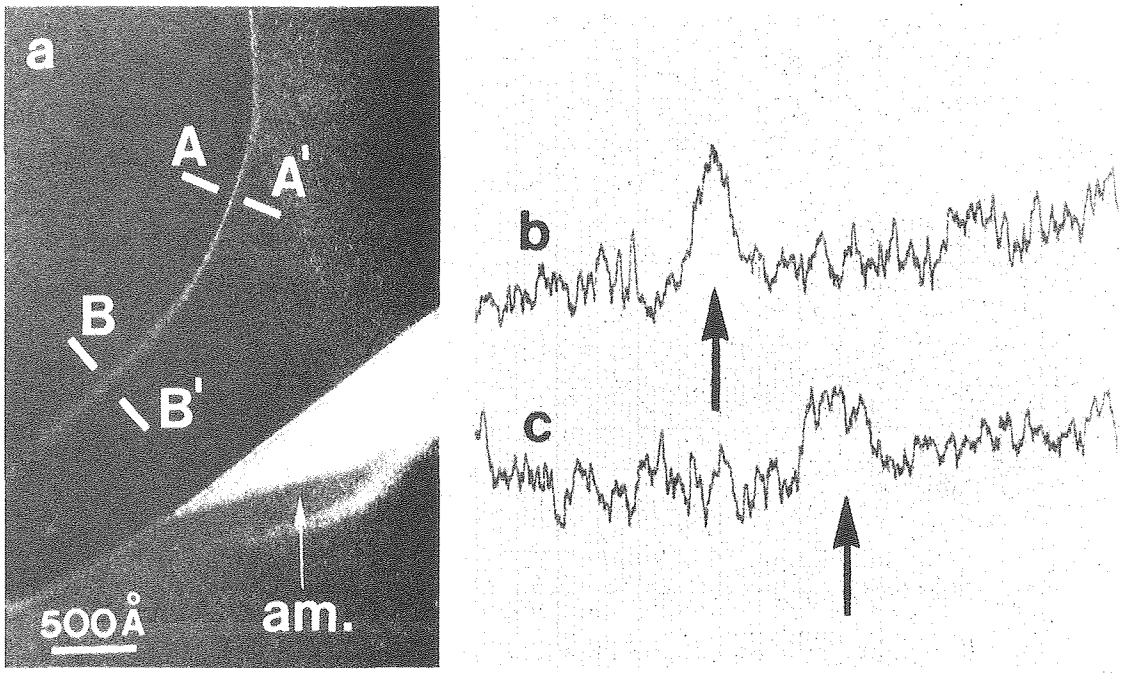


XBB 786-6922

Figure 37

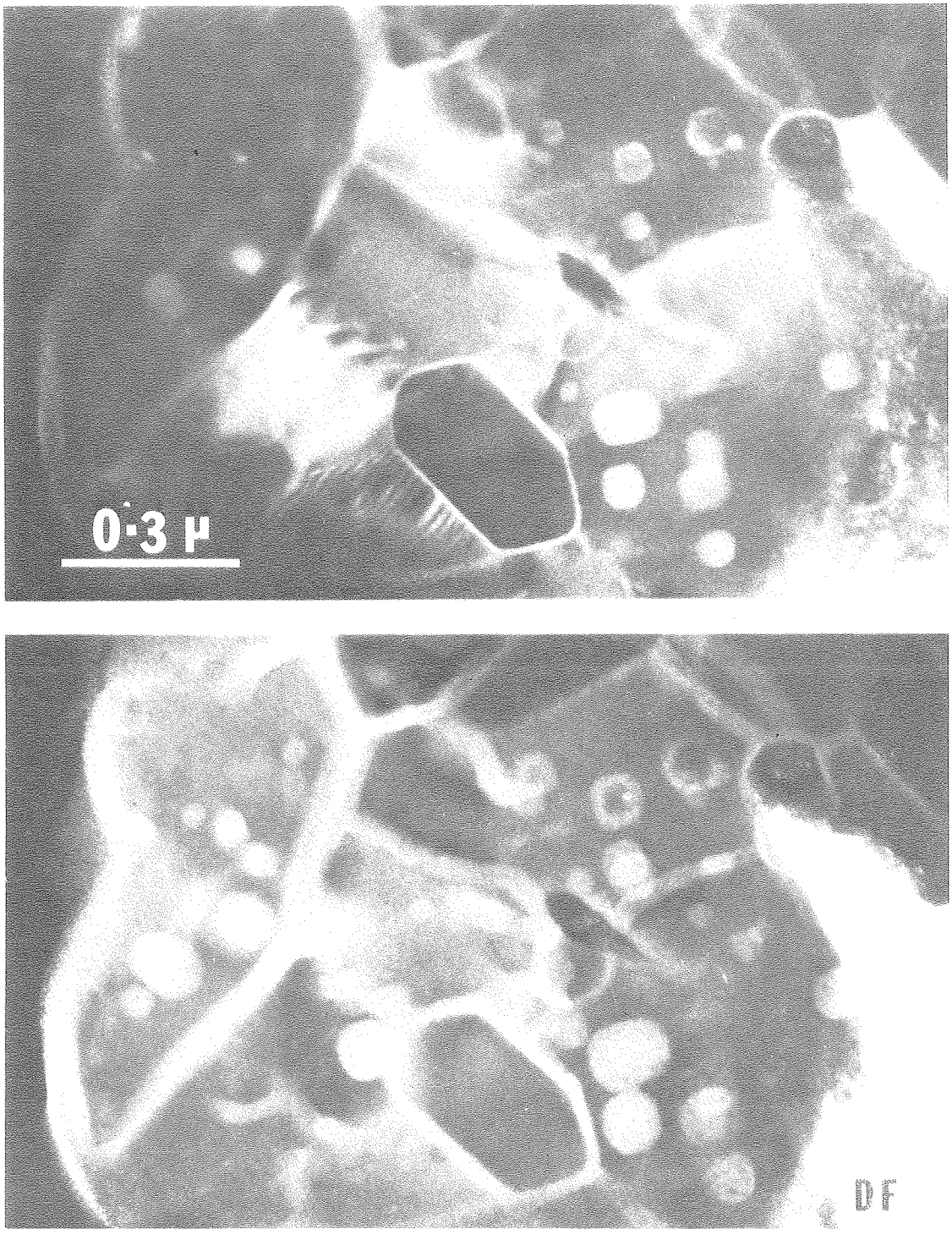


XBB 807-8755

Figure 38